Establishing the Kinematics of the North East Region of South Africa with the use of GPS Data

Prepared by Ahmad Desai under the supervision of Dr. George Sithole and co-supervision of Prof. Ludwig Combrinck

A thesis presented for the degree of
Master of Science

Department of Architecture, Planning and Geomatics
University of Cape Town
South Africa
August 2015

Plagiarism Declaration

I know the meaning of plagiarism and declare that all the work in the document, save for that which is properly acknowledged, is my own.

Signature Signed by candidate

Signature Removed

Acknowledgements

I would like to express my appreciation to my supervisor, Dr. George Sithole. This dissertation is testament to your guidance and patience. Your perspective on research, South Africa, and life has truly broaden my horizon. I thank you.
To my co-supervisor, Professor Ludwig Combrinck, your genius in summing up a problem and providing a solution almost instantaneously set me in the optimal research direction. I am very thankful. Your vast array of technical abilities and sacrifice for not only Geodesy, but for the various South African and global scientific communities are applauded.
To Dr. Ramesh Govind, I thank you for always making time to hear my thesis queries, to discuss Geodesy and to discuss South Africa and Geodesy. I admire your humility and humbleness. You are a true inspiration. South Africa, your motherland welcomes you home.
To the Department of Rural Development, Chief Directorate: National Geospatial Information, thank you for affording me the opportunity to complete my Masters in Science. To Aslam Parker I thank you for always showing interest and making time to review my thesis write up. Lindy-Anne Siebritz, thank you for being my voice of reason.
To the Ismial and Banderker families, I thank you for all the support and for the Tuesday and Wednesday night dinners. The great laughs are appreciated.
To my sisters Mumtaz, Thakira and Fairoza I thank you for always being there. I thank my parents Ebrahiem and Fatima for the love and the support, however I reserve special praise for my mother; of your many qualities, I draw strength from your perseverance. Verily your sacrifice has not gone unnoticed.

Abstract

The Nubia-Somalia boundary is one of the least well defined plate boundaries. The southern extension, as it extends through the latitudes that are co-incidental to South Africa's geographical extent has not been defined.

This project analyses Trignet data, supplemented with other available Nubian GPS data, to determine whether the North East Region of South Africa is segregated from the Nubian Plate. A ten year GPS time series (processed using the Bernese 5.0 precise GNSS software) is minimally constrained to the ITRF2008, using the reprocessed IGS08 products. This processed data was managed to alleviate GPS time series bias, which includes seasonal effects, the determination of GPS velocity uncertainty using a white+flicker noise model, discontinuity detection using Roggero's (2012) discontinuity algorithm and an outlier detection using an algorithm developed for this project for each of the 104 stations incorporated in the network.

The computed velocities were compared to the ITRF2008 published velocities and a RMS of the post fit residuals of 0.4, 0.4 and 0.7 mm/yr for the North, East and Height were computed respectively. This RMS is of similar magnitude to the WRMS of the post fit velocity residuals in computing transformation parameters from ITRF2005 to ITRF2008, suggesting that the threshold of ITRF2008 velocity precision has been obtained. The resultant Euler vector was scrutinised on three fronts: an Euler vector representing the geographical extent of South Africa, an Euler vector in which the height velocity was minimised to zero and an Euler vector representing the North East Region of South Africa. All computed Euler vectors are consistent, suggesting a uniform South African GPS velocity field. The Euler vector representative of South Africa's uniform velocity field has an angular velocity of 0.273 deg/Myr, with a pole of rotation at lat 50.85 and long -82.83 degrees and is consistent with the Euler vectors computed by Altamimi et al. (2012) and Malservisi et al. (2013) for Africa and South Africa respectively.

The consistency of the Euler vector suggests that South Africa is underlain by a single plate (i.e. the Nubian Plate), and that the East African Rift valley does not extend into South Africa. Hence, for future tectonic studies and long term reference frame solutions, stations such as HARB, HRAO and RBAY should be included, as they are not located in deformation zones.

Contents

List of Figures

Chapter 1

Introduction

1.1 Introduction

German scientist Alfred Lothar Wegener in 1912 argued that the land masses of the various continents are dynamic, adding that at one stage all of the modern day continents formed one land mass known as Pangaea, which, over time, split up into the various continents observed today (Saigeetha and Banyal, 2005).

This theory was based on archaeological and geological evidence. Plants and animals of similar species found on different continents were used to support this theory. It was further supported after the discovery of the Mid-Atlantic ridge and the spreading thereof (Prawirodirdjo, 2004).

The advent of the Global Positioning System (GPS), the continuous addition of stations into the International GNSS Service (IGS) (url: `https://igscb.jpl.nasa.gov/`, accessed: 27 August 2015) global network as well as the development of Continuously Operating Reference Stations (CORS), have facilitated accurate positions to be determined on a global scale. Furthermore, the amalgamation of Global Navigation Satellite System (GNSS) with other space Geodetic techniques such as Satellite Laser Ranging (SLR) and Very Long Baseline Interferometry (VLBI) have together made it possible for velocities of the various plates to be accurately modelled (Fernandes et al., 2004; Nocquet et al., 2006).

One of the early applications of space geodetic techniques (such as GPS) was the determination of the motion of continental plates (DeMets et al., 2010). Initially, estimates of plate kinematics determined from space geodetic observations agreed well (within the expected uncertainty of 3 mm/yr) with geological models (Sella et al., 2002). However, with the increase in the number of global GPS sensor stations and with the improvement in

the ephemerides, significantly refined geodetic models (i.e. plate kinematic models) highlighted important tectonic information that was not sensed by the more crude geologically propagated angular velocity models and by the early space geodetic models (Sella et al., 2002).

The reasons for the difference between the refined geodetic models and the geological models are partially due to the observation techniques and in the difference in the temporal nature of the observed data.

Geological models are based on a 3.2 million year average of spreading rates and thus any change in the rate of motion in that period is not considered (Prawirodirdjo, 2004). However, space geodetic techniques have a data span of approximately 20 - 30 years and the derived velocity estimates are geologically instantaneous representing the plate motion for the last 10 000 to 100 000 years (Prawirodirdjo, 2004), so the change in plate motion cannot be solved with space geodetic techniques alone.

One of the more robust kinematic models that is based on geological data is the NUVEL-1A (DeMets et al., 1990, 2010) model. This model takes into account the kinematics of 14 major plates and these rates are obtained primarily from seafloor spreading data (Nocquet et al., 2006). This seafloor spreading rate obtained at the plate boundary is then assumed by the entire plate that is associated with that boundary (Nocquet et al., 2006).

The NUVEL-1A served as a kinematic model to compute the ITRF (url: `http://itrf.ensg.ign.fr/`, accessed: 27 August 2015) realizations between and including ITRF88 and ITRF1997.

With the increase in the number space geodetic sensor stations (such as Very Long Baseline Interferometry (VLBI), Global Navigation Satellite System (GNSS),etc.) an improved ITRF 2000 reference frame was computed. ITRF 2000 and subsequent ITRF realizations are independent of geological models (Prawirodirdjo, 2004). Failing to acknowledge the African plate as two independent plates compromises the accuracy of the NUVEL-1A model and is one of the major sources of discrepancies between the NUVEL-1A model and geodetic derived kinematics (Nocquet et al., 2006). The exclusion of the Nubia-Somalia boundary in the NUVEL-1A model is attributed to the lack of earthquakes and volcanic activity along the entirety of the respective boundary (Nocquet et al., 2006).

1.2 The Kinematics of the African Plate - The Nubia-Somalia Plate Boundary

It has been established that seismic activity such as earthquakes and volcanoes are associated with plate boundaries. The characteristic of the plate boundary may either be what is called a constructive plate boundary, whereby more "earth plates" are being generated (e.g. mid-atlantic ridge) or one that is destructive, whereby a plate is consumed by the mantle (e.g. New Zealand's transform fault).

The Nubia-Somalia plate boundary is characterised by earthquakes and volcanoes as well as shown in Figure 1.1. This boundary has a general north-south orientation that falls within the latitude range of 10 degrees north and 48 degrees south, and is constrained in the north by the Red Sea and Gulf of Aden, and in the south by the South West Indian Ridge (SWIR).

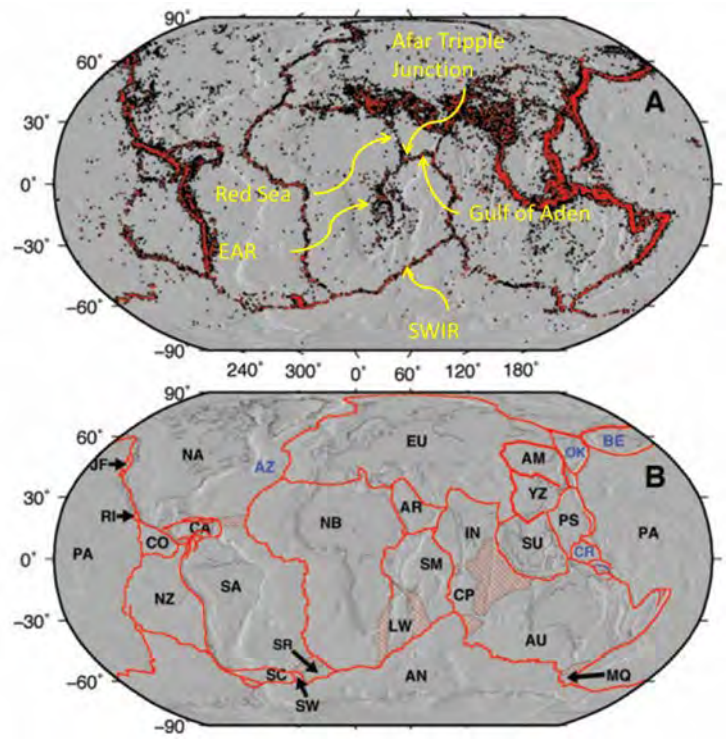

Figure 1.1: Red dots in the 1st image (top) depicts seismic activity registering above 4.5 on the Richter scale. The 2nd image (bottom) outlines the plate boundary based on the seismic activity. The pate abbreviations are: NB-Nubian, AR-Arabian, SM-Somalia, LW-Lwandle, AN-Antarctica plates, IN-Indian and EU-European (DeMets et al., 2010).

The northern terminal of the boundary is characterised by a triple junction, known as the Afar triple junction. The Red Sea, the Gulf of Aden and the East African Rift (EAR) Valley constitutes this triple junction.

In previous kinematic models such as NUVEL-1A, the understanding of the Afar triple junction and its implications on a global kinematic model was limited. The EAR was not considered and the African plate was treated as a single plate. Jestin et al. (1994) suggest that a two plate African system, and a single Indian Plate better fits the existing geological data.

The East African Rift (EAR) Valley forms the southern arm of the Afar triple junction. It is topographically distinctive with volcanic and earthquake activity from about 5 degrees north to about 20-22 degrees south. Moving down south, at about 5 degrees south the EAR splits into a western and eastern arm (see Figure 1.2). The western arm extends southwards from the northern end of the Kenyan Rift Valley through Tanzania and Lake Tanganyka, through Malawi and Lake Malawi, and through Mozambique; whereas the eastern arm traverses through Kenya, the Davie Ridge and the Mozambique Channel connecting with the western arm in the southern part of Mozambique (Fernandes et al., 2004; Hayes et al., 2014). The western arm is subjected to higher seismic activity than the eastern arm and is generally accepted as the Nubia-Somalia boundary (Le Gall et al., 2004).

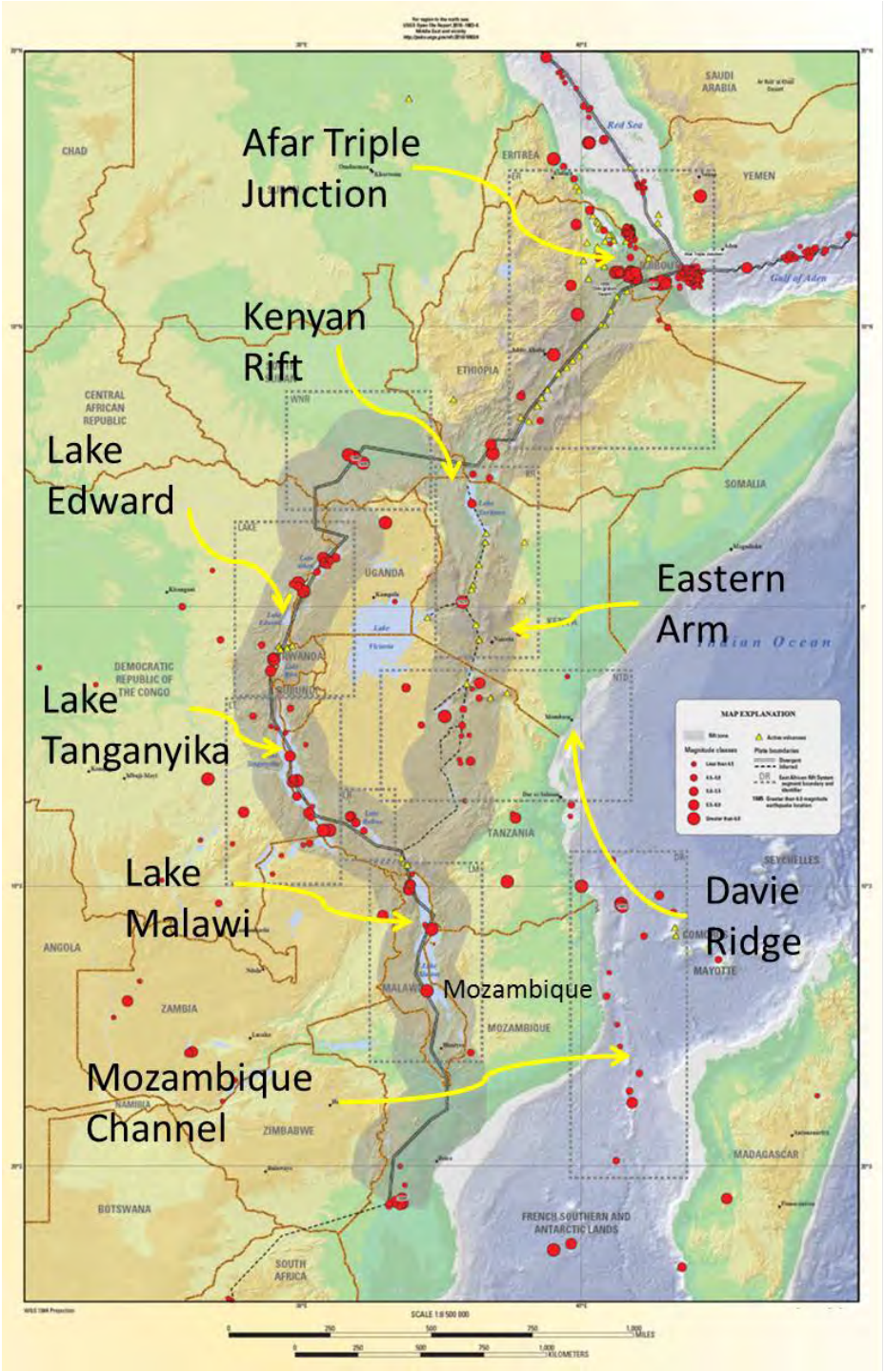

Figure 1.2: Seismic activity of the EAR from 1900 to 2013. Each red circle indicates an epicentre of an earthquake, with more reds circles (seismic activity) along the western arm of the EAR. The size of the circle indicates the earthquake intensity, with the smallest circle suggesting earthquakes with a magnitude of less than 4.5 (Hayes et al., 2014).

Between these arms, Jestin et al. (1994) suggest a minor plate, the Victorian Plate, and later Fernandes et al. (2004); Calais et al. (2006); Nocquet et al. (2006) and Stamps et al. (2008), suggested that two more plates (Rovuma and Lwandle) exist within the Nubia-Somalia region as illustrated in Figure 1.3. These suggestions were born from the variant velocity fields derived from Continuous GPS (CGPS) network and slip vector data in the respective areas. The seismic activity decreases as one moves south of the Malawi Rifts and the activity ceases as one approaches South Africa, which suggest incipient rifting (Fairhead and Henderson, 1977).

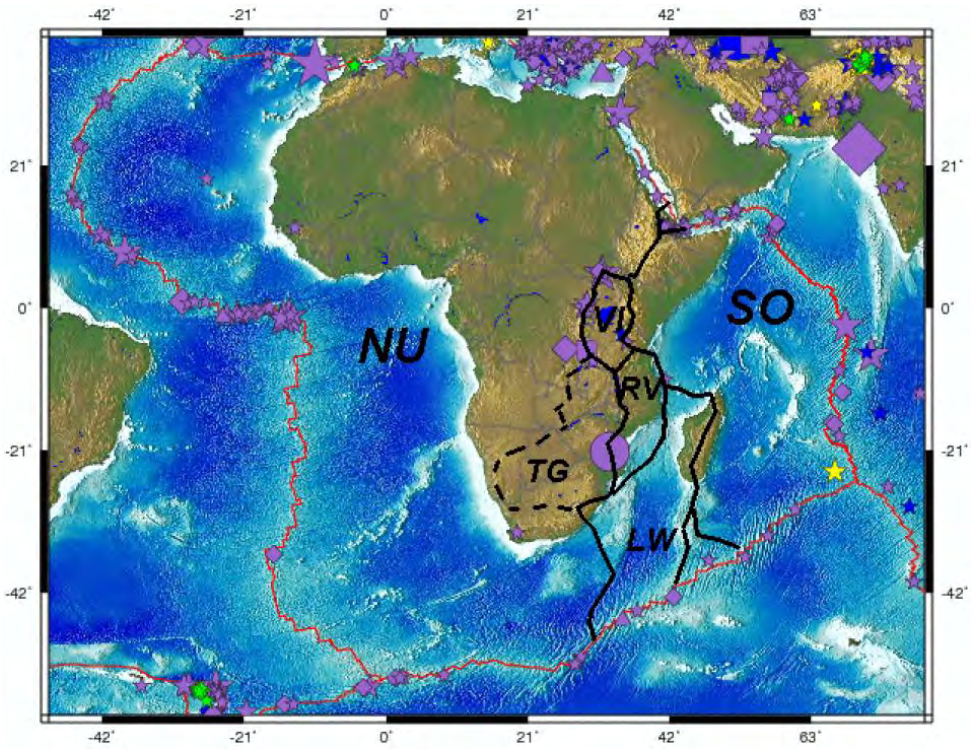

Figure 1.3: Depiction of the minor plates within Nubia-Somalia boundary dynamics. Nu-Nubia, So-Somalia, VI-Victorian, RV-Rovuma, LW-Lwandle, TG-Transgariep plate (Hartnady et al., 2007)

Seismic activity in South Africa is of fairly low intensity and is generally associated with mining particularly in and around the Gauteng area. The seismic activity that is evident in KwaZulu-Natal (KZN) and in the Southern Cape are, however, of a different nature.

In KZN the seismic activity is tectonic based, and Jestin et al. (1994) suggests that KZN may be the location of incipient rifting of the EAR. The

seismic activity in the Southern Cape is the result of the isostatic adjustment of the earth's crust that is associated with large scale erosion in the area (Hales and Gough, 1960). Hales and Gough (1960) observed negative isostatic anomalies in the area between the escarpment and the ocean (i.e in the Southern Cape). They suggest that these anomalies are as a result of the large scale erosion of the African escarpment in the Southern Cape and that the lithosphere is adjusted isostatically.

The portion of the Nubia-Somalia boundary as it traverses through and exits South Africa towards the SWIR has not been determined (Chu and Gordon, 1999; Bird, 2003; Hartnady et al., 2007; Pisani et al., 2009). This may be attributed to the slow rifting rate (6-7 mm/yr at the Afar junction) and the diffuse nature of the southern region of the boundary.

This study attempts to clarify the kinematics of the North East Region of South Africa (the region in which the proposed Nubia-Somalia boundary traverses South Africa), with the use of South African Trignet data along with global IGS stations.

1.3 Project Objectives and Hypothesis

The objective of this project is to establish whether the North East Region of South Africa has a different velocity field to the rest of South Africa. The velocity field will be established with the use of Trignet and IGS GPS data.

The working hypothesis for this project is that the angular velocity of North East Region of South Africa is different to the rest of South Africa.

1.4 Research Questions

To address the research objective, which is the establishment of the kinematics of the North East Region of South Afica, the derived research questions are divided into two sections. These sections are Time Series Management and Euler Vector Computation.

1.4.1 Time Series Management

Time Series Management addresses GPS time series factors that compromise the accuracy of the velocity that has been estimated from that time series. The research questions are:

1. How extensive should the data series be to determine a high quality Euler Vector for South Africa.
2. What aspects (e.g discontinuities, noise, outliers, etc.) of the time series should be considered to compute a reliable velocity?
3. How should station velocity be computed from a Trignet GPS time series.

1.4.2 Euler Vector Computation

Euler Vector Computation addresses factors that compromise the consistency of the computed Euler vector. The research questions are:

1. How is tectonic plate stability determined with the use of GPS data?
2. Should velocity uncertainty be taken into account when computing an Euler vector for South Africa?
3. How should different velocity fields (i.e South African, North East Region of South Africa, etc. velocity fields) be distinguished?

1.5 Methodology

The methodology addresses Time Series Analysis and Euler Vector Computation research questions.

1.5.1 Time Series Management

South African Plate kinematics were obtained with the use of a Trignet time series, and supplemented the series with data from the relevant GPS stations on the Nubian and Somalia plates. These supplementary stations were either IGS stations or they were owned by other organisations and/or agencies. Trignet data are hosted by National Geo-spatial Information (NGI), an agency of the Department of Rural Development and Land Reform.

The process of selecting IGS stations to comprise this project's network included an investigation of the minimal GPS time series period to determine an acceptable GPS velocity. This analysis also considered an acceptable period for a Trignet network, as different Trignet stations were introduced

at different times into the Trignet network.

Once the network and observation period was decided and the GPS data processed, aspects that are typical to a GPS time series that negatively affect velocity estimates were determined and managed such that a representative site velocity may be estimated. These factors were determined by investigating previous studies that addresses velocity uncertainty, plate kinematics and reference frame definitions.

Thereafter, a strategy (that incorporates the necessary GPS time series factors) to compute a homogeneous linear solution (position and velocity) for the adopted time series period was investigated. From this computation acceptable site velocities are estimated.

1.5.2 Euler Vector Computation

South Africa's kinematics in this study is described by an Euler Vector/s. The velocities that were computed after the GPS time series have been managed served as the input site velocities to determine a South African Euler Vector.

The factors that affect the Euler vector consistency are the accuracy of the input velocity estimates and the tectonic plate stability (the existence of plate boundaries, intra-plate deformation, tectonic lithospheric nature, etc. affects tectonic stability). The manner in which to assess South African plate tectonic stability was investigated. Certain factors were considered: The understanding of the nature of the African GPS status, the understanding of the South African GPS status, how these GPS status either enhance or compromise the integrity of the South African stability status, and how to establish plate stability from a GPS velocity field.

The determination of the consistency of the computed Euler vector was in turn determined by following methods that were practised by previous authors of plate motion models and plate tectonic research. The computed velocities and Euler vectors that were computed for this study were compared to relevant previous studies to validate their computation and consistency.

1.6 Outcomes of this project

The main outcome of this project is a South African velocity field constrained to the ITRF2008. The methodology (which incorporates the automation of computing GPS data within a Bernese Processing Software

environment) is foreseen to be replicated by NGI to produce a daily network of Trignet co-ordinates. The byproducts, such as the solved for tropospheric parameters of the computed co-ordinates could facilitate South African weather research (based on integrated water vapour content) and climate once longer term time series are available.

The behaviour of stations within the processing period will also become apparent with this study, and this information can be used for future planning and assess behaviour patterns of Trignet stations under certain geophysical and atmospheric conditions.

With respect to the research objectives, the Nubia-Somalia boundary will be less ambiguous as this project aims to establish the kinematics of the North East Region of South Africa. This region has been proposed by Chu and Gordon (1999), Bird (2003), Hartnady et al. (2007), Pisani et al. (2009), etc. as being segregated from the rest of South Africa by the Nubia-Somali boundary.

For the derivation of global kinematics with the use of GPS, a more informed selection of southern African stations will be possible. Furthermore, the IGS relies on stations that are on the stable parts of plates when computing the ITRF, this study could aid this process.

For the South African Trignet and AFREF, the understanding of the Nubia-Somalia boundary is essential for a long term stable reference frame. Unlike other continental plates, GPS stations are few and far in between and the selection of stations that have high noise levels have a profound negative effect on the diminished network. On the other hand, excluding stations that are not in the deformation zone, but deeming them as unstable stations based on assumptions may also negatively affect the computations because of the small number of stations available (longer baselines have to be computed then, which are susceptible to less successful GPS ambiguity resolutions).

1.7 Dissertation Structure

The dissertation is split into the following 5 sections:

Chapter 2 contains a literature review that relates to the computation of an Euler vector. The aspects addressed are time series management (noise and discontinuity detection), Euler vector Computation and Plate Rigidity.

Chapter 3 contains a description of the aspects considered for IGS and Trignet station selection. Also, seismic events between 2003 and 2013 is provided.

In Chapter 4 a methodology for noise detection, discontinuity detection, outlier detection, velocity field computation and Euler vector computation is presented.

The results of the detection algorithms as applied to this project's GPS processing output are provided in Chapter 5, along with an assessment of the velocity field and computed Euler vector/s.

A discussion of the implications of the dissertation findings and recommendations are presented within Chapter 6.

Chapter 2

Theoretical Concepts

2.1 Plate Kinematics

In earlier years, geological data formed the corner stone in formulating a global kinematic model. Global kinematics have been described since the 1970's, with the first model (i.e. RM2) described by Minster and Jordan (1978) as quoted by Altamimi et al. (2012). This model, and later models (such as the NUVEL-1A and "ITRF2008 plate motion model" among others), whether geodetic or geological incorporates the Euler inversion model that is described by Minster et al. (1974).

Global Euler inversion models such as RM2 and NUVEL-1A comprise multiple Euler vectors that describes each tectonic plate in the respective model.

An Euler vector incorporates an angular velocity that is referenced to a pole of rotation.

If the angular velocity is known, then the velocity at a position $\boldsymbol{r}$ may be represented with the equation:

$$\boldsymbol{V_r} = \boldsymbol{\Omega} \times \boldsymbol{r} \tag{2.1}$$

with $\boldsymbol{V_r}$ representing the instantaneous velocity at position $\boldsymbol{r}$ and $\boldsymbol{\Omega}$ the plate Euler vector (DeMets et al., 1990).

The inversion model, in which the Euler vector is solved for, is derived by using instantaneous velocities at positions on the relevant tectonic plate/s. These instantaneous velocities are generally observed by geological techniques (such as slip vectors and seafloor spreading) and by space geodetic techniques (such as GNSS, VLBI etc.). Hence, plate kinematics may be represented by geological only models, by space geodetic only models or by

a combination of techniques seated in these two disciplines.

2.1.1 Determining an Euler Vector

Figure 2.1 graphically represents the relationship between the instantaneous velocity $\boldsymbol{V_r}$ at position $\boldsymbol{r}$ and $\boldsymbol{\Omega}$ the plate angular velocity. This relationship is expressed in equation 2.1.

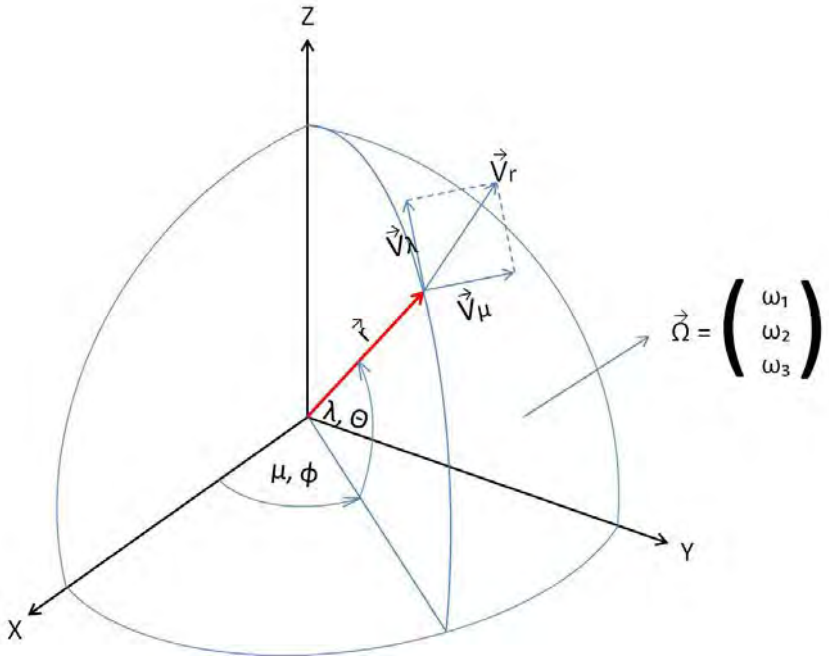

Figure 2.1: Geographical representation of an instantaneous velocity vector at a position $\boldsymbol{r}$ on a tectonic plate with Euler vector $\boldsymbol{\Omega}$.

In Figure 2.1, vector $\boldsymbol{r}$ may be spherically expressed with the components (a, λ, μ), with spherical radius a, latitude λ and longitude μ. Similarly, $\boldsymbol{\Omega}$'s vector components (ω_1, ω_2, ω_3) may be expressed in terms $\boldsymbol{\omega}$, Θ and Φ (see Equation 2.2), with ω the rate of rotation of the respective plate, and Θ and Φ are the latitude and longitudinal position of the pole of rotation of that plate (Minster et al., 1974).

The cartesian components of $\boldsymbol{r}$ and $\boldsymbol{\Omega}$ may be described as :

$$r = \left\{ \begin{array}{l} acos(\lambda)cos(\mu) \\ acos(\lambda)sin(\mu) \\ asin(\lambda) \end{array} \right\} = \left\{ \begin{array}{l} X \\ Y \\ Z \end{array} \right\} \quad \Omega = \left\{ \begin{array}{l} \omega cos(\Theta)cos(\Phi) \\ \omega cos(\Theta)sin(\Phi) \\ \omega sin(\Theta) \end{array} \right\} = \left\{ \begin{array}{l} \omega_1 \\ \omega_2 \\ \omega_3 \end{array} \right\}. \tag{2.2}$$

Introducing the least squares principle:

$$V = A\boldsymbol{X} - \boldsymbol{l}, \tag{2.3}$$

with V, A, $\boldsymbol{X}$ and $\boldsymbol{l}$ representing the residuals, the design matrix, the solution vector and the observation vector respectively.

Introducing the cartesian components into the least squares solution, Equation 2.3 may be interpreted as:

$$\boldsymbol{V} = \begin{bmatrix} 0 & Z & -Y \\ -Z & 0 & X \\ Y & -X & 0 \end{bmatrix} \begin{bmatrix} \omega_1 \\ \omega_2 \\ \omega_3 \end{bmatrix} \quad - \quad \begin{bmatrix} V_x \\ V_y \\ V_z \end{bmatrix}. \tag{2.4}$$

The solution vector is :

$$\boldsymbol{\Omega} = (A^T P A)^{-1} A^T P l, \tag{2.5}$$

with P the weight matrix.

2.1.2 Plate Rigidity

An important estimation in the study of plate kinematics is plate rigidity, as lithospheric blocks falsely modelled as rigid blocks biases the velocity computation (Nocquet and Calais, 2004). Rigidity refers to a tectonic plate's aptness to maintain physical form. The factors that deforms a lithospheric plate are temperature and pressure, and the lithospheric thickness and rock type determines how the plate behaves under such conditions (Buck, 1997). Brittle rocks tend to "snap", whereas ductile rocks tend to bend and fold under intense pressure and temperature (Buck, 1997).

Mathematically, rigidity of a lithospheric block is determined by doing a χ^2 test per degree of freedom. Degrees of freedom in this case are the number of GPS sensors used to estimate the Euler vector of a particular block, less the 3 Euler vector parameters solved for per plate. The three Euler vector parameters are angular velocity, latitude and longitude as described in section 2.1.1. A χ^2 per degree of freedom of unity suggests a rigid lithospheric block (Horner-Johnson et al., 2007). Rigidity is an important characteristic of a block for the a posteriori plate closure condition to be implemented as it (i.e. plate closure) assumes plate rigidity.

Plate closure refers to the sum of the relative angular velocities of a series of plates that completes a circuit. The condition for plate closure is that this sum equates to zero (within expected tolerance). This sum is a measure of plate closure. Also, the relative velocity of a plate may be computed within a circuit. This computed relative velocity may be compared to relevant observed data (e.g slip vector data), and the agreement between the computed and observed kinematic values may also be a measure of plate closure (Horner-Johnson et al., 2007).

In the ideal case the condition of plate closure would be met. This is not the case when we apply real data to determine plate kinematics, and the plate closure condition is not met. Depending on the magnitude of the misclosure and the associated uncertainty, the misclosure may be related to either noise in the data, to the existence of unknown plates or deforming plates within the kinematic system (Horner-Johnson et al., 2007). Any significant tectonic activity (e.g earthquakes of magnitude in excess of 4.5 on the Richter scale), isostatic adjustment or aseismic activity may classify a plate as non rigid (Nocquet and Calais, 2004). Aseismic activity is tectonic activity in the absence of any notable earthquake; however surface displacement is evident (Nocquet and Calais, 2004)

Establishing Nubian Plate Rigidity

Stamps et al. (2008) follow the procedure set forth by Nocquet et al. (2006) to establish plate velocity estimates and rigidity. Both studies compute a χ^2 value of 1.5 using 14 and 16 estimated velocities respectively, and allude to a rigid Nubian plate based on this χ^2 value.

The investigation by Sella et al. (2002) included an assessment of the North American Plate and reports that when computing the entire North American network of 84 GPS stations , a χ^2 per degree of freedom of 1.63 is calculated. However, when he excludes the 20 sites that are prone to glacial isostatic adjustment, then a χ^2 value of 1.05 is calculated. Even though the North American Plate is geographically unrelated to this study, Sella et al. (2002) demonstrates that the influence of isostatic adjustment on plate rigidity is quite significant. Sella et al. (2002) also demonstrates the importance of site selection and the understanding of the nature of the plate to determine its rigidity.

However, the number of Nubian sensor stations are limited and excluding stations from the already diminished network might weaken the solution. Hence, the value of 1.5 may suggest a large element of noise within the Nubian data, a part of the Nubian Plate being non rigid, a part of the plate being subject to isostatic adjustment and\or the existence of minor plates

within the Nubian Plate.

The study by Malservisi et al. (2010), "How Rigid is a Rigid Plate" investigates the rigidity of South Africa from a Trignet data set. It concludes that South Africa is a rigid region with the χ^2 value of 1.13. Within the study, each baseline's ellipsoidal distance is computed, and the rate of change of the distance is divided by its initial geodesic distance Malservisi et al. (2013). The study also computes baseline uncertainties of the obtained time series. The uncertainties were obtained following the procedure by Hackl et al. (2011), who investigated the Allan variance of the rate (AVR) method using a Trignet data series. The areas with the highest RMS (uncertainty) baselines are in the north east of the country and in the Western Cape Province as depicted in Figure 2.2. It is understood that the north eastern part of South Africa and the KwaZulu-Natal Province may not form part of the Nubian Plate and may, instead, form part of the minor Rovuma Plate, or the Somalia Plate.

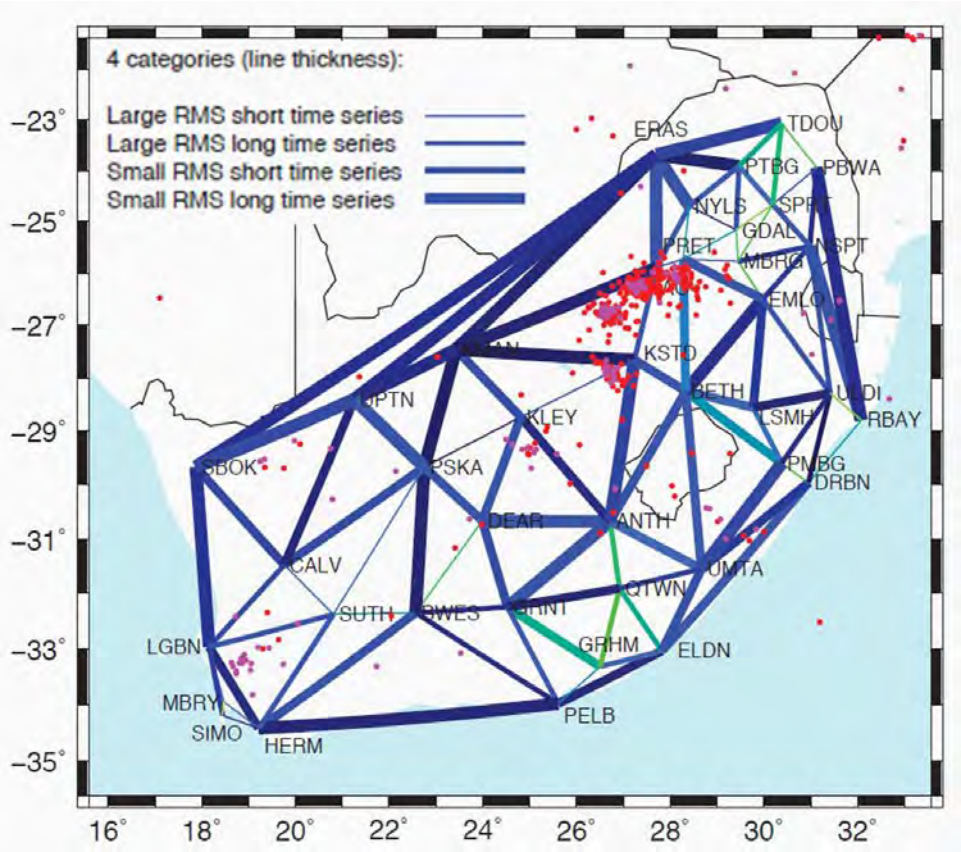

Figure 2.2: Baselines computed by Malservisi et al. (2010), using a 5 year Trignet data series. The dark bold lines are baselines with low RMS, and the light thin lines are high RMS baselines. These baselines are further distinguished with short and long data spans as shown in the table within the figure.

The observed magnitude of the Western Cape seismic activity is less than the established magnitude of 4.5 suggests that there exists no plate boundary and there has been no evidence of aseismic activity. Rather, the seismic activity is related to isostatic adjustment as the result of erosion in the Western Cape as described in the Fairhead and Henderson (1977) study, which made use of seismic data only.

2.2 Estimating an Euler Vector with the use of GPS observations

Three factors needs to be considered when using GPS data to resolve an Euler vector. These factors are outliers, noise within the data series and discontinuities. Discussions on GPS noise and discontinuities are presented.

2.2.1 Noise within GPS time series

Velocity is generally derived by applying linear regression to a GPS data series. Linear regression is a least squares adjustment, in which the day to day error is assumed to be uncorrelated. The noise associated with this assumption is white noise. The derived uncertainty from the amplitude of white noise only within a GPS time series is underestimated or overly confident (Williams, 2003*b*).

Incorporating time correlated noise along with white noise gives a more realistic GPS derived velocity uncertainty (Zhang et al., 1997; Mao et al., 1999; Williams, 2003*b*, 2004). The time correlated noise types that are referred to are random walk noise and flicker noise. Flicker noise is related to Earth's Polar motion, uncertainty in atomic clock time measurements, sunspot variability, etc.; and random walk noise is associated with the establishment of GPS beacons (Williams, 2004). Of the noise types (i.e white, random walk and flicker), the amplitude of a white plus flicker noise model best describes GPS velocity uncertainty (Zhang et al., 1997; Mao et al., 1999; Williams, 2004). This relationship between GPS data series time length and the velocity uncertainty related to a white plus flicker noise model is highlighted in Figure 2.3.

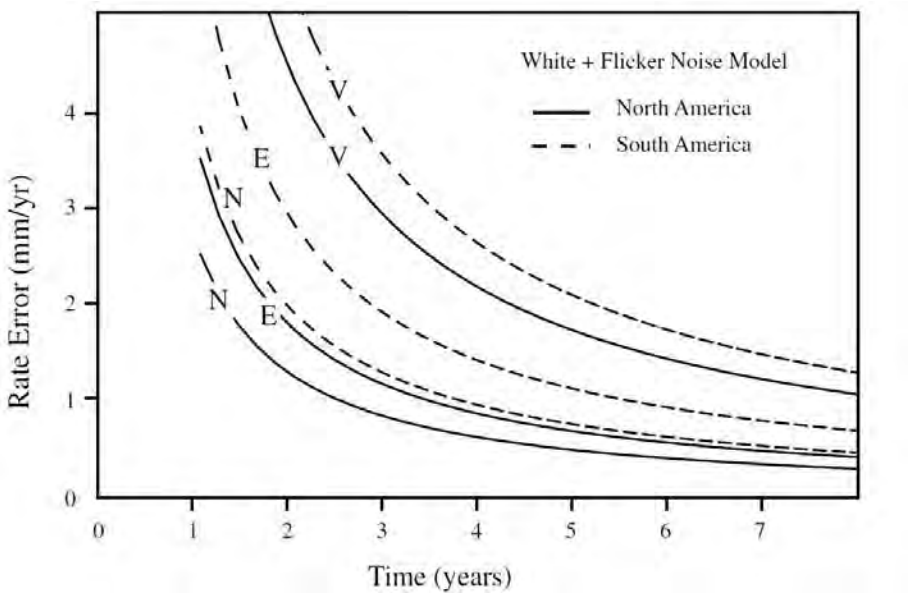

Figure 2.3: Effect of White + Flicker noise on GPS data series. Noise influences decreases substantially with increase in the time length of the GPS data series. The solid line represents a North American GPS station, whereas the dashed lines represent a single station in the South American network. The symmetry is quite evident (Sella et al., 2002).

Also, spatial correlated noise should be considered. This may be split into regional and global networks. For regional networks, the baselines are short and the spatial correlated noise is reduced with a prolonged data series. For global analysis, the baselines are much longer, and hence sensor sites are deemed to be uncorrelated.

2.2.2 Discontinuities in GPS time series

Offsets or discontinuities are almost inevitable in a GPS time series (Williams, 2003*a*). These offsets may be as a result of natural events such as earthquakes or may be humanly induced.

Unaccounted for discontinuities in a GPS time series biases both the computed velocity and its uncertainty (Santamaría-Gómez et al., 2011). This is because the linearisation of the time series that is representative of the velocity is sensitive to time series breaks.

Discontinuities in GPS data series may be as a result of a change in GPS model, processing strategy, reference frame (Nikolaidis, 2002), GPS equip-

ment or a change in the environment (e.g tree pruning) (Dong et al., 2002). Williams (2003*a*) also emphasises that stations with discontinuities may introduce discontinuities at other station time series in the network.

The velocity uncertainty is increased with the increase in discontinuities. The worst case scenario is if the discontinuities are evenly spaced, in which the uncertainty is amplified by a factor equivalent to the number of resultant segments (Williams, 2003*a*).

Discontinuity Algorithm

The algorithm presented here refers to the work by Roggero (2012). The algorithm incorporates the following system of equations which incorporates a state vector $\boldsymbol{x}$, (which is a position and velocity) and vector of observations, $\boldsymbol{y}$ developed through a series of epochs t $(t = 1, ..., n)$,

$$\begin{aligned} \boldsymbol{x}_{t+1} &= T_{t+1}\boldsymbol{x}_1 + B_{t+1}\boldsymbol{b}_t + V_{t+1}, \\ \boldsymbol{y}_{t+1} &= H_{t+1}\boldsymbol{x}_{t+1} + C_{t+1}\boldsymbol{b}_{t+1} + V_{t+1} + \varepsilon_{t+1}, \\ \boldsymbol{b}_{t+1} &= \boldsymbol{b}_t. \end{aligned} \tag{2.6}$$

In Equation 2.6, V and ε refers to system noise and observational error respectively (Roggero, 2008). The dynamic matrix is represented by T, and H is the design matrix of coefficients linking the state vector $\boldsymbol{x}$ and observation vector $\boldsymbol{y}$. Variables B and C are matrices of discontinuities for $\boldsymbol{x}$ and $\boldsymbol{y}$ respectively. Vector $\boldsymbol{b}$ is a bias and is constant.

With respect to GPS, for a constant velocity model

$$T = \begin{bmatrix} 1 & \delta t \\ & 1 \end{bmatrix} \tag{2.7}$$

and Equation 2.6 may then be interpreted as

$$\begin{aligned} p_{t+1} &= p_t + \boldsymbol{\nu}_t \\ \boldsymbol{\nu}_{t+1} &= \boldsymbol{\nu}_t \ , \end{aligned} \tag{2.8}$$

with p and $\boldsymbol{\nu}$ position and velocity respectively. For Equation 2.8 $B = C$ and are composed of 1's and 0's with each row referring to a an epoch of observation and each column to a discontinuity. The relationship of the discontinuity matrix C and the time series is graphically illustrated in Figure 2.4.

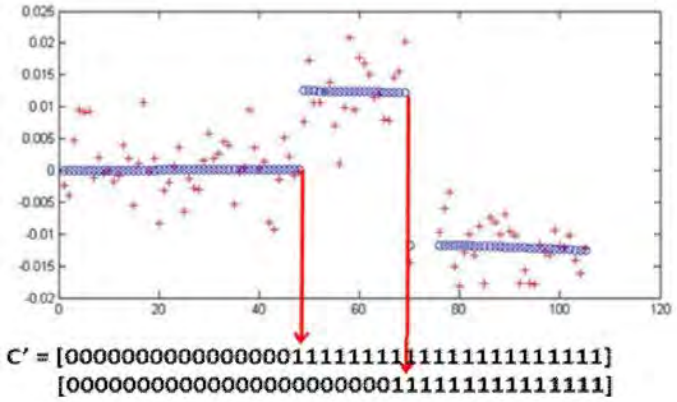

Figure 2.4: Illustration of discontinuities and how these discontinuities may be interpreted in the C matrix. The red crosses refers to the observations y as in Equation 2.6, with the blue circles referring to the state vector x (Roggero, 2012).

The detection algorithm is structured such that the null hypothesis H_0 assumes no discontinuities, and the alternative hypothesis H_A assumes discontinuities:

$$H_0 : \begin{cases} \triangle(y) = Hx \\ \sum(y) = Q_y \end{cases} \quad H_A : \begin{cases} \triangle(y) = Hx + Cb \\ \sum(y) = Q_y \end{cases} . \tag{2.9}$$

From this equation a variance of unit weight σ_0 and σ_A may be obtained for the null and alternative hypothesis respectively.

Discontinuities may now be tested using the ratio $\frac{\sigma_A^2}{\sigma_0^2}$ and the chi squared distribution (χ^2) with confidence level $\propto$ such that:

$$\frac{\chi^2_{(\frac{\propto}{2})}}{n-r} < \frac{\sigma_A^2}{\sigma_0^2} < \frac{\chi^2_{(1-\frac{\propto}{2})}}{n-r} . \tag{2.10}$$

The symbols n and r refer to the number of observations and unknowns respectively. If the ratio exceeds these limits, then the alternative hypothesis is true and the epoch of observation referring to the relative row in matrix C is indeed an epoch of discontinuity.

Chapter 3

Data

An important step in determining a velocity field is station selection (Altamimi et al., 2012). The integrity of a plates kinematic computation ultimately is reliant on the quality of the GPS sensor station network. For this reason an effort is made to select the best possible stations using the available information.

The investigation of suitable stations may be divided into two sections i.e. IGS and Trignet stations. This division is because the IGS and the Trignet serve two very different purposes with respect to datums, and hence their beacon construction and management may be different. The IGS is concerned with a homogeneous global datum, along with the associated products such as EOP's and satellite orbits. Trignet provides a real time positioning service and provides users with daily GPS observations made available in RINEX formatted files for static processing. Trignet is not concerned with a homogeneous long term solution, although the Directorate of National Geospatial Information (NGI) provides a Trignet realization of the ITRF every two years that is based on two weeks of relevant GPS data (latest realization: Trignet 2014).

3.1 Station Selection Factors

When selecting stations for this project then the same factors are considered for both IGS and Trignet stations. These factors are GPS Beacon Construction, Extensiveness of Data Period, Number of Antenna Changes and Proximity to Tectonic Boundaries.

3.1.1 GPS Beacon Construction

The optimal station is one that is tied to bedrock (Combrinck and Chin, 2001). This limits the movement of the station with respect to the tectonic plate, which minimises the noise element and hence minimises the velocity uncertainty (Johnson and Agnew, 1995). Not all stations are tied to bedrock, and this bedrock factor is compromised. Stations that are constructed on buildings that are tied to bedrock may suffice. If there is a lack of stations constructed on bedrock, then stations with solid foundations may be suitable. Stations that are constructed on unstable ground should be avoided.

3.1.2 Extensive Logging Period

Stations with extensive data that covers the full 10 year period for this project should be selected. However, this is not possible for all stations. The selected stations should then have at least 2.5 - 3 years of discontinuity free data to accommodate for seasonal affects (Blewitt, 2002). Seasonal effects are largely due to atmospheric pressure and hydrology (Williams, 2003*b*). The stations with lesser data may not be used to compute a velocity, but may aid in aligning the network to the daily ITRF realization or to improve the network geometry for the period of data availability of that station.

Computation of velocity uncertainty is also adversely affected by data spans shorter than 2.5 years (Santamaría-Gómez et al., 2011). Short time spans yield underestimated velocity uncertainties as the time correlated noise is masked in the determination of the trend of the data series (Williams, 2004; Santamaría-Gómez et al., 2011).

3.1.3 Network Geometry

The IGS stations should be globally distributed such that the network can be aligned to the ITRF. At least 30 IGS global stations should be included in the network to avoid the network effect (i.e. a shift between the computed network and the ITRF) (communicated by Zuheir Altamimi at the CATREF course, 2012, Paris). Trignet stations are generally well distributed with baselines less than 300 km. Also, a well distributed network will limit the length of baselines between the network stations, easing the cycle slip and integer ambiguity resolution.

3.1.4 Antenna Changes

The need for station maintenance is unavoidable. Station maintenance may include the change of antenna. A change in station position may be observed as a result, with a shift in either the height component, the North component, the East component or a combination of the three components. This change in position may be evident as a discontinuity in the GPS computed time series of the respective station. Unaccounted for discontinuities adversely effect the accuracy of the computed velocity at that station, and ultimately the reliability of the computed Euler vector (Williams, 2004).

The time gap between discontinuities is also essential (assuming there are sufficient time series observation points within the time gap). Time gaps of lengths less than 2.5 years weaken the solution as it succumbs to seasonal effects. This point is emphasised in the Rebischung et al. (2011) study, in which a minimum threshold period of 3 years between station discontinuities is applied in establishing the IGS08.

3.1.5 Proximity to Plate Boundaries

Stations with minimum noise levels, that has a continuous velocity with zero break should be selected to form part of the network for this project (Rebischung et al., 2011). Hence stations that are close to tectonic boundaries, which renders them to abrupt change in velocities, should be avoided. Tectonic boundaries are associated with earthquakes and volcanoes, which destabilises that part of the tectonic plate. In the Bird (2003) study a tectonic boundary buffer zone of 100 km is proposed when computing global kinematics.

3.2 IGS selected stations

To summarise the station selection results, a network of 104 global sensor stations was selected. These 104 global stations are composed of 51 IGS stations, and 63 Trignet stations with 10 stations being common to both the IGS and Trignet. The common stations are: HARB, RBAY, SUTH, ULDI, DEAR, ULDI, UMTA, MFKG, SBOK and HNUS.

Selected IGS stations for this project had to form part of the IGS core network. Thereafter, the analysis of the IGS station logs were used to select the optimal stations from the IGS core network, such that an optimal network geometry is maintained too.

3.2.1 Station Distribution

An initial step of selecting a subset of IGS core stations for this project. Africa has a sparse GPS network, hence additional IGS stations were added to the selected IGS core stations to optimise the network geometry as depicted in Figure 3.1. These IGS stations are: ANTC, RABT, SEY1, OHI1, ADIS and MAL2; and for the stations that are common to the IGS and Trignet network: TDOU, HRAO, DEAR and SBOK were added.

The selected IGS stations serve to satisfy two purposes i.e. for the daily alignment of the network to the ITRF 2008 (using the IGS daily realization) and to constrain the selected IGS velocities to obtain a reference frame to compute velocities for stations in the network.

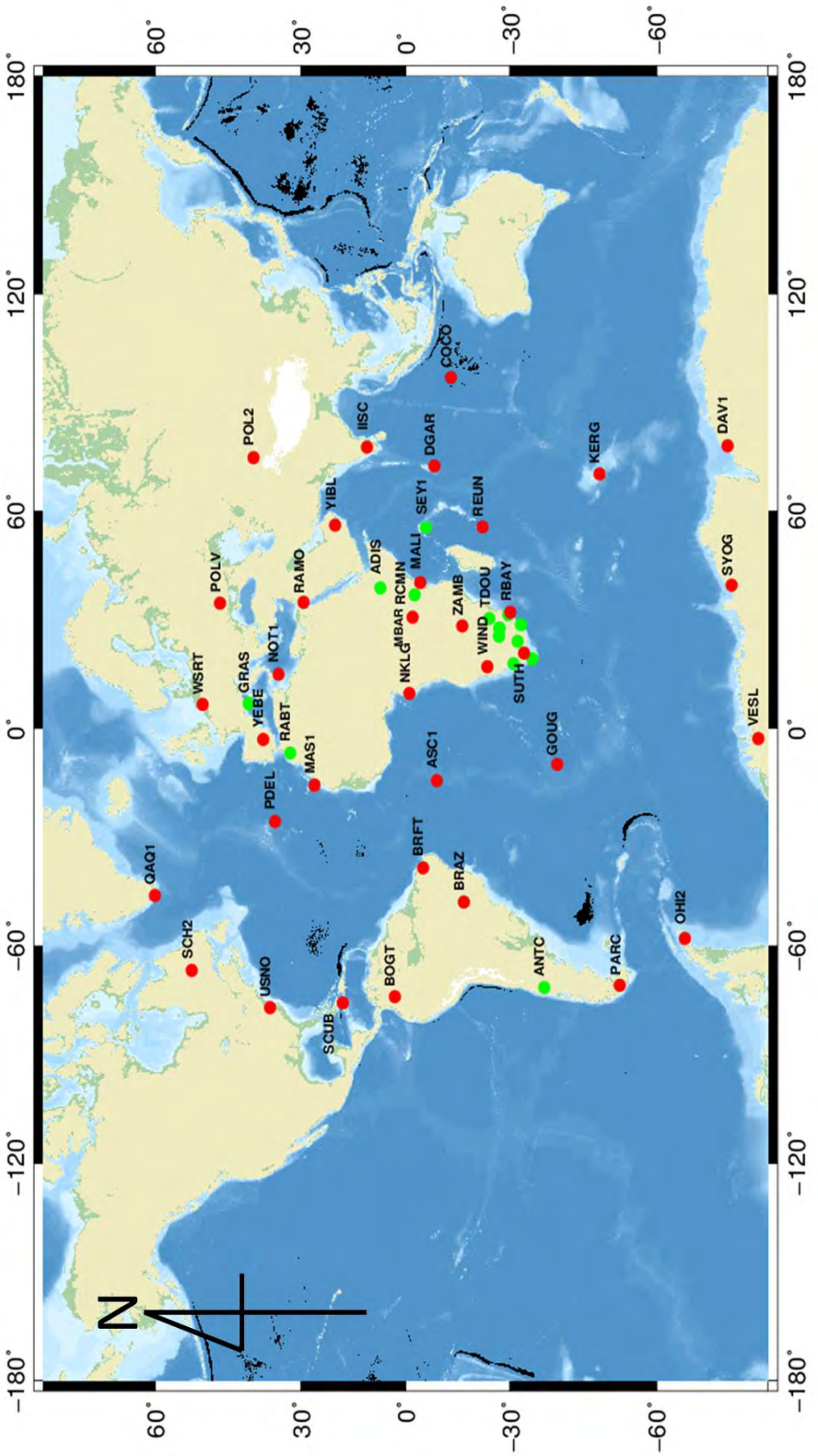

Figure 3.1: IGS stations that were selected for this project which serves to both align the network to the ITRF and to constrain the South African velocity field. The red IGS stations forms part of the IGS Core network and the green IGS stations compliments this subset network. The South African IGS stations are labelled in Figure 3.2.

The optimal IGS station (assuming that its stable with acceptable noise quality and remains true to its reference position as determined by the ITRF linear model (Rebischung et al., 2011)) is a station that has a daily IGS realization (IGS08 daily realizations in this case) and an IGS velocity Ṫhis is not the case for all IGS stations, and although many stations have IGS daily realizations, they do not necessarily have IGS published velocities. Ten IGS listed station in the network do not have published IGS velocities, 7 of which are listed as Trignet stations. The Trignet stations are DEAR, MFKG, SBOK, HNUS, ULDI, UMTA and TDOU; with MAL2, RCMN, and ADIS being the remaining IGS stations that do not have published velocities.

These IGS stations with absent velocities are used for the daily alignment to ITRF if the IGS has computed daily co-ordinates for them. If no co-ordinates are computed for them by the IGS, then they serve to densify the network, improve the network geometry and decrease the average baseline lengths.

The Trignet stations that are listed as IGS stations but do not have published IGS velocities have less than 400 computed IGS daily realizations for each station (within the time period considered for this project), and this may be a contributing factor for these stations not having an IGS velocity.

Station MALI no longer exists, but the station's archived data is extensive and realistic velocity estimates may be computed for MALI. Hence station MALI is included in the network.

3.2.2 IGS GPS Beacon Construction

Table 3.1 summarises the station site information, the station tectonic plate and the number of antenna changes within the period 2003-2013 for each station. Stations tied to bedrock minimise random walk noise and are recommended (Williams, 2004).

Table 3.1: Summary of the selected IGS station information

IGS Stations	Date Installed	Site Information	Tectonic Plate	No. of Antenna Changes Btwn. 2003-2013
ADIS	30-Jun-07	Bedrock	African	1
ANTC	01-Jan-02	Bedrock	S.American	0
DAV1	18-Nov-93	Bedrock	Antarctica	2
GRAS	10-Feb-95	Bedrock	Eurasian	3
HRAO	05-Sep-96	Bedrock	African	6
IISC	20-Jan-95	Bedrock	Indian	1
OHI2	14-Feb-02	Bedrock	Antarctican	1
POL2	10-May-95	Bedrock	Eurasian	1
QAQ1	15-Oct-01	Bedrock	N.American	3
RAMO	10-Jun-98	Bedrock	African	1
REUN	16-Dec-98	Bedrock	African	2
SCH2	29-Jun-97	Bedrock	N.American	2
SEY1	15-May-95	Bedrock	African	4
SUTH	05-Dec-97	Bedrock	African	1
SYOG	15-Mar-95	Bedrock	Antarctica	0
VESL	18-Dec-97	Bedrock	Antarctica	0
WSRT	23-May-97	Bedrock	Eurasian	0
PDEL	17-May-01	Roof Top (Bedrock)	African	1
RABT	07-May-00	Roof Top (Bedrock)	African	0
SCUB	31-May-95	Roof Top (Bedrock)	N.American	0
YEBE	30-Nov-92	Roof Top (Bedrock)	Eurasian	0
ASC1	20-Apr-96	Roof Top	African	0
BRAZ	03-Mar-95	Roof Top	S.American	1
BRFT	06-Sep-05	Roof Top	S.American	0
DGAR	11-Apr-96	Roof Top		1
PARC	01-Jan-99	Roof Top	S.America	1
POLV	01-Mar-00	Roof Top	Eurasian	0
ULDI	01-Jul-00	Roof Top	African	0
USNO	24-Mar-97	Roof Top	N.American	0
WIND	24-Jun-03	Roof Top	African	1
ZAMB	28-Mar-02	Roof Top	African	0
DEAR	08-Jul-97	Rock	African	0
HNUS	29-Feb-00	Rock	African	2
RBAY	10-May-00	Concrete pier	African	1
COCO	30-Jul-92	Sand	Australian	1
MBAR	20-Mar-03	Clay	African	0
MFKG	08-Sep-01	Gravel Sand	African	0
TDOU	23-Feb-01	Gravel sand	African	0

Table 3.1 continued.

IGS Stations	Date Installed	Site Information	Tectonic Plate	No. of Antenna Changes Btwn. 2003-2013
RCMN	13-Mar-07	Gravel	African	0
UMTA	23-Feb-01	Clay	African	0
GOUG	08-Jan-98	N/A	African	0
KERG	01-Nov-94	N/A	Antarctica	2
MAL2	01-Jul-08	N/A	African	1
MALI	12-Nov-95	N/A	African	0
MAS1	11-Apr-94	N/A	African	2
NKLG	10-Feb-00	N/A	African	1
NOT1	15-Sep-00	N/A	Eurasian	0
SBOK	08-Feb-00	N/A	African	0
YIBL	11-Jul-03	N/A	Arabian	0
BOGT	04-Nov-94	N/A	S.American	6
HARB	26-May-97	N/A	African	2

Of the 51 IGS selected stations, 17 were tied to bedrock directly. A further 4 stations were constructed on buildings that were built on bedrock minimising random walk noise.

Eleven stations were constructed on roof tops, vulnerable to building and ground motion which may increase noise in the data.

Six stations (of which 4 are South African stations) were not tied to bedrock, instead using a concrete foundation that is settled in the available ground. Depending on the nature of the area and the activity (such as hydrological pumping (Malservisi et al., 2013)), these stations may be highly susceptible to noise.

Eleven of the station log files do not stipulate any geological or site information (or it is not clearly communicated in these files) and their susceptibility to random walk noise is unknown at this stage of the project. These stations are noted with N/A under site information in Table 3.1.

3.2.3 Antenna changes

Antenna changes may introduce unnecessary discontinuities, which stands to bias station velocity computation. For this reason, stations are selected

with a minimum number of antenna changes. The average number of IGS antenna changes is 1 per every 9 years (Williams, 2004). This project adheres to this statistic, in which on average 1 antenna change occurs for the 10 year period between 2003-2013. Table 3.1 summarises antenna changes for the IGS stations. The stations with the most antenna changes are HRAO and BOGT with 6 each. Twenty-three stations had zero antenna changes.

3.2.4 Plate Boundary Proximity

Altamimi et al. (2011) and Altamimi et al. (2007) incorporates IGS GPS stations situated within deformation zones for the alignment of the IGS daily network and for computing a long term datum.

In light of this practise, stations in deformation zones are included in the alignment to the ITRF and combination solution of this project (provided no station velocity discontinuity exist). The number of stations that are in deformation zones (excluding southern Africa as it is the research area) as prescribed by Bird (2003) are 13.

3.3 Trignet Station Selection

The manner in which Trignet stations are analysed is different to that of the IGS analysis. This is because Trignet does not have available station logs. Hence an analysis of geological information, site information and station events are not available. However, record is kept of receiver and antenna type that are in place in a station information file.

Trignet stations are not used to align the network and, hence, all available Trignet stations were selected for processing (as depicted in Figure 3.2) and an aposteriori analysis is presented in sections 5 and 5.3.

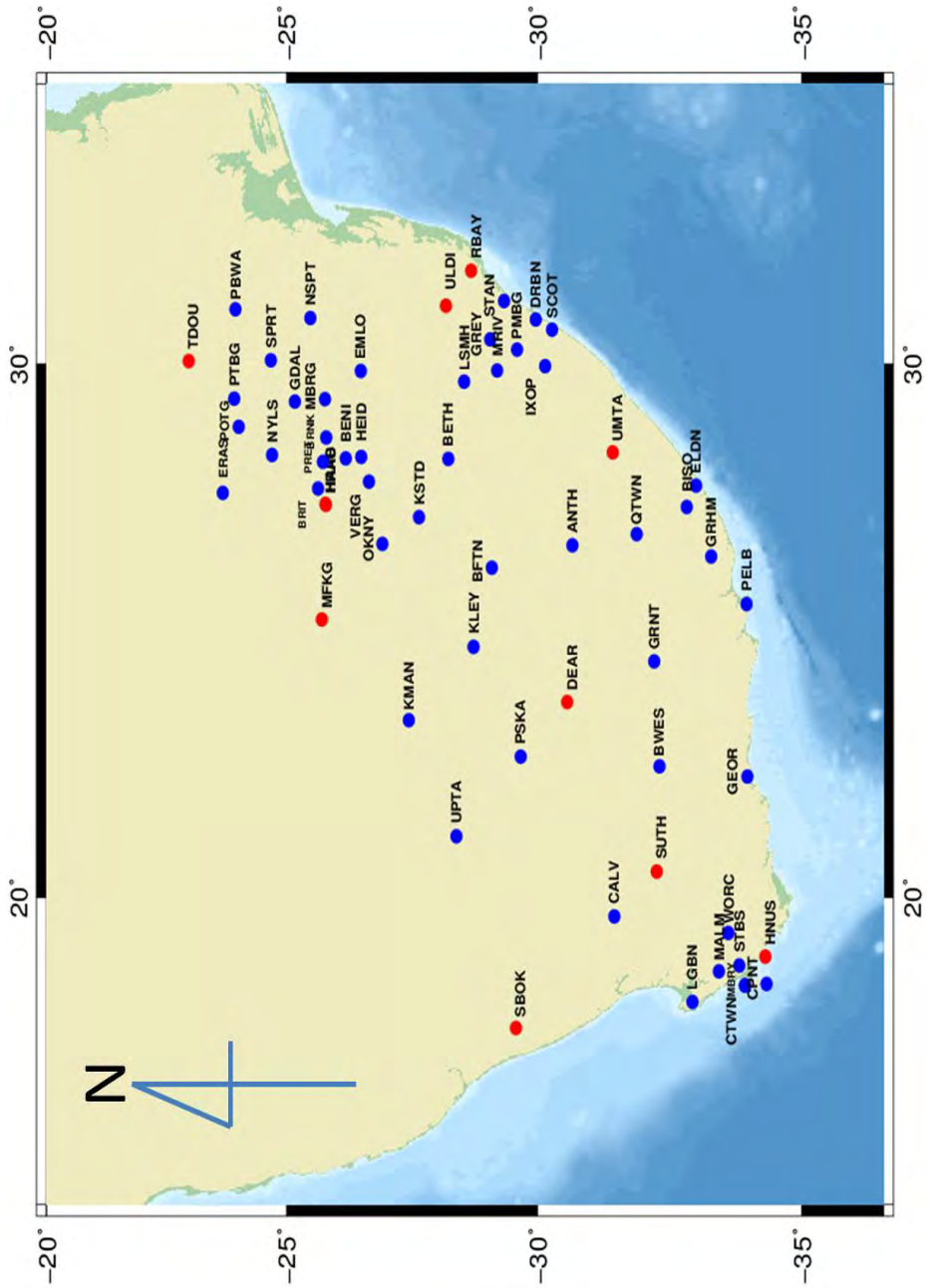

Figure 3.2: South African Trignet stations that were selected for this project. The red dots are IGS stations and the blue are Trignet stations.

However, there are station issues that had to be accounted for before proceeding with the processing of the GPS network. These issues relates to stations TDOU, SUTH, GEOR and to the years 2003-2005.

The station information provided for station TDOU by NGI is different to that of the IGS. NGI accounts for an antenna change on 2008-02-14, whereas the IGS does not. The station information as provided by NGI was adopted in this instance.

Station SUTH and SUT1 share the same antenna, with independent receivers. Station name SUTH was adopted despite some of the GPS data decoded by a different receiver.Station GEOR was physically relocated on 4 occasions, and hence is removed from the analysis.

In years 2003, 2004 and 2005 only 14 hours of data were observed at a large number of Trignet stations. To include Trignet stations between 2003 and 2005, the 20 hour threshold (as suggested by Sella et al. (2002)) was eased to a 12 hour threshold.

One of the main reasons for easing the threshold between 2003 and 2005 is that if the remaining 7 years were only accounted for and discontinuities are introduced, then the number of eligible segments (segments with data spans exceeding 2.5 years) may be diminished. In turn a smaller network of reliable velocities would be available to compute a dependable Euler vector and determine its consistency.

3.4 South African Seismic Activity

South Africa experiences seismic activity as described in section 1.2. The record of seismic activity for South Africa between the dates 2003.0 to 2013.0 was acquired from the United States Geological Survey (USGS).

According to the USGS records, there were 76 seimic events that registered with magnitude greater than 3.5 within South Africa. These events are shown in Figure 3.3.

Figure 3.3: Each white circle represents a seismic event with a magnitude of greater than 3.5 between the dates 2003.0 to 2013.0. These data were supplied by the USGS.

These events may help understand the discontinuities that are computed for Trignet stations as discussed in sections 4.3 and 5.1.2.

Chapter 4

Computational Standards and Procedure

The primary objective of this project is to establish the kinematics of the North East Region of South Africa with the use of GPS data. To accomplish this, a GPS velocity field has to be computed. From this velocity field an Euler vector or vectors which describes the southern African kinematics may be established.

South Africa hosts Trignet, which satisfies the need for GPS sensor stations. To optimise Trignet's available GPS data, 10 years of GPS data are processed and the resultant time series are analysed to address seasonal effects, data discontinuities, velocity uncertainty, etc. as discussed in chapter 2.2. These factors are discussed as resolved for this project. An overview of the methodology (as depicted in Figure 4.1) to determine South Africa's kinematics is now presented.

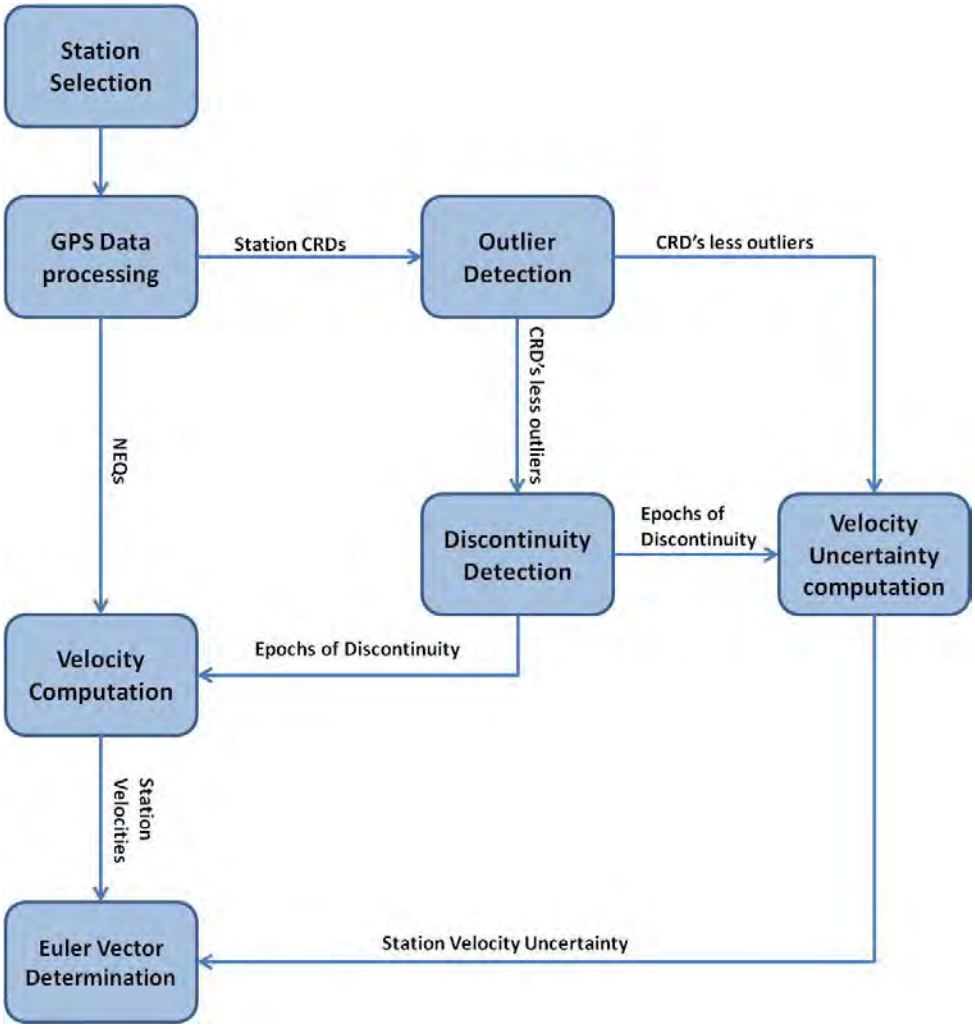

Figure 4.1: Overview of Methodology

4.1 GPS Data Processing

Precise daily co-ordinates are needed to meet the primary objective of this project, with the solution represented in Normal Equation (NEQ) format. These daily Normal Equations are then combined for the computation of station velocities.

To establish daily NEQ's, the Bernese 5.0 Precise GNSS Software (Dach et al., 2007) (url: `http://www.bernese.unibe.ch/`, accessed: 27 August 2015) is used. The factors that the Bernese software accounts for are presented.

4.1.1 Site Displacement Modelling

Each GPS station is attached to the Earth, and hence succumb to the motion of the Earth. These motions are tectonic motion, solid earth tides, polar motion, ocean loading, and precession and nutation, etc., which are considered in the Bernese 5.0 software.

Solid Earth Tides

Solid Earth Tide refers to temporal variation of Earth's crust. Solid Earth tides may account for as much as 30 cm and 5 cm in height and horizontal displacement respectively (Leick, 2004). The Bernese 5.0 algorithm models for Solid Earth tide and are in accordance with the IERS 2003 convention.

Ocean Loading

Ocean loading refers to the deformation of Earth's crust as a result of the tidal redistribution of Earth's water. The displacement may be up to 5 cm and 2 cm in height and horizontal respectively (Leick, 2004). Station specific coefficients are obtained from http://www.oso.chalmers.se/loading/ to compensate for this effect.

4.1.2 Earth Orientation

Precession and Nutation

Precession and Nutation refers to the Earth's instantaneous axis of rotation in space with Precession referring to the long-period lunisolar motion, and nutation referring to the short-period lunisolar motion (Leick, 2004). The IAU2000 model to compensate for this motion type is adopted.

Polar Motion

Polar motion refers to the change in position of the intersection of Earth's instantaneous rotational axis and Earth's static crust (Hoffmann et al., 1994). The Bernese 5.0 software accommodates for this motion by employing the subdaily pole model IERS2000.

4.1.3 Space Geodetic Products

The products that were used in the Bernese routine processing for this project are precise orbits, EOPs, IGS weekly co-ordinates and antenna phase calibrations.

Orbits

The Standard Product #3 (sp3) IGS orbits were employed for the daily processing of the network's GPS data. The current accuracy of the sp3 orbits are 7.3 $\pm$ 0.5 mm (Griffiths and Ray, 2009), and are made available with a two week delay.

Earth Orientation Parameters

EOPs (obtained from the IGS), which compensates for polar motion, and precession and nutation are introduced as well. The accuracy of the EOPs for the x and y components are 10,10 micro-arc-seconds (Altamimi et al., 2011).

IGS Weekly Coordinates

IGS weekly co-ordinates are also obtained from the IGS which is a realization of the ITRF2008. The co-ordinates are a combined solution of the 7 analysis centres realizations. The intrinsic GPS precision of the co-ordinates are 1.7 mm, 1.6 mm and 4.4 mm for the North, East and Vertical components respectively (Altamimi et al., 2011).

For the period prior to 2008, the IGS reprocessed products were used, which included co-ordinates, orbits and EOPs. Absolute antenna phase calibrations "IGS08.atx" were incorporated in the routine processing.

4.1.4 Overview of GPS Data Processing

An overview of the GPS data processing as employed by this project is presented in Figure 4.2.

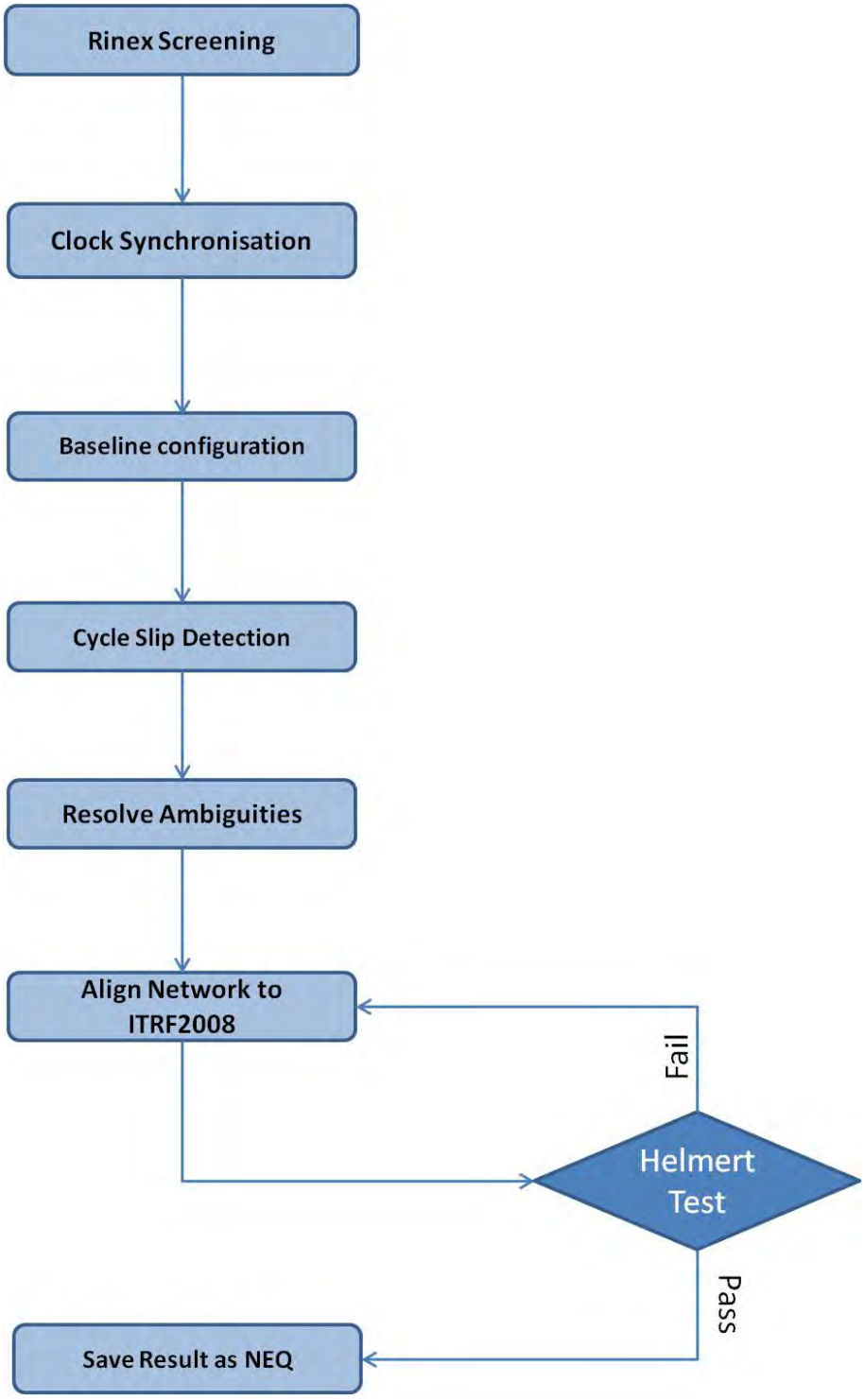

Figure 4.2: GPS Processing Overview implemented using the Bernese 5.0 Precise GNSS software

Each step in the processing overview as shown in Figure 4.2 is now discussed.

4.1.5 RINEX Screening

Screening of GPS data is the first step in computing accurate co-ordinates, in which all GPS data that are filed in RINEX (url: `ftp://igscb.jpl.nasa.gov/igscb/data/format/rinex210.txt`, accessed: 27 August 2015) format are analysed. A threshold for the minimum number of observations in the file is set at 2400, which equates to 20 hours of 30 second observations (Sella et al., 2002). At this stage bad observations are earmarked and excluded. Thereafter GPS stations and satellite clocks are assumed synchronised to GPS time.

4.1.6 Baseline Configuration

Once the clocks are synchronised the optimal network of baselines can be configured. Baselines are configured such that the baseline's terminal GPS stations have the maximum number of observations to common satellites.

4.1.7 Cycle Slips and Integer Ambiguity

These established baselines are analysed for cycle slips and integer ambiguities. A cycle slip is the event in which the tracking and observing of the incoming carrier phase at the receiver end is disrupted. The partial observation phase is not affected, but the number of whole cycles observed is abruptly changed (Hoffmann et al., 1994).

Integer ambiguities are those unknown number of L1 and L2 carrier phases that are present in the observable. The reader is referred to Dach et al. (2007) for the Bernese algorithm employed to solve for cycle slips and resolving integer ambiguity.

4.1.8 Aligning to the ITRF2008

Aligning the network of baselines that are cycle slip and integer ambiguity free to the daily IGS08 realization is achieved through a 7 parameter transformation.

This realization of Trignet should maintain its characteristics, and any deficiency (daily or long term) within the network should be managed or accounted for. This analysis is done on a daily basis, ensuring an optimal time

series.

At this stage of the processing methodology, the network is referenced to the apriori input co-ordinates (i.e. ITRF2008 co-ordinates at epoch 2005.0 propagated to the relevant epoch). The baselines in this network are translated, scaled and orientated based on the daily IGS08 realization using a minimum constrained 7 parameter transformation. This minimum constrained solution maintains the intrinsic daily datum characteristics of the proposed network (i.e. network composed of Trignet and IGS stations) and highlights any deficiencies in this network (Altamimi et al., 2008). If fixed constraints are applied instead of a minimum constrained solution, then any deficiency in the network is masked and distributed through the network (the IGS stations in the network should reveal the agreement/disagreement of the computed network with that of the IGS08 daily realization) (Altamimi et al., 2002; Altamimi, 2003).

4.1.9 Helmert Transformation

Once the transformation parameters are derived, they are applied to all the co-ordinates including the computed co-ordinates of the IGS stations. A Helmert transformation is then applied to determine the agreement between the resultant IGS08 co-ordinates and the published weekly IGS08 co-ordinates. A threshold agreement between the computed and published co-ordinates is set at 1.5 cm for each of the horizontal ordinates and 3 cm for the vertical component. These thresholds take into account the GPS intrinsic precision as discussed by Altamimi et al. (2011), the diminished African IGS network and the difference in network geometry between this project's network and the IGS network in computing the relevant IGS08 weekly realization. IGS stations with residuals exceeding the set threshold are highlighted and excluded. The network realization of the ITRF is then recomputed excluding the IGS problematic stations. This process is iterated till the desired consistency is obtained.

This process is repeated for each GPS day between the years 2003 and 2013. To obtain an acceptable velocity precision as implied by Altamimi et al. (2011) and Altamimi et al. (2012), the resultant time series has to be analysed such that the velocity uncertainty can be determined along with the associated discontinuities and outliers at each station.

4.2 Velocity Uncertainty Computation

Each day of GPS precise processing within the 10 year period yields a set of co-ordinates for each station in the network (that is if the GPS data are

available for that day). Therefore each station has a resultant time series of co-ordinates. Each station may behave differently (difference in noise amplitudes) over time and this behaviour pattern may be evident when analysing their time series (Williams, 2003*b*). The patterns may be attributed to phenomena such as plate tectonics, isostatic adjustment that may be related to large scale ice melting, long term atmospheric conditions, solar flares, antenna changes, GPS satellite geometry and the spatial distribution of GPS stations (Williams, 2004).

These factors that affect the behaviour may be evident in the noise pattern of GPS stations. As described in section 2.2.1, a white+flicker noise model best describes GPS station uncertainty Williams (2003*b*). From these noise models, the uncertainty in velocity at each station may be computed using the Maximum Likelihood estimator (MLE). The reader is referred to the work by Williams (2004) for a detailed description of the MLE and its use to determine the amplitudes of white and flicker noise.

4.2.1 Input Data and Parameters

To compute the uncertainty at each station in the network, the Create and Analyze Time Series (CATS) software (Williams, 2008) was employed. This GPS coordinate time series analysis software applies least squares to fit a multi-parameter (intercept, trend, annual and semi annual sinusoidal signals and offsets) model to a GPS time series, and analyses the resultant residuals to determine the magnitude of the stochastic noise (Williams, 2008). The reader is referred to Williams (2008) for a more comprehensive overview of the CATS software. The input parameters used to estimate the uncertainties using the CATS software are: white+flicker noise model, an epoch resolution of 1 day, and an annual and semi-annual seasonal effect considered. The CATS software considers the individual North, East and Up ordinates for each station independently and quotes the uncertainty in North, East and Up as well.

Discontinuities and outliers (as computed for this project) are accounted for and excluded respectively in computation of the velocity uncertainty. The employed discontinuity and outlier algorithms are now discussed.

4.3 Discontinuity Detection

In general, a discontinuity may be described as an abrupt change in the trend (velocity) of a time series at a specific epoch (Williams, 2003*a*). This abrupt change also coincides with an abrupt change in position between the

epoch of discontinuity and the epoch prior to the discontinuity.

To determine the discontinuities that the time series are subject to, two methods are investigated. Both methods apply least squares linear regression. However, Method 1 analyses the change in velocity, whereas Method two analyses the change in ratio of the variance of unit weight between an apriori least squares solution (solving for linear velocity) and a least squares solution in which a discontinuity is introduced into the linear solution.

4.3.1 Method 1 : Variation of Velocity

Method 1 considers the change in velocity to detect discontinuities. It employs a shifting window that is 2.5 years wide to avoid the effect of seasonal bias. The window is then shifted by 1 month (30 days), each time linearising the 2.5 year window for each ordinate (North, East and Up). Therefore in a 10 year period approximately 120 computations are generated.

The output of this method for each shift is a velocity and an intersection for each ordinate. It is expected that the velocity to be consistent from shift to shift if no discontinuities are present. However, an abrupt change in velocity would suggest a discontinuity. The discontinuity would occur in the 30 day shift that corresponds to the local maximum or minimum of the shifting window velocity computations. Figure 4.3 graphically explains this algorithm.

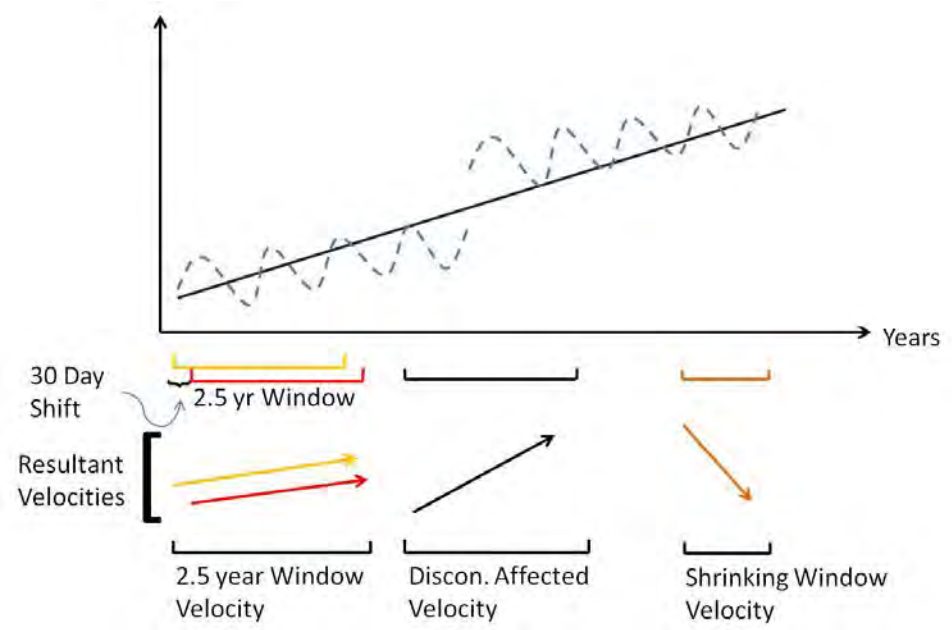

Figure 4.3: Two and a half year window that has a 30 day shift. A velocity is computed within each 2.5 year window. An abrupt change in velocity from window to window suggest a discontinuity.

There are two major limitations to this method. The first is that the shift that corresponds to the discontinuity has a 30 day temporal resolution, which may not be fine enough to sufficiently negate discontinuity bias within a network solution.

The second major limitation (which is shown in Figure 4.3) is that unreliable velocities are computed for shifting windows that coincides with the final 2.5 years of the time series. The shifting window shrinks by 30 days for each consecutive computation as it traverses the final 2.5 years, hence the computed velocities relating to these windows are subject to seasonal effects making these computed velocities unreliable in their use to detect discontinuities. These limitations led to the investigation of a second method.

4.3.2 Method 2: Variance Factor Discontinuity Algorithm

This method is described in section 2.2.2. For this method, discontinuities are detected by analysing the variance of unit weight (Roggero, 2012). The variance of unit weight σ_0 and σ_A of the least squares velocity solution refers to the null and alternative hypothesis respectively. The null hypothesis assumes no discontinuities, and the alternative hypothesis assumes discontinu-

ities in the least square velocity solution (Roggero, 2012). The ratio $\frac{\sigma_A^2}{\sigma_0^2}$, as described in section 2.2.2 from here onwards is referred to as the sigma ratio. An overview of the discontinuity detection algorithm is shown in Figure 4.4.

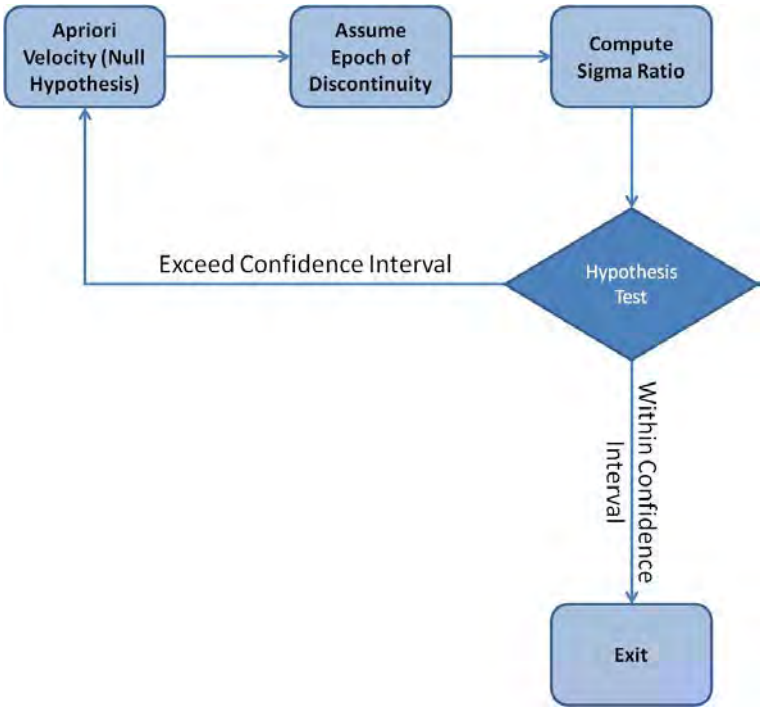

Figure 4.4: Overview of the discontinuity algorithm

A discontinuity is assumed at an epoch and the resultant σ_A^2 of the least squares linearisation is compared to the apriori linearisation's σ_0^2. Here the σ_0^2 relates to the linearisation with no discontinuities as shown in Figure 4.5 (or to an apriori solution which may include epochs of discontinuities). The ratio of σ_A^2 to σ_0^2 is used to test the chi squared 95% hypothesis (Roggero, 2012). All epochs (relevant to the investigated time series) are tested for discontinuities.

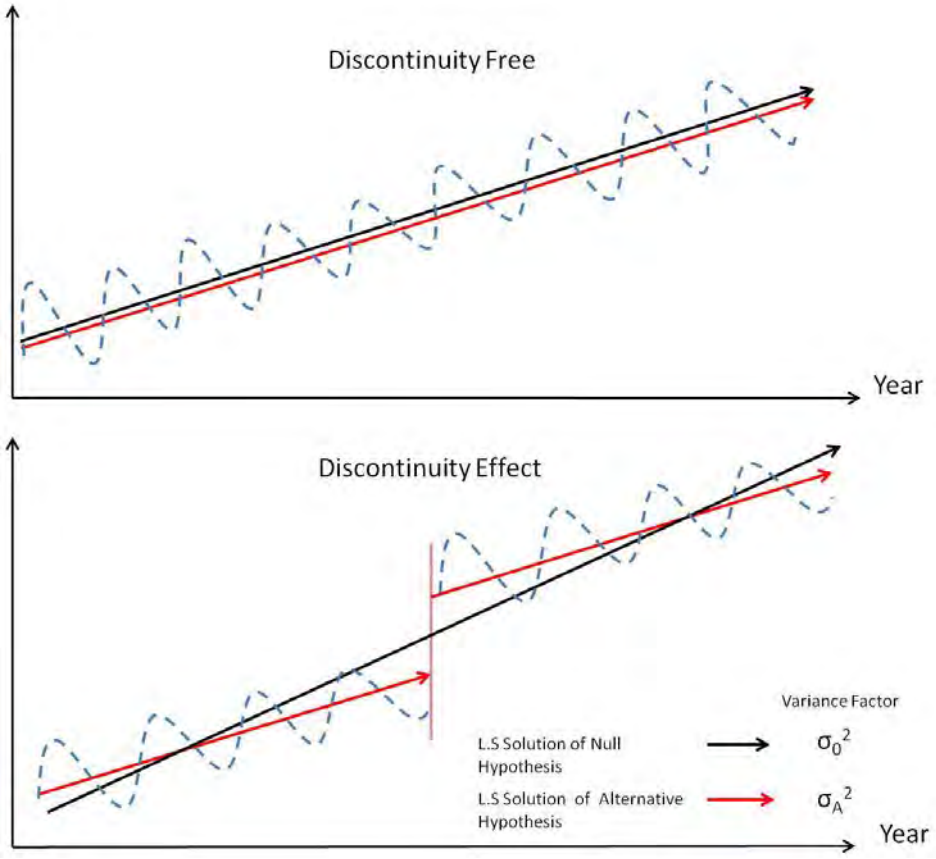

Figure 4.5: Figure illustrating the concept of the Variance Factor Discontinuity Algorithm in which the ratio of the variance factors of the null and alternative discontinuity hypothesis is analysed. The least squares solutions relating to the null and alternative hypothesis solutions in the top "Discontinuity free" image are depicted with separation for ease of view.

If the alternative hypothesis is true, i.e. if the computed sigma ratio exceeds the 5 % confidence interval, then the epoch at which the discontinuity is introduced is in actual fact an epoch of discontinuity (Roggero, 2012). There may be more than one discontinuity in the time series and each needs to be detected.

To illustrate this concept, Figure 4.6 contains a plot of the sigma ratio over time for the North component of station COCO. A discontinuity occurs at the ratio's local minimum at the beginning of 2012 (i.e. if this ratio exceeds the χ^2 5% confidence interval).

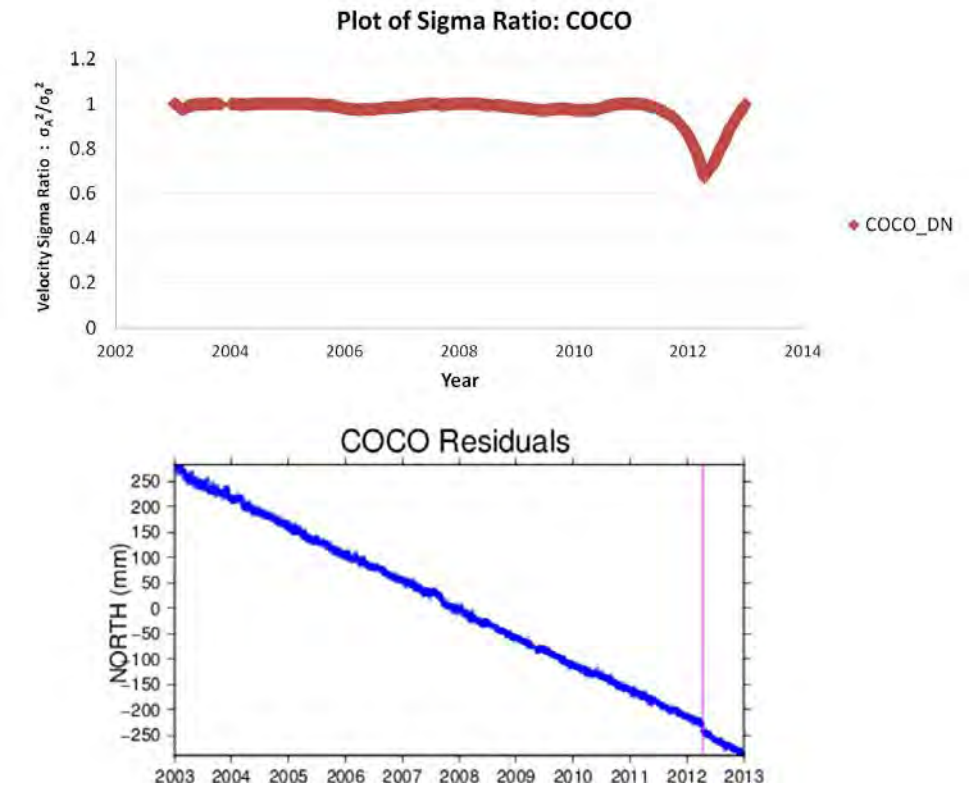

Figure 4.6: Top Image : Plot of velocity sigma ratio vs. Time for the North component of station COCO. Bottom Image : The corresponding North ordinate time series of station COCO. The local "Sigma Ratio" minimum aligns with the discontinuity in year 2012.

This method as it is described in section 2.2.2 has limitations and hence the method needs to be enhanced.

Limitation of Method 2

The limitation with this method is that the individual time series of each ordinate is analysed independently. Thus, a discontinuity that is evident in one ordinate may not necessarily be evident in the station's other co-ordinate components. Also a discontinuity detected at a specific epoch in an individual ordinate, may be offset by a few epochs in another ordinate because of the least squares minimisation of residuals. The small time offset may deem one of these discontinuities as unnecessary. Thus, when 10 years of NEQ's are combined to compute velocities within a network, then unnecessary epochs of discontinuity may be introduced. This weakens the network solution and the reliability of the estimated velocity becomes questionable. This is especially true when the time span of the resultant segments are less

than 2.5 years. This detection of discontinuities in different ordinates with a small time offset (between discontinuities) is illustrated in Figure 4.7.

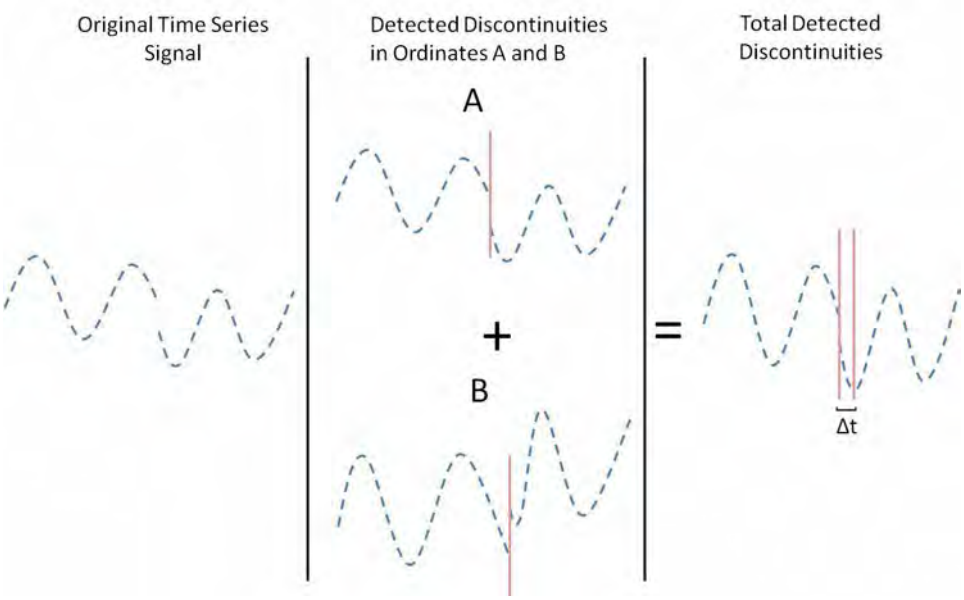

Figure 4.7: Limitation of the Variance Factor Discontinuity Algorithm, in which unnecessary discontinuities are accounted for in a combined network solution.

This small Δt between detected discontinuities in different ordinates is circumvented by using apriori input epochs of discontinuities. These apriori epochs of discontinuities are derived from the detected epochs of discontinuities in the time series of the related ordinates. The enhancement of Roggero's (2012) algorithm addresses this issue.

Enhancement of Method 2

The objective of the enhancement of Method 2 is to eliminate unnecessary computed epochs of discontinuity (EoD) as described in section 4.3.2. The algorithm is explained as follows:

Algorithm

Firstly, discontinuities are detected in the 1st ordinate (which may be any of N, E or H) using the method as described in section 2.2.2.

These EoD are then accounted for in the second ordinate, by forming the apriori input EoD for that ordinate as depicted in Figure 4.8.

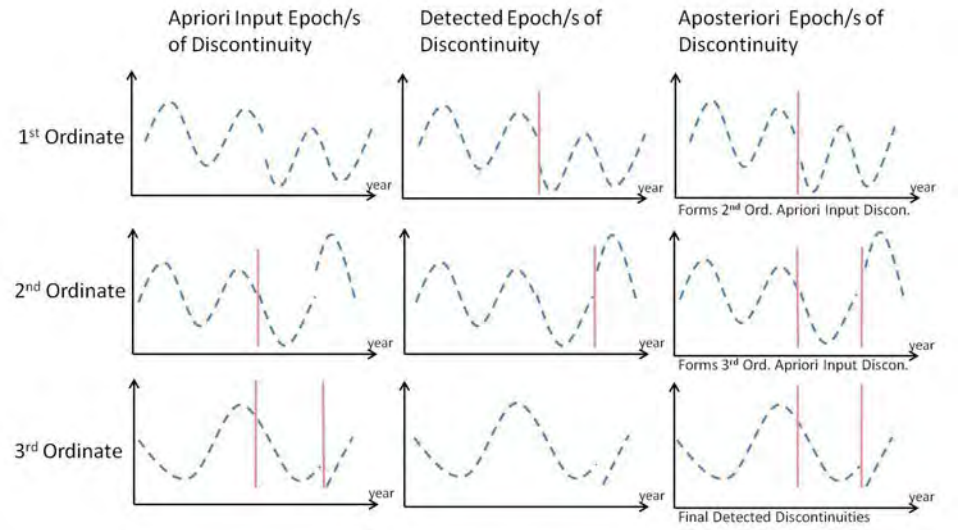

Figure 4.8: Figure illustrating the Variance Factor Discontinuity Algorithm, in which the apriori solution adopts previously detected discontinuities of the associated ordinates.

Now, discontinuities in the second ordinate are detected (with the first ordinate's detected EoD forming the apriori EoD input). If additional EoD are detected, then the 1st set of EoD and the additional detected EoD are introduced to detect discontinuities in the third ordinate. Again, the previous EoD forms the apriori input.

The weakness of this approach is that depending on the sequence in which the ordinates are analysed to detect discontinuities, a different set and number of discontinuities may be computed. So depending on the apriori epoch of discontinuities, the solution (and hence the discontinuities) are adjusted such that the residuals satisfy minimisation criteria.

To obtain the optimal solution, all possible combination of sequences are computed. That is six combinations for each station. The optimal solution would be the sequence that coincides with actual events of discontinuities such as antenna changes, equipment changes, earthquakes, etc. If the computed discontinuities do not coincide with actual events, then the optimal solution is the sequence with the least number of discontinuities.

4.3.3 IGS Official Discontinuities

Discontinuities are computed for all stations, including the IGS stations. The detected discontinuities of the IGS stations using this project's discon-

tinuity method are compared to the published IGS discontinuities.

It must be noted that because this project's and IGS time series characteristics are different (as a result of different processing strategies, difference in network geometry, etc.) there may be differences in computed discontinuities.

4.4 Outlier Detection

Outliers are detected to avoid their adverse effect on the discontinuity least squares solution and the uncertainty computation as described in sections 4.3.2 and 4.2 respectively. Discontinuities are to be introduced into the combination solution as described in section 4.6.3 and the velocity uncertainty introduced in the Euler vector determination as described in section 5.3. Hence, the detection of outliers is an integral step to maintain the integrity of the overall solution.

4.4.1 Factors Considered for the Outlier Algorithm

Seasonal effects that impact on the GPS time series are considered along with the GPS achievable accuracy. Seasonal effects may affect the position in the region of 1.5 cm to 3 cm for horizontal and vertical components respectively (Collilieux et al., 2010). These far exceed the expected accuracy for GPS as discussed by Altamimi et al. (2011). The accuracy quoted for North, East and Height are 1.6 mm, 1.7 mm and 4.4 mm respectively. This difference emphasises the need for the outlier algorithm to consider seasonal effects. The outlier detection method is as follows:

4.4.2 Outlier Detection Algorithm

Each of the ordinates are treated independently. The outliers that are identified will be excluded from not only the associated ordinate, but from the observations of each of the North, East and Height co-ordinate components of a particular station that relates to the epoch at which the outlier has been detected.

To accommodate for seasonal affects, the time series is segregated into individual weeks and analysed on such a basis. This algorithm is illustrated in Figure 4.9.

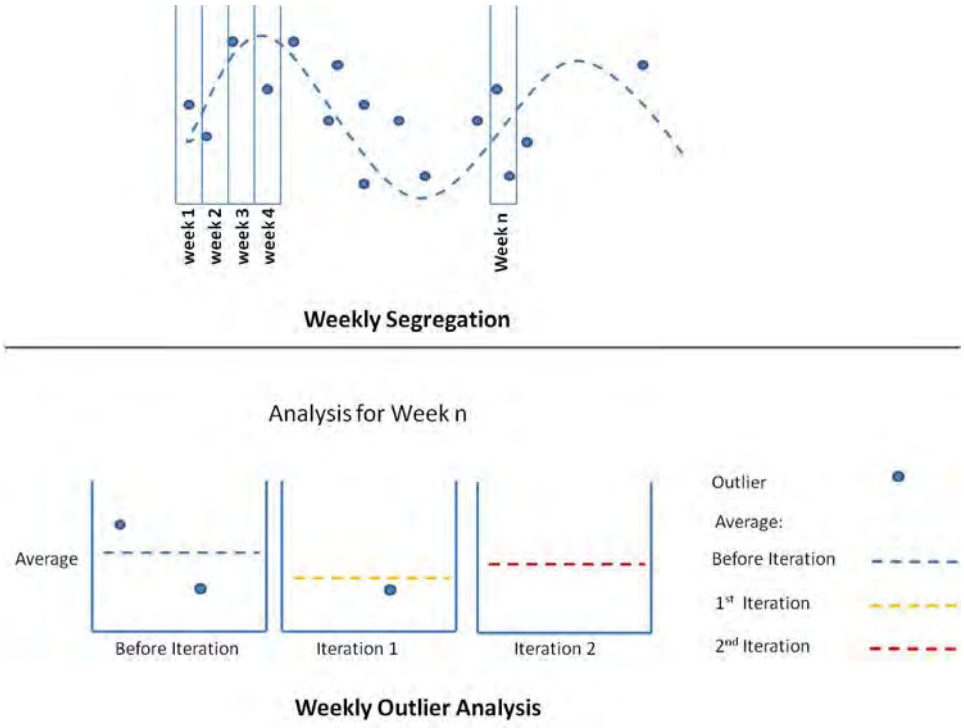

Figure 4.9: Illustration of the Outlier Algorithm. Top figure depicts the weekly segregation. Bottom figure illustrates the weekly analysis and the iteration in removing outliers.

The average for the week is computed for each of the ordinates. Then each daily solution is compared to the weekly average. If the daily observation exceeds the weekly average by a given threshold (described in section 4.4.2), then it is identified as an outlier and excluded. The weekly average is then recomputed excluding the outlier, and each individual solution is again compared to the newly calculated average. If outliers are detected, then the process is repeated.

The minimum number of observations in a week for this process to commence is 3 (2 observations to compute a least squares average, 3 for redundancy), if less than 3 observations are available then this process is terminated and the following week is analysed.

Adopted Thresholds

The threshold for classifying an observation as an outlier is 10 mm for the North and East components, and 20 mm for the Height component. The reason for the seemingly lenient threshold as compared to GPS accuracies

referred to by Altamimi et al. (2011) is that the GPS solutions used to compute the accuracies by them are weekly, multi-centre (various AC solutions) combined solutions (which is more accurate than any single AC solution (Altamimi and Collilieux, 2008)) using an optimal global network.

The network that is used for this project is not optimal as Africa's GPS network is very sparse; the observations comprising this project's time series are based on individual days; and there are no multi-centre combined solutions. Hence, each day in the week also succumbs to weekly sinusoidal effects; and each day is based on a single computation as opposed to a multi-centre solution. For these reasons the daily solutions may not be as accurate as implied by Altamimi et al. (2011) and instead of using 3σ (with sigma referring to the GPS intrinsic accuracy) the adopted thresholds are adjusted to be more representative of this project's time series.

4.5 Euler Vector Computation

The velocity field is computed using a network solution within the Bernese 5.0 Precise GNSS software environment. All daily solutions for the 10 year period are in the Bernese NEQ format. These 10 years of daily solutions are combined to obtain a single homogeneous solution which represents a position and velocity at a chosen epoch (which is arbitrary for this project) for each station in the network. This combined solution makes use of the ADDNEQ2 program, which is part of the Bernese package and is much like the solution as described by Altamimi et al. (2011) (for more information on the ADDNEQ2 solution the reader is referred to the work by Thaller (2008)). However, here only GPS data are considered and the focus is on a velocity field rather than a homogeneous reference frame.

4.6 Establishing a Velocity Field

The velocity field is computed using the combination theorem as described by Thaller (2008). The following is discussed : Reference Frame Selection, Accounting for Discontinuities, and the Algorithm employed to establish a velocity field.

4.6.1 Reference Frame Selected

For the computation of the velocity field a reference frame is needed. Therefore this project is aligned to the ITRF2008 by minimally constraining the IGS stations co-ordinates and velocities. As discussed by Rebischung et al.

(2011), the ITRF2008 is accessible through the IGS08 to maintain the GPS intrinsic precision and this project adheres to this practice.

4.6.2 Accounting for Discontinuities

An important apriori step to computing velocity for station in the network is the detection of discontinuities (Rebischung et al., 2011). The discontinuities that are detected as described in section 4.3 are introduced into the combination step. The manner in which Bernese handles these discontinuities is by introducing a new station for each resultant segment (Dach et al., 2007). The number segments is equal to n+1, with "n" equal to the number of discontinuities.

The number of segments at a station may be numerous and therefore the manner in which these segments are handled plays a crucial role in obtaining a reliable solution. This is especially important for the IGS stations that are used to constrain the network.

A single station can not have two or more solutions, so, an important step is to select a segment that best characterises the actual station behaviour. Adopting all segments (each segment treated as an individual station then) that are related to the IGS stations to align the network may weaken the solution as there may be IGS segments that have time spans of less than 2.5 years (hence, succumb to seasonal effects). This is also true for non IGS stations.

If all segments of a station are to be used, then the more segments (hence discontinuities) at a particular station means that, that station has greater influence on the final solution (each resultant segment treated as an individual station in the combination), which may bias that solution. It is desired for stations with more discontinuities to have less influence on the final solution and not vice versa.

4.6.3 Algorithm

To select the optimal station segments to represent the IGS station velocity for this project, an iterative approach is adopted.

The IGS station segments are analysed and the longest segments are chosen to represent their respective stations as control. This forms the first step of establishing the velocity field as depicted in Figure 4.10. The adopted

segments must span at least 2.5 years.

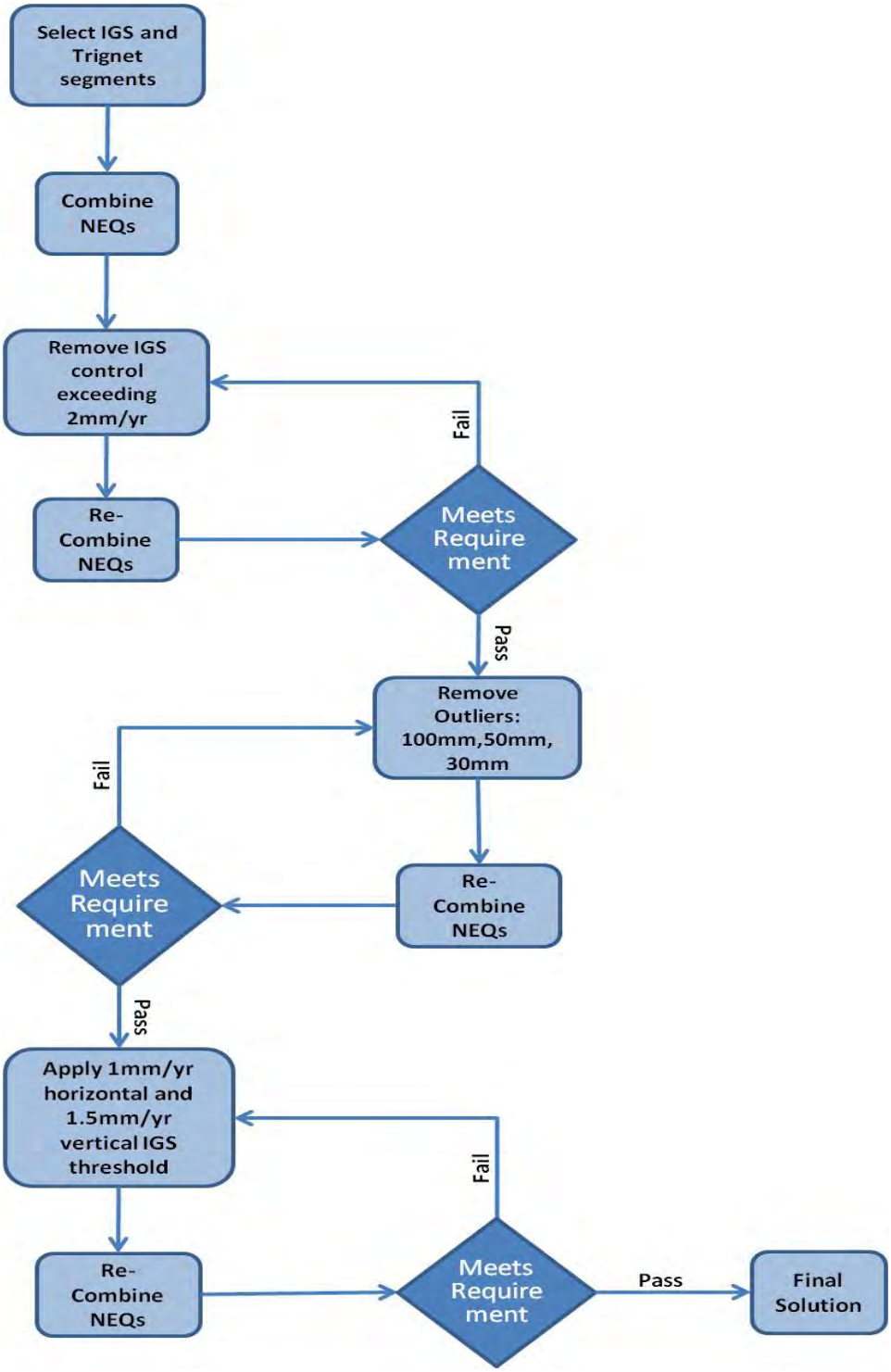

Figure 4.10: Overview of the Combined Velocity Solution

An initial velocity computation is then made, using the longest IGS segments to align the network. This step is mainly carried out to identify poorly behaving IGS stations (or poorly selected segments to represent the IGS stations) that were intended as control, by comparing the estimated IGS station velocity to the published IGS station velocity. If the IGS station comparison exceeds 2 mm/yr for either of the horizontal components, and/or exceeds 3 mm/yr in the height component then that station segment is analysed, and a different segment may be chosen to represent that station. That station may also be excluded from aligning the velocity network.

The difference in the analysis of the Trignet segment selection as compared to the analysis of the IGS segement selection is that no official velocities exist for Trignet. Hence, the criterion for selecting the segments that represent the station velocities is based on the time span of the segments. Segments with the longest time span are selected to represent a Trignet station's velocity, with an underlying prerequisite of a minimum time span of 2.5 years. Once the segments are selected, the velocity field is recomputed using an updated control list to align the network to the ITRF2008.

The next set of iterations are used to eliminate daily outliers at each station in the network. First, all daily solutions with residuals greater than 100 mm in any of the station ordinates are eliminated from the solution. The velocity is then recomputed. This process is then repeated for residuals exceeding 50 mm, and then finally for residuals exceeding 30 mm, each time recomputing the solution (this technique of eliminating outliers iteratively was adopted from the CATREF course in Paris, 2012).

The estimated IGS velocities are again compared to the IGS official velocities. By this stage, a combined solution that accounts for discontinuities, with optimal segments selected and outliers eliminated has been obtained. The combination velocity accuracies at this stage are expected to be better than 1 mm/yr for the horizontal co-ordinate components and 1.5 mm/yr for the height component. This expectancy stems from the velocity precision histogram depicted in the description by Altamimi et al. (2011) of the ITRF2008. This histogram (as shown in Figure 4.11) shows that a vast majority of station velocity precisions are better than 1 mm/yr. For this project, if an ordinate comparison exceeds the set threshold (compared to official IGS velocities), then the respective station is excluded from aligning the network to the ITRF2008 and the velocity field is recomputed.

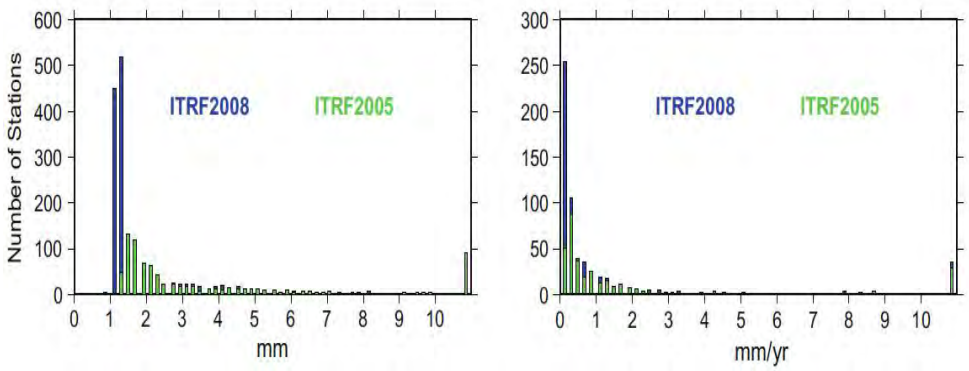

Figure 4.11: Improvement in position and velocity from ITRF2005 to ITRF2008 (Altamimi et al., 2011).

4.7 Euler Vector Computation

The Euler vector is calculated for South Africa, using Trignet station velocities that are computed as described in the previous section. All Trignet station velocities computed are based on at least 2.5 years of GPS data. The uncertainty computed using a white + flicker noise model described in sections 2.2.1 and 4.2 is used to weight the least squares Euler Vector solution. The weight matrix is constructed using the conventional inverse of the squared uncertainty ($\frac{1}{\sigma^2}$), with σ representing station velocity uncertainty.

4.7.1 Test for consistency

The computed Euler vector consists of a pole of rotation (latitude and longitude) and an angular velocity. To validate the output Euler vector for South Africa, two tests are performed. The first test is a 3-sigma-3 test proposed by Altamimi et al. (2012), and the second test is a chi squared goodness-of-fit test.

Three-Sigma-Three test

The 3-sigma-3 test has two parts to it. The first phase analyses the residuals of the least squares Euler vector solution. Stations with residuals exceeding 3 mm/yr are classified as outliers (Altamimi et al., 2012). The second phase of the test scrutinises the ratio of the residual to the apriori uncertainty (uncertainty computed as described in section 4.2). The ratio should be less than 3, otherwise the respective input station velocity is deemed as an outlier (Altamimi et al., 2012). The reason for a ratio of better than 3 in

the second phase is that the uncertainty has a confidence of 1 sigma (Altamimi et al., 2012), hence outliers exceeding 3 sigma are considered outliers.

Goodness-of-fit test and Plate Rigidity

The second part of the consistency analysis is the chi squared goodness-of-fit (GoF) test. The chi squared per degree of freedom formula adopted for this project is $\frac{\sum \frac{Residual^2}{\sigma^2}}{n-3}$, with *Residual* being the residual of each observation, σ is the velocity uncertainty at each station and (n-3) is the degree of freedom with n equal to the number of observations (station velocities).

A chi squared per degree of freedom value of 1 suggests a rigid lithospheric block (Horner-Johnson et al., 2007). Values greater than 1 alludes to a deforming lithospheric block, or that the station velocities are of two or more independent tectonic plates moving at different velocities.

Chapter 5

Results and Analysis

To maintain the integrity of the velocities and Euler vector that is computed for this project, then the management of the network's noise, discontinuities and outliers becomes essential. An effort is made to manage the daily solutions, such that the network of velocities obtained are at the confidence level alluded to by Altamimi et al. (2011). An analysis of the Time Series, Velocity Computation and Euler Vector Estimate is provided in this chapter.

5.1 Time Series Analysis

5.1.1 Velocity Uncertainty

Velocity uncertainty is computed using a Maximum Likelihood Estimator (MLE) in which a white + flicker noise model is incorporated as is described by Williams (2004). The uncertainty is to be used in establishing an Euler vector of South Africa, and the resultant residuals will be analysed using a 3-sigma-3 test and chi squared goodness-of-fit test to determine whether South Africa is a single plate, or conforms to a multi-plate tectonic system.

The uncertainty computation also reveals the behaviour patterns of stations. This detail may prove valuable for selecting core stations (stations with better uncertainty) in establishing a datum, similar to the ITRF.

The average velocity uncertainty computed for stations in this project's network is 0.377 (stdev:0.27), 0.37 (stdev:0.40) and 0.765 (stdev:0.580) mm/yr for the North, East and Height components respectively. As expected the Height component is associated with the higher uncertainty. Analysing GPS intrinsic precision, the horizontal components for the positional precision is approximately 2.6 times that of the height (Altamimi et al., 2011). The velocity uncertainty ratio computed for Height to either of the North or East component is approximately 2 (H/N: 0.765/0.37).

To obtain a reasonably accurate velocity, a minimum of 2.5 years of data are required to alleviate seasonal effects (preferably 5 years of data are required for accurate velocity estimates (Blewitt, 2002)). Comparing the number of observations to the uncertainty then a significant correlation is evident. The increase in the number of observations yields a more representative velocity estimate. This equates to a correlation of -0.69 and this relationship is shown in Figure 5.1 (an increase in observations is associated with a decrease in velocity uncertainty).

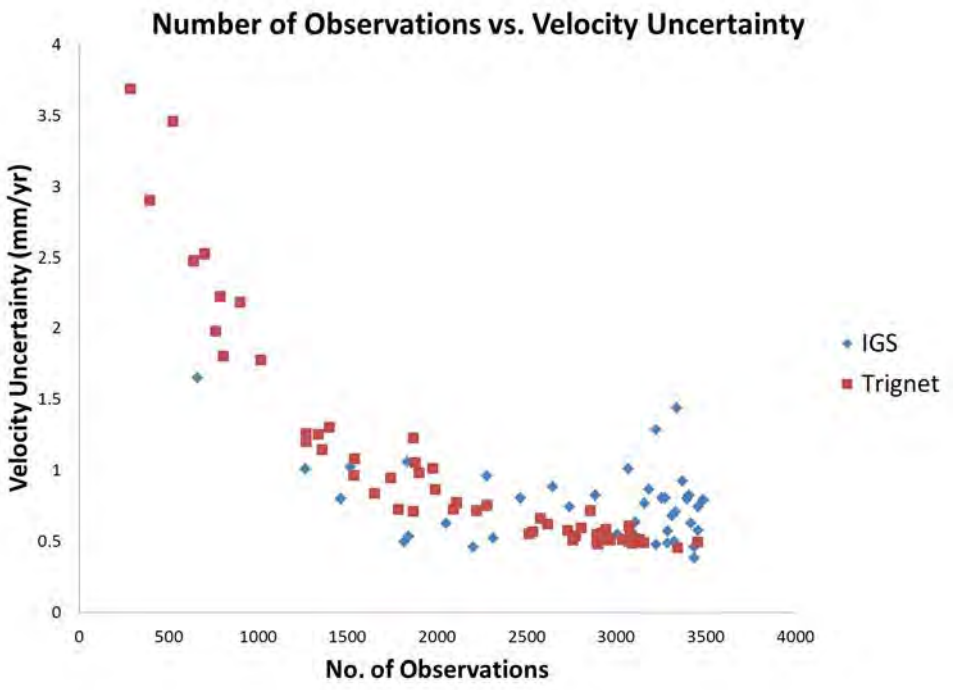

Figure 5.1: Graph illustrating the correlation between the number of GPS observations and GPS velocity uncertainty. The red and blue series are Trignet and IGS stations respectively.

Besides negative correlation, Figure 5.1 reveals the difference in uncertainties between the IGS and Trignet stations. Analysing the graph, the IGS stations have lower overall uncertainty as compared to the Trignet stations. However, the Trignet stations that behave poorly have fewer observations (less than 1000). That said, there is a threshold of observations of approximately 1500 (equating to about 4.5 years) after which the improvement is minimal with the increase in observations. This echoes the finding in the Blewitt (2002) study, which emphasises that beyond 4.5 years of observed

GPS data, the precision gained in velocity estimate is negligible. The improvement beyond this threshold are then linked to other factors such as monumentation, network design, etc (Blewitt, 2002; Williams, 2004).

The IGS outlier in Figure 5.1 (top right of the graph) refers to station ANTC that experienced an earthquake in 2010. Figure 5.9 illustrates the non-linear velocity recovery after the earthquake.

5.1.2 Discontinuities

In section 4.3 two discontinuity algorithms were described. Method 2: Variance Factor Discontinuity Algorithm (described in section 4.3.2) was adopted for this project because of Method 1: Variation in Velocity algorithm's (described in section 4.3.1) susceptibility to seasonal effects. Hence only Method 2 results are discussed.

The discontinuity analysis based on Method 2's algorithm may be split into two sections, i.e. an IGS section and a Trignet section. IGS has an official list of discontinuities that is adopted (on the whole) for this project, whereas Trignet on the other hand does not have an official list of discontinuities. To assess the performance of the discontinuity algorithm described in section 4.3.2, the computed discontinuities for the IGS stations are compared to the IGS official discontinuities and for those that are computed for Trignet stations are analysed and events (such as antenna changes and equipment changes) that co-incide with the computed discontinuities are identified.

IGS Discontinuities

To assess the efficiency of the discontinuity algorithm, the detected discontinuities for the IGS stations are compared to the official IGS list. By and large, the official IGS list of discontinuities was adopted for this project.

Of the 10 Trignet stations that are common to the IGS network, only HRAO, HARB, SUTH, HNUS and RBAY has published discontinuities. The remaining 6 stations in this event do not have IGS listed discontinuities and are excluded from the IGS discontinuity analysis.

Comparison with Official IGS list
Each of the 44 IGS stations (51 IGS stations less the 7 Trignet stations that do not have official IGS discontinuities) has a series of IGS discontinuities listed. Of the 44 series, 37 were adopted for this project. Each station's computed discontinuities were compared to the official IGS discontinuities. Twenty six of the stations discontinuity series were in agreement with the IGS official list. A summary of the IGS station discontinuity comparison is given in Table 5.1.

In the cases of disagreements, the Jet Propulsion Laboratory (JPL) discontinuities computed for the IGS stations common to this project would be analysed to determine which set of discontinuities to adopt. If the JPL solution is more harmonised with either of the solution, then that solution is adopted (only in the cases of disagreement). These disagreements may be attributed primarily to large data gaps in the series that the algorithm used for this project does not account for.

Difference in IGS discontinuities
Eighteen IGS stations discontinuities as computed in this project were in disagreement with the official IGS list. Two of these stations showed more agreement with JPL, and the remaining 16 showed no agreement to either JPL or the IGS. The disagreement sequences comprises 6 stations that have large data gaps, 3 stations in which the official IGS discontinuities were adopted and 7 stations that showed unique solutions. These are discussed under the headings JPL Discontinuity Agreement, Stations with Minimal Data, IGS Adopted Discontinuities for Stations with Disagreement, and Unique Discontinuities.

Table 5.1: Matrix Summarising the Comparison of Station Discontinuities detected using this Projects Algorithm and the Official IGS discontinuities

Station Name	**IGS Adopted Discons**	**Similar Detected IGS Discons**	**Different Detected IGS Discons**	**No Discons**	**No Agrment**	**JPL Agrment**	**Uniquely Computed Discon**	**Minimum Data**	**Notes**
PARC	✓	✓		✓					
NOT1	✓	✓		✓					
RCMN	✓	✓		✓					Large Data Gaps
ADIS	✓	✓		✓					
USNO	✓	✓		✓					
NKLG	✓	✓							
MAL2	✓	✓							
HARB	✓	✓							
ANTC	✓	✓							Earthquake Detected
DAV1	✓	✓							
KERG	✓	✓							
DGAR	✓	✓							Earthquakes Detected
COCO	✓	✓							Earthquakes Detected
RAMO	✓	✓							
PDEL	✓	✓							
MAS1	✓	✓							
MBAR	✓	✓							Noisy Data

Table 5.1 continued.

Station Name	IGS Adopted Discons	Similar Detected IGS Discons	Different Detected IGS Discons	No Discons	No Agrment	JPL Agrment	Uniquely Computed Discon	Minimum Data	Notes
SCH2	✓	✓							Noisy Data
WSRT	✓	✓							
POL2	✓	✓							
IISC	✓	✓							
GRAS	✓	✓							
MALI	✓	✓							
BRAZ	✓	✓							
SEY1	✓	✓							Large Data Gaps
RBAY	✓		✓	✓				✓	Large Data Gaps
ZAMB	✓		✓	✓				✓	Large Data Gaps
OHI2			✓				✓		Introduced Discon
ASC1	✓		✓	✓				✓	Large Data Gaps
GOUG	✓		✓	✓				✓	Large Data Gaps
VESL	✓		✓	✓				✓	Sparse Data
YEBE	✓		✓	✓		✓			JPL Discon at 2010.011
RABT			✓				✓		
REUN			✓				✓		
HRAO			✓				✓		Antenna Changes

Table 5.1 continued.

Station Name	IGS Adopted Discons	Similar Detected IGS Discons	Different Detected IGS Discons	No Discons	No Agrment	JPL Agrment	Uniquely Computed Discon	Minimum Data	Notes
SYOG			✓				✓		
WIND	✓		✓					✓	Large Data Gaps
BRFT	✓		✓		✓				2011 not Detected
YIBL			✓				✓		Discon in 2004
BOGT	✓		✓		✓				2005 and 2007 Detected
SCUB	✓		✓			✓			Discon similar to JPL
QAQ1	✓		✓		✓				
SUTH			✓				✓		2007 Antenna Change

JPL Discontinuity Agreement
Stations SCUB and YEBE have different series of discontinuities to those of the official IGS, yet have similar discontinuities to JPL (Figure 5.2 illustrates the agreement for station YEBE). The official IGS discontinuities for these stations were retained because the series of discontinuities computed for these stations using this project's algorithm were subtle and may have a little influence on the velocities.

Expanding on this, analyses of the discontinuity sigma ratios as described in section 4.3.2 for SCUB and YEBE are all greater than 0.9, which is borderline discontinuity classification. Therefore, these discontinuities as computed using this projects algorithm for these stations were disregarded and the official IGS discontinuities adopted.

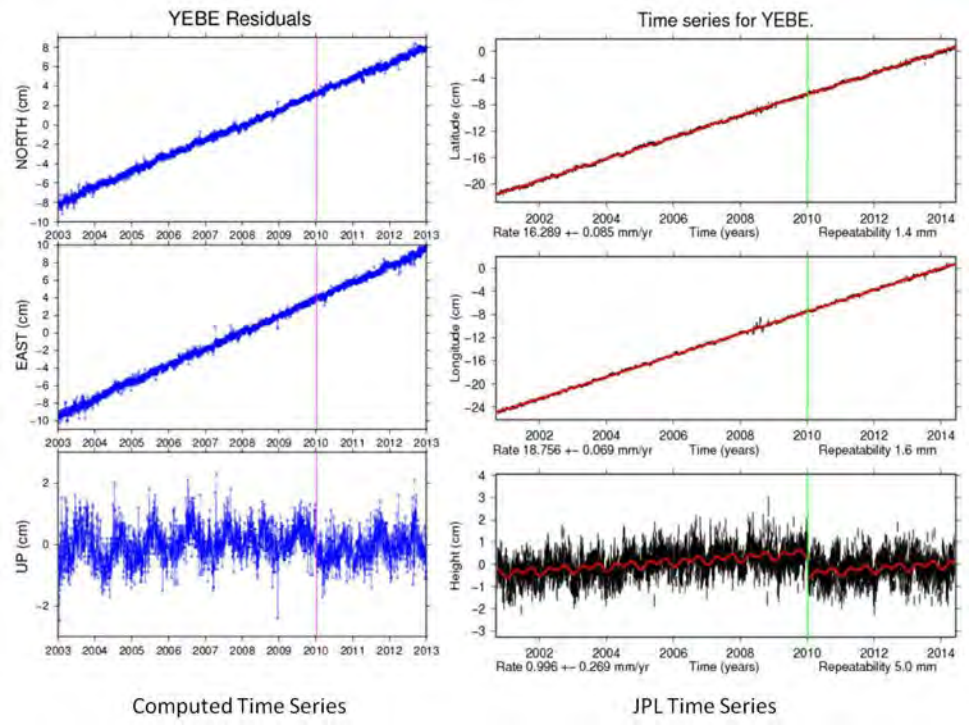

Figure 5.2: Comparison of computed discontinuities (magenta vertical line) for YEBE to that of JPL (green vertical line). JPL's solution is the time series on the right

Stations with Minimal Data
Station ZAMB, WIND, GOUG, RBAY and ASC1 shows significant data gaps in the plotted time series. These data gaps affect the computed least

squares solution. This solution may be different and more true if the time series were free of significant data gaps. The algorithm does not take into account data gaps and therefore the IGS discontinuities were adopted for these stations.

Similarly, station VESL has very sparse data between 2003 and 2011, in which 6 of the 8 years has less than 300 days of data (a 300 day threshold is suggested by Sella et al. (2002)). Hence, the official IGS discontinuities were adopted for this station. Figure 5.3 illustrates the large data gaps and sparse data in these stations time series (3 of the 6 stations are shown for ease of illustration).

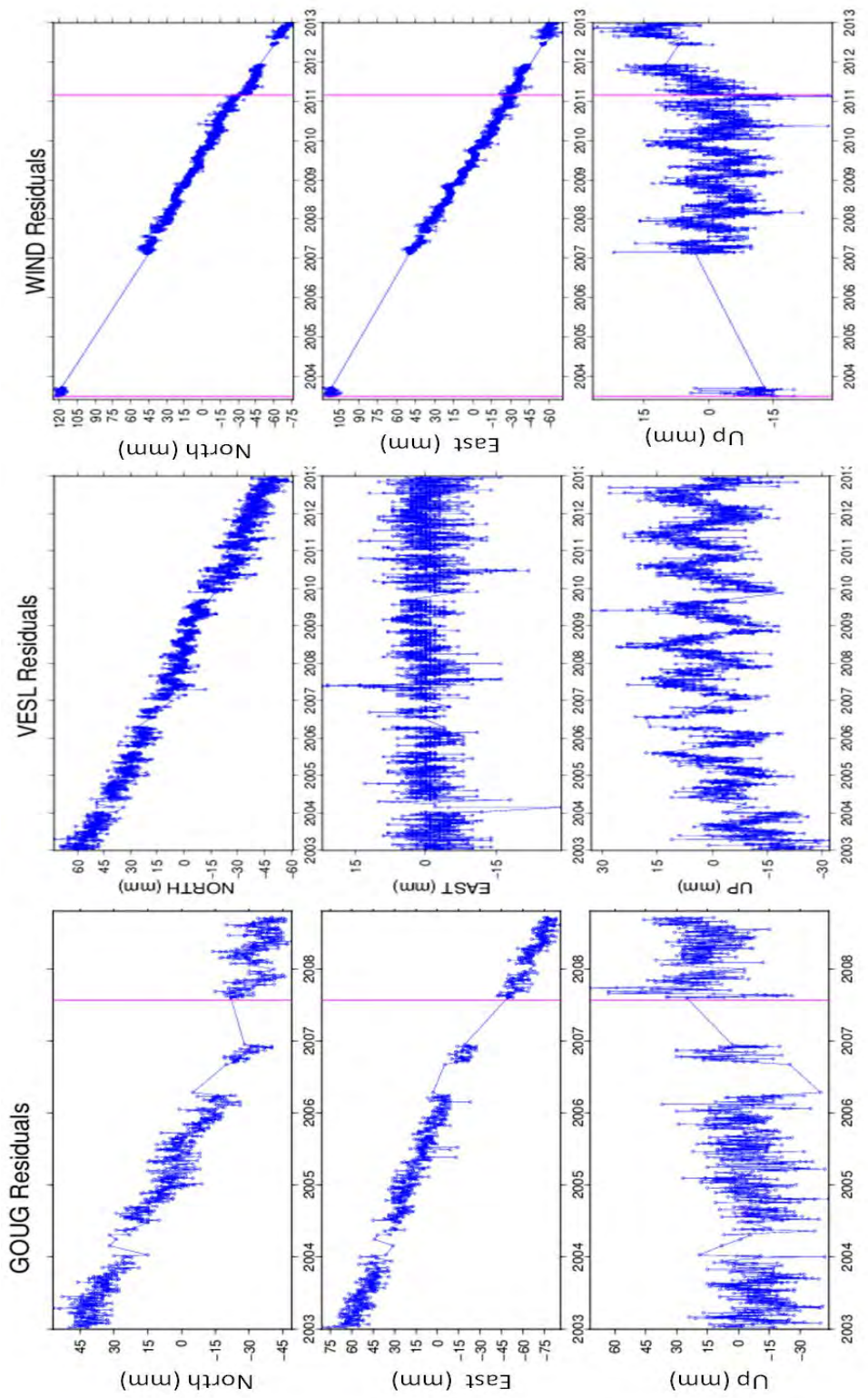

Figure 5.3: Time series of VESL, GOUG and WIND. GOUG and WIND time series shows large data gaps with VESL showing more sparse data series, compromising the performance of the discontinuity algorithm

IGS Adopted Discontinuities for Stations with Disagreement

Three stations showed no agreement with the IGS, yet the IGS discontinuities were adopted for this project. These stations are BRFT, BOGT and QAQ1.

At station BRFT, the step in data in year 2011 (as evident in Figure 5.4) is not detected by this project's discontinuity algorithm. This step in data occurs at the beginning of 2011 and the trend is restored 3 months on. A major draw back of this discontinuity algorithm is that the entire series is being analysed to generate a variance of unit weight. An improvement to the algorithm would be to mimic the procedure that would be adopted if discontinuities were computed near real time (ie. three month delay to accommodate the discontinuity least squares solution).

To accomplish this the algorithm should be adjusted by including a 3 month incremental window. Starting with a minimum period of 2.5 years and then incrementing this period by three months until the entire 10 year period is incorporated, searching for discontinuities with each increment. This would allow steps such as the step in 2011 BRFT time series to be detected. As a result, the IGS official discontinuities for BRFT were adopted.

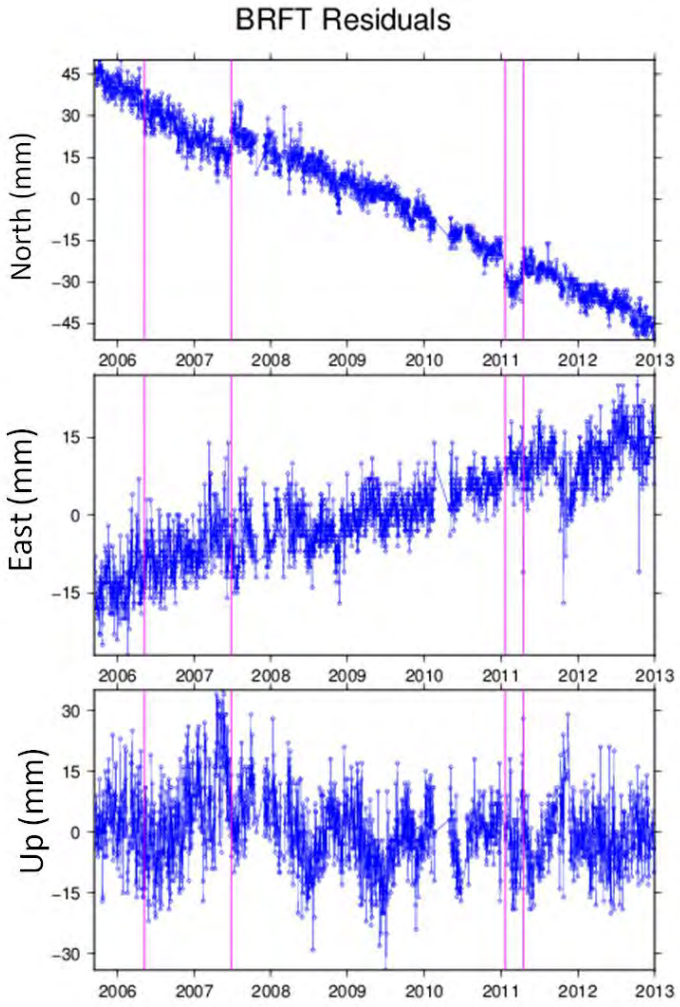

Figure 5.4: Discontinuities (magenta vertical lines) computed and adopted for station BRFT. The step in data occurs in 2011 (which is very evident in the North component), introducing two discontinuities that were not detected by this project's algorithm.

Only two of the four IGS listed discontinuities were detected by this project for station BOGT. As described for station BRFT, the algorithm needs to be adjusted so that the period is analysed incrementally. Since the entire series is analysed to generate a variance factor, the solution is given for the entire period, not for a near real time solution. Again, the IGS official discontinuities were adopted for the station BOGT.

Station QAQ1 discontinuities as computed for this project shows no agree-

ment with the IGS discontinuities, nor to that of JPL. The JPL and IGS discontinuities computed for QAQ1 are not consistent. The number of discontinuities computed for QAQ1 is alarming large using the algorithm adopted for this project, and hence the discontinuities as computed by the IGS were adopted.

Unique discontinuities
Seven stations adopted the discontinuities as computed by this project. These stations discontinuity sequence were not in complete agreement with the IGS list. These stations are HRAO, REUN, SUTH, YIBL, SYOG, OHI2 and RABT.

The algorithm employed detected a discontinuity in 2005 for station REUN, along with the only IGS detected discontinuity in 2008 as depicted in Figure 5.5. The discontinuity in 2008 relates to equipment and antenna change.

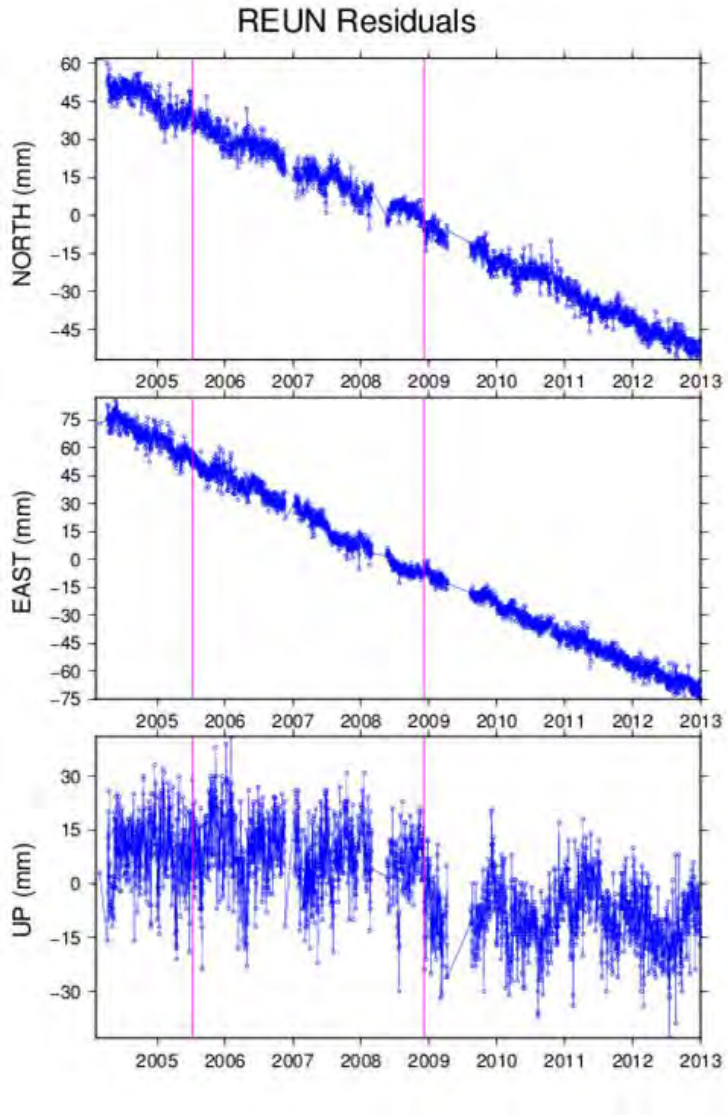

Figure 5.5: Discontinuities computed (magenta vertical lines) and adopted for station REUN. Discontinuity in 2008 relates to antenna change at station REUN

Analysing station HRAO, additional discontinuities towards the end of 2004 and beginning of 2006 were detected by the algorithm. These discontinuities were not published as part of the IGS list, however, the discontinuities at the beginning of 2008 and 2009 (which were also detected by this project's algorithm) as depicted in Figure 5.6 were detected.

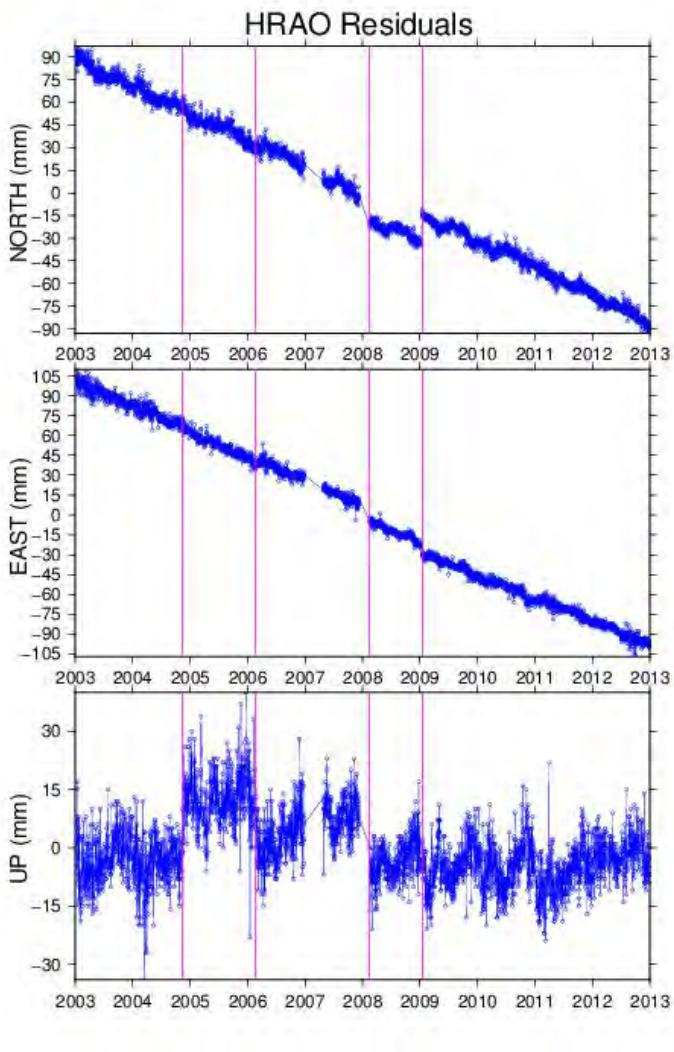

Figure 5.6: Discontinuities computed and adopted for station HRAO

Discontinuities at 2004 08 04 and 2007 11 08 were detected for YIBL and SUTH respectively, but are not IGS listed. The discontinuity relating to station SUTH coincides with an antenna change and hence is maintained. The discontinuity in YIBL time series is significant yielding a sigma ratio of 0.70 and is likewise maintained.

Both RABT and OHI2 share a discontinuity in 2008 that is not detected by the IGS and since the discontinuities are significant as detected for this project, it is maintained. Station OHI2 has a very noisy data series.

SYOG, which is in Antarctica shows discontinuities that are not IGS listed.

These discontinuities occur at 2006 12 31 and 2009 10 11 as shown in Figure 5.7, which is detected when analysing the Height and North components respectively. The sigma ratio computed for the height discontinuity is 0.79, which is quite significant. This may be attributed to Glacial Isostatic Adjustment (GIA), which is not taken into account in this project. The sequence of discontinuities as computed by this project was adopted, because of the significant sigma ratios.

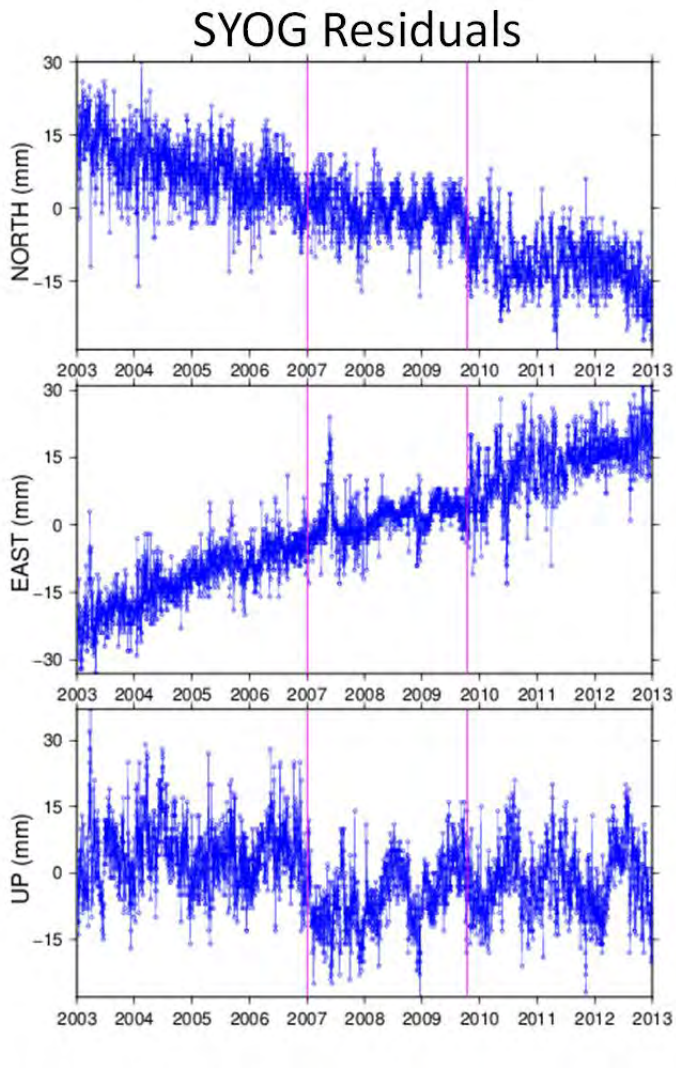

Figure 5.7: SYOG is in Antarctica. This station may succumb to GIA, which is not accounted for in this project. This may account for the discontinuities in 2006 and 2009 for station SYOG.

Earthquakes detected

The algorithm computation also revealed events of earthquakes at stations COCO, DGAR and ANTC. COCO and DGAR experienced the same earthquakes at epochs 2004 12 26 and 2012 04 11 (resultant discontinuities shown in Figure 5.8, relates to earthquakes registering 9 and 8.6 on the Richter scale respectively). COCO and DGAR are situated on two different plates i.e. DGAR on the Somalia Plate and COCO on the Australian Plate. Both of these stations are fairly distant from a plate boundary.

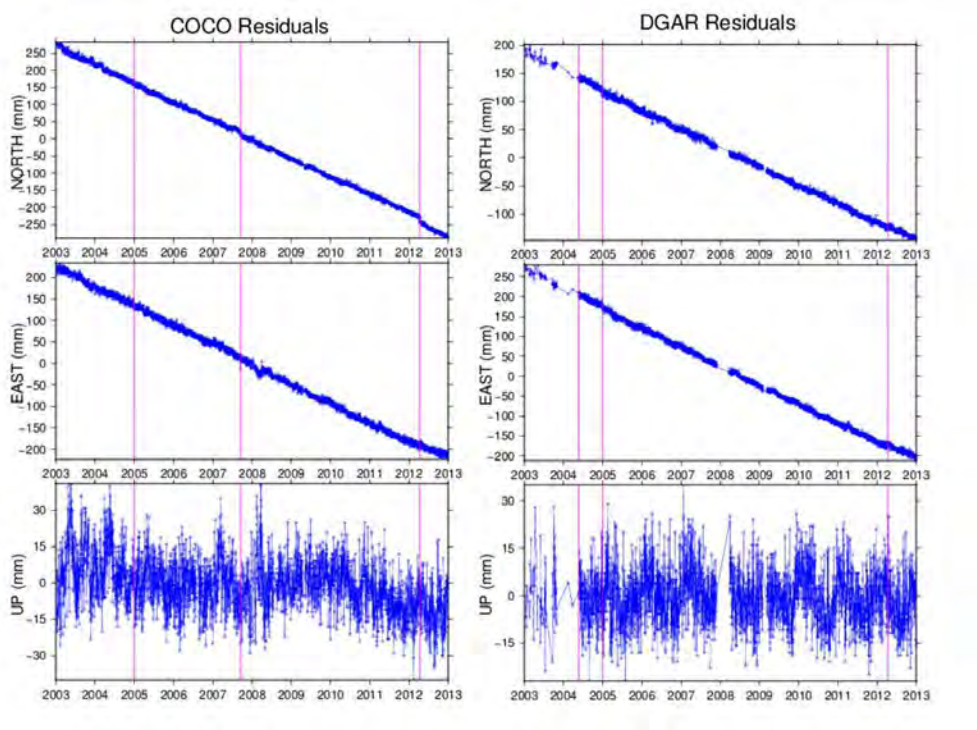

Figure 5.8: Time series of DGAR and COCO showing the same discontinuities at the end of 2004 and in the year 2012 which corresponds to earthquakes. The earthquake on the day of the 26th December 2004 corresponds to the Tsunami that hit South East Asia

.

ANTC on the other hand is situated on the South American Plate close to a plate boundary. The Chile earthquake on 2010 02 27 is detected by the algorithm, which measured 8.8 on the Richter scale. The manner in which ANTC recovers from the earthquake is different to that of COCO and DGAR, which may be because of its close proximity to the plate boundary. ANTC experiences a "hangover effect" long after the earthquake has occurred and this post-seismic effect is evident in the time series.

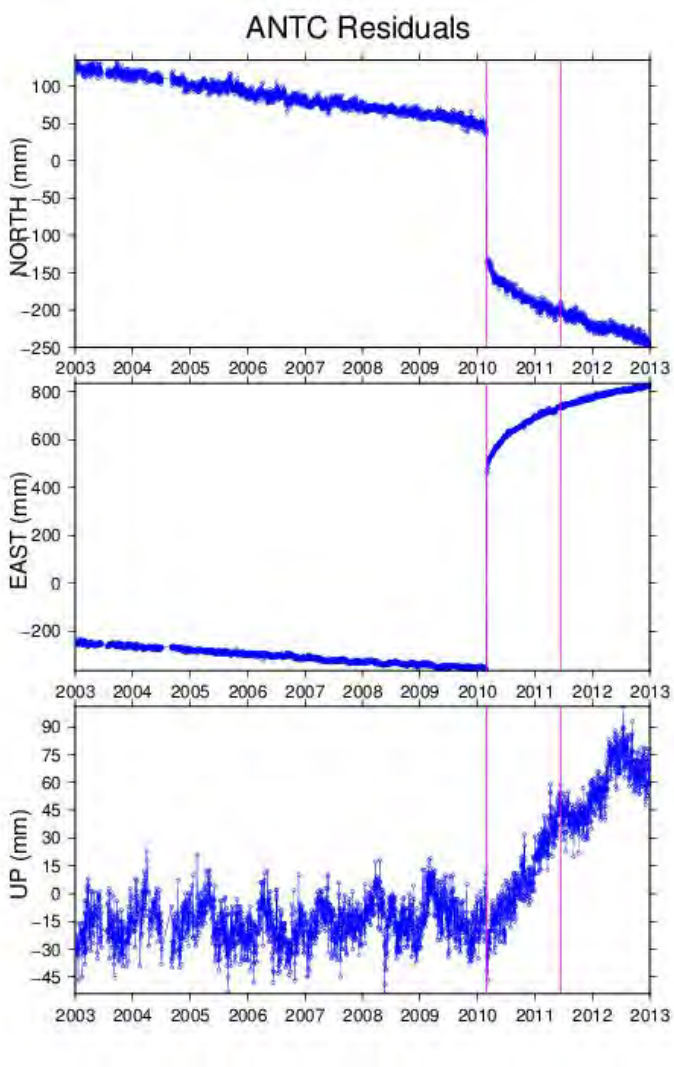

Figure 5.9: Time series of ANTC showing the recovery after the Chile earthquake in 2010.

Analysis of Trignet Discontinuities

There is no official discontinuity list for Trignet, none the less this project has revealed some interesting information with respect to Trignet station behaviour.

Although a large number of the discontinuities are unaccounted for (unaccounted for discontinuities are not out of the ordinary), which is partly

attributed to the lack of logging of Trignet maintenance activity.

Antenna and equipment changes
A total of 67 Trignet discontinuities were detected. Of this 67 discontinuities, only 22 coincide with antenna changes, and 1 discontinuity with equipment changes.

Antenna Baseplate Change
Communication with Trignet staff revealed that antenna base plate changes occurred at stations GEOR, PELB and ELDA in the week of 2005 02 16. Station GEOR has four different positions as mentioned in section 3.3, and is excluded from the analysis. This base plate change was not detected at station ELDA, but this change coincides with the discontinuity in week 2005 02 16 of station PELB. This again illustrates the need to log station maintenance.

Antenna Changes
Analysis of the station information file used by NGI to process Trignet data reveal antenna changes in week of 2007 11 08 for stations GDAL, KSTAD, VERG, SUTH, EMLO and BETH. These antenna changes were detected as discontinuities using this project's algorithm. Figure 5.10 shows the 2007 11 08 discontinuity that relates to antenna changes at stations EMLO, GDAL and VERG.

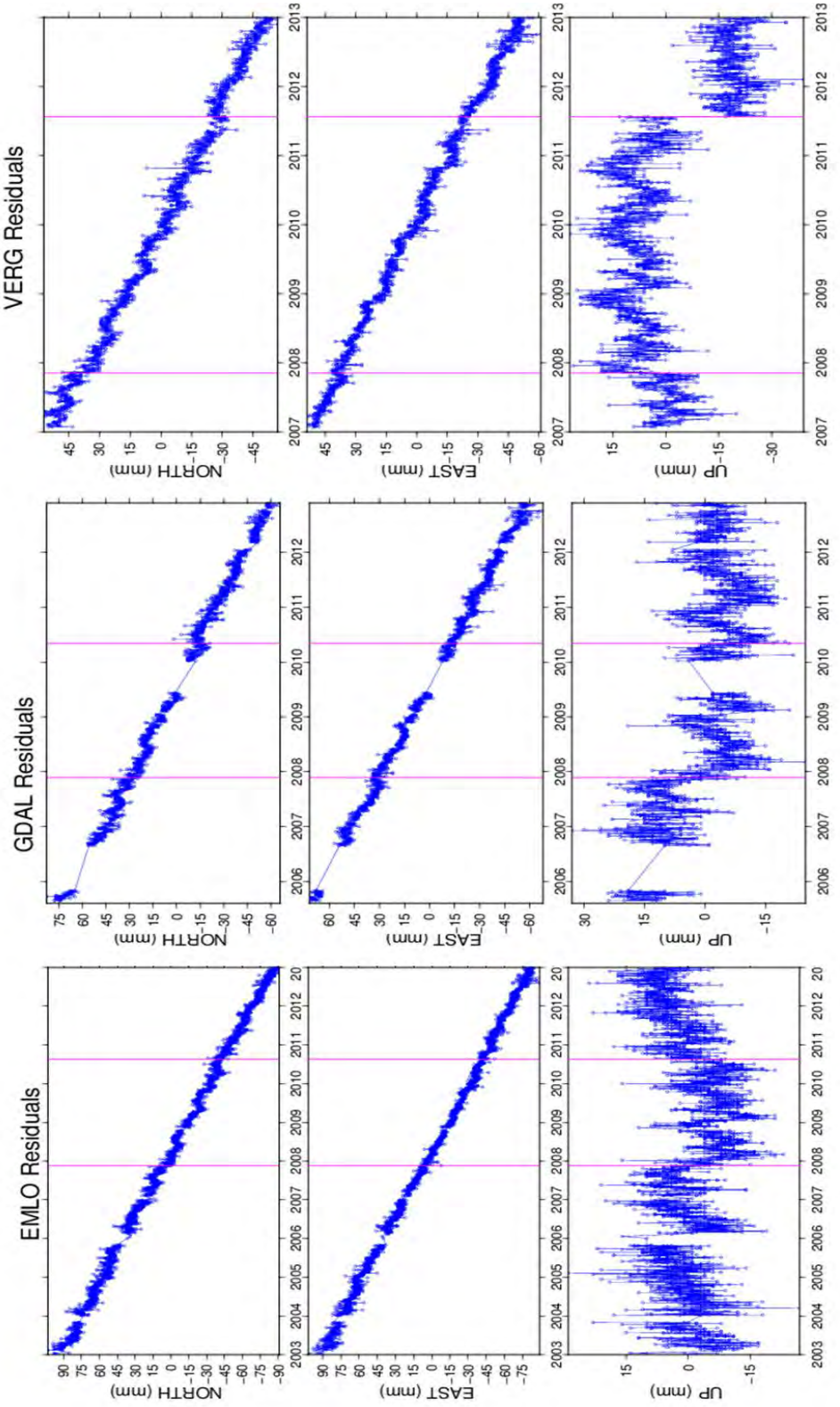

Figure 5.10: Time series of EMLO, GDAL and VERG each having a discontinuity in the same week of 2007, which corresponds to antenna change at this epoch for these stations.

However, there are stations that share an epoch of discontinuity that cannot be accounted for. In the week of 2011 01 15, four stations experienced a discontinuity in that week (i.e. ELDN, NYLS, PMBG, TDOU). ELDN has an antenna change in that week and can be accounted for, however discontinuities at NYLS, PMBG and TDOU are unaccounted for.

Likewise in week 2008 01 09 BWES, ERAS and CALV experience discontinuities which are unaccounted for. Analysing these three stations time series shown in Figure 5.11, it is quite evident that a change in height occurs in that week.

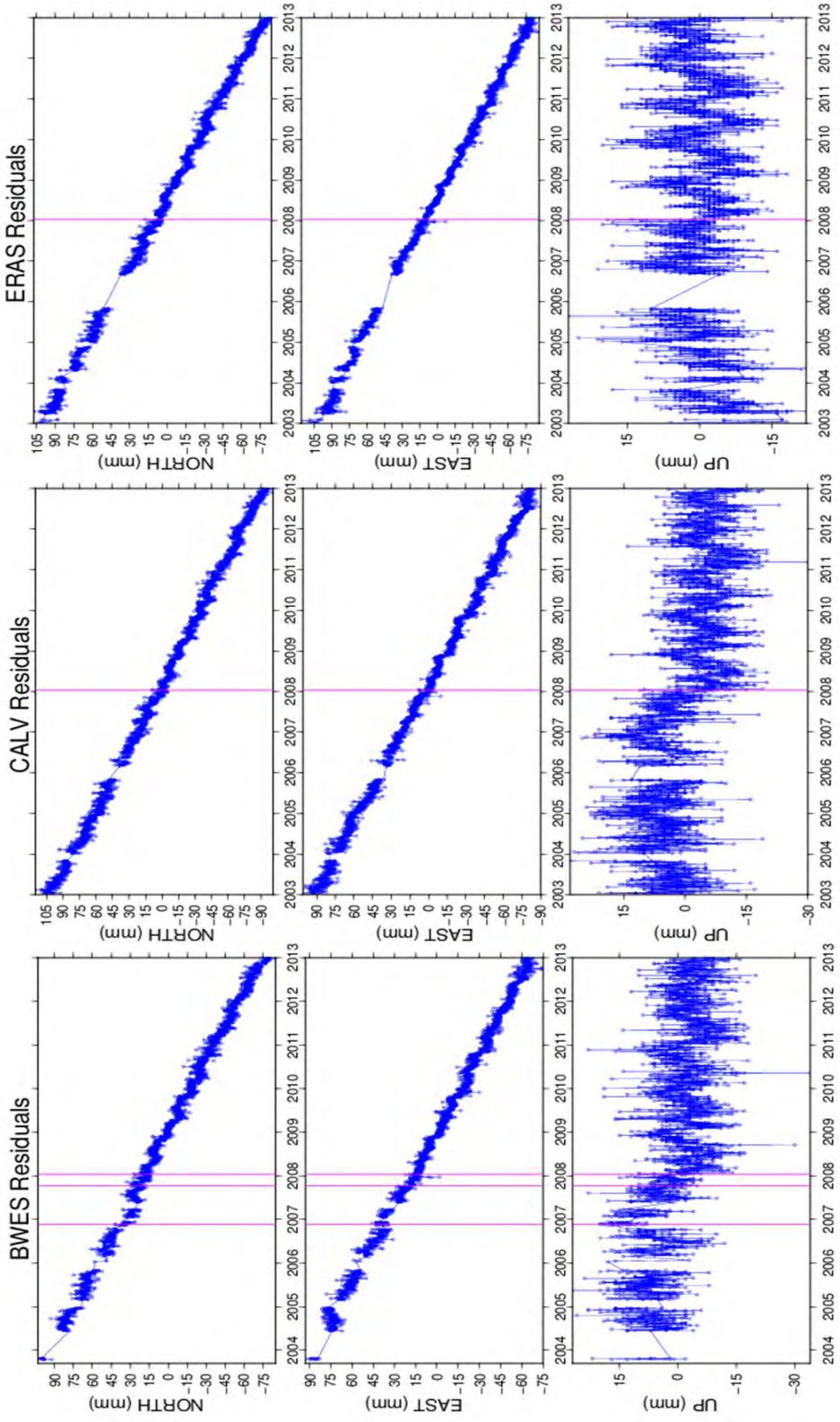

Figure 5.11: BWES, CALV and ERAS show the same discontinuity in the week of 2008 01 09.

There are two seismic events for the period 2007 10 15 to 2008 03 30 as shown in Figure 5.12. In this period, stations VERG, GDAL and EMLO (which have discontinuities that have been accounted for) are closer to the seismic events than stations CALV, BWES and ERAS which have unaccounted for discontinuities. Thus, detected GPS time series discontinuities do not necessarily relate to mining or hydrological seismic activity, despite the detected discontinuities co-inciding with seismic events of such nature.

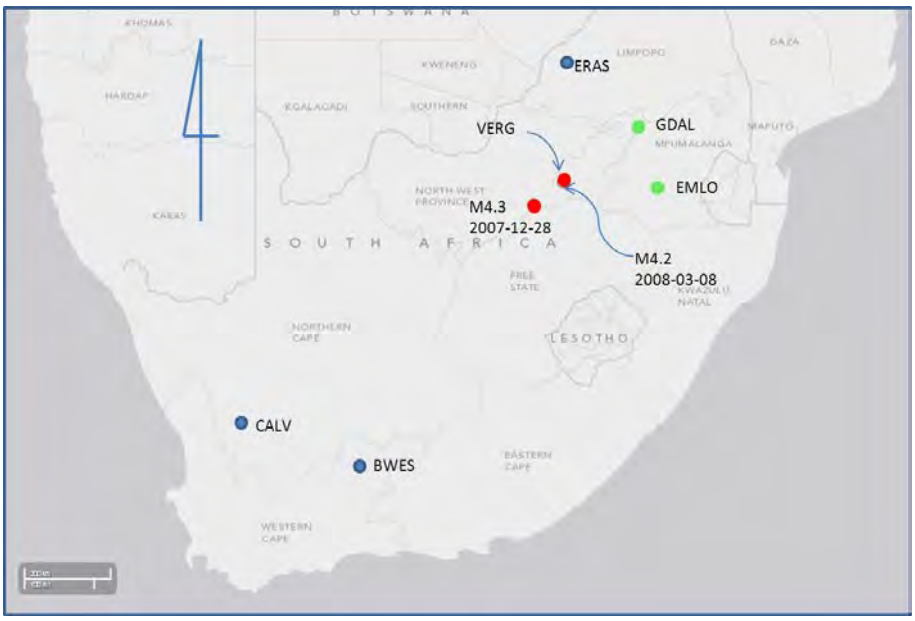

Figure 5.12: Seismic activity for the period 2007 10 15 to 2008 3 30. Seismic activity above 3.5 are depicted with red circles. Stations with accounted for discontinuities are for this period are shown in green, and stations with unaccounted for discontinuities are shown with blue circles. Station VERG is in the same vicinity as a seismic event, and is annotated as such for ease of view. Station VERG discontinuities are accounted for.

Similarly, for stations NYLS, PMBG and TDOU, their unaccounted for discontinuities are not related to seismic activity. Figure 5.13 shows the geographical relation between the seismic activity and stations NYLS, PMBG and TDOU for the period 2010 11 30 to 2011 02 28. Four of the five seismic events occurred between 2011 01 07 and 2011 01 25 with magnitudes 4.1, 4.2, 4.4 and 4.4, with the fifth registering at 4.6 on 2011 02 21. The unaccounted for discontinuities occurred on the 2011 01 15, but is geographically unrelated.

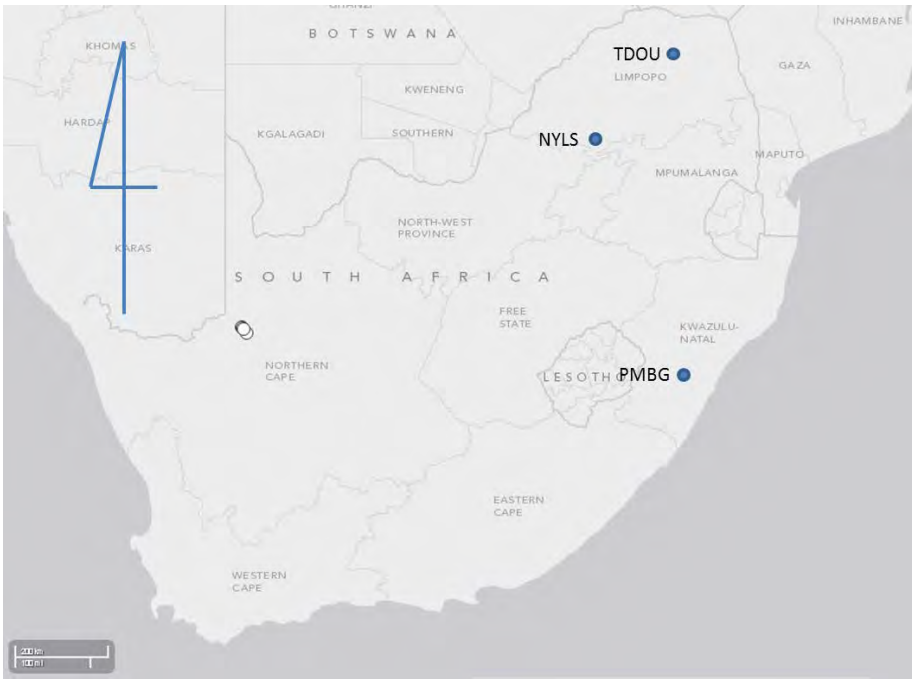

Figure 5.13: Seismic activity for the period 2010 11 30 to 2011 02 28. Seismic activity above 3.5 are depicted with white circles. Five such events occurred in the said period. Stations with unaccounted for discontinuities are shown with blue circles.

Station BFTN has unexplainable behaviour too as is illustrated in Figure 5.14. BFTN is excluded from the calculation of a South African network velocity and Euler vector because of its large number of outliers computed in the combined solution.

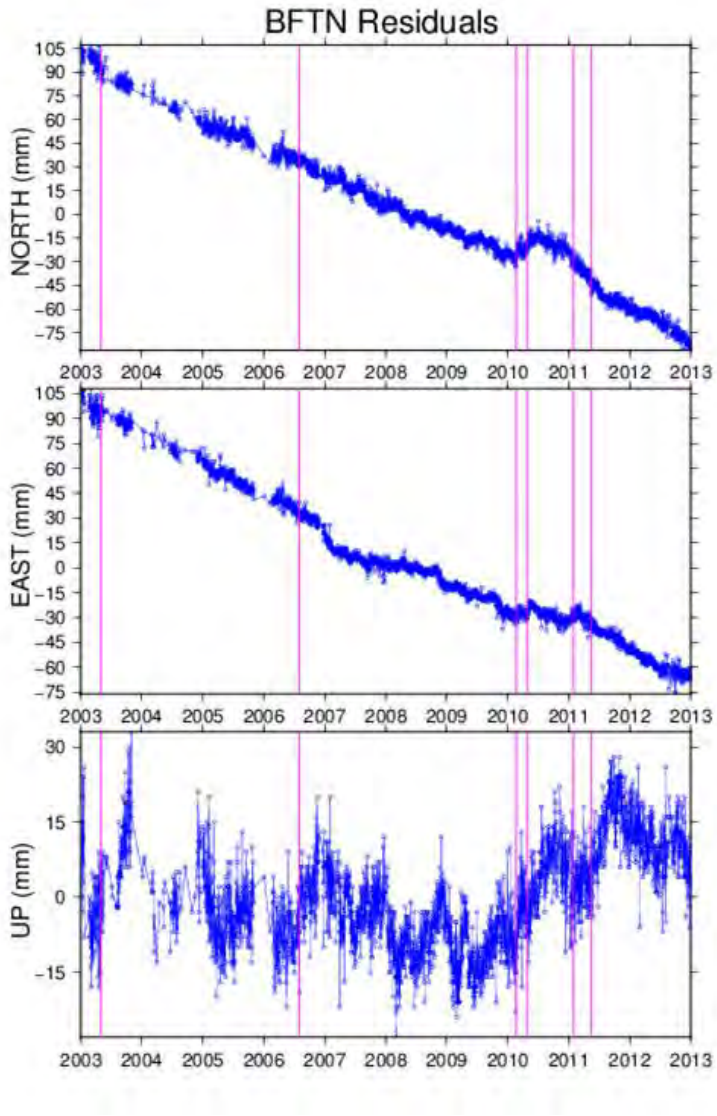

Figure 5.14: Time series of BFTN in which the station behaviour is unaccounted for.

Working with limited station information is challenging, and it becomes difficult to answer questions that relate to station behaviour. It becomes even more challenging when dealing with a topic such as plate tectonics, in which discontinuities may be misinterpreted as tectonic activity. For this project, the computed velocities are key to establishing an Euler vector. Stations with low velocity certainty may erroneously deem that South Africa is underlain by more than one plate, or vice versa.

Beyond this project, if an African Reference Frame (AFREF) is to be established, then Trignet, AFREF and the ITRF has to be in sync. At this moment in time, with the lack of logging of metadata (such as station maintenance), this condition may be difficult to satisfy.

5.2 Outliers

A total of 7034 outliers were detected. This equates to 2.7 % of the total population of 252475 observations. That is 97 % of the observations are retained to compute discontinuities and the uncertainty at each station. This 97 % of retained data is indicative of the maintenance of the station behaviour.

The graphic in Figure 5.15 is indicative of the improvement made to the time series once the outlier algorithm is applied.

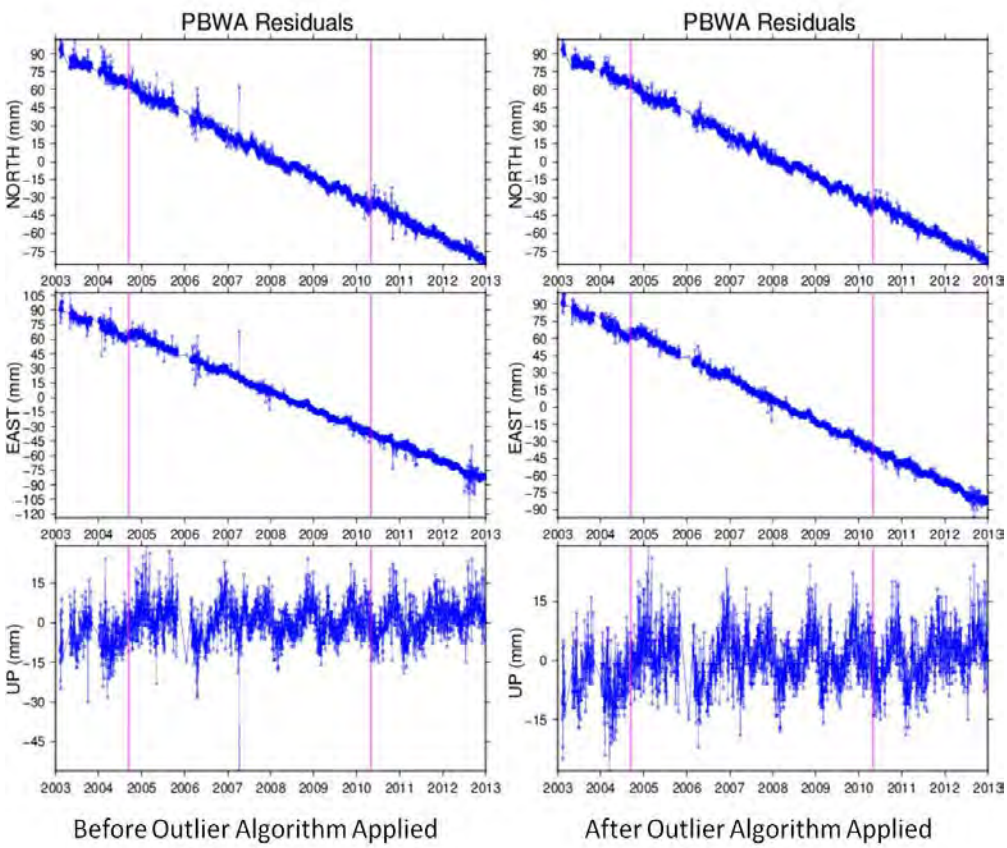

Figure 5.15: Station PBWA time series showing the improvement once the outlier algorithm is applied to its data Series. The series on the left is before the algorithm is applied and the series on the right is the resultant outlier free data set.

Comparing the two time series in Figure 5.15, the large number of outliers (especially around 2004) has reduced after the algorithm has been applied. The series on the right also emphasises that the station behaviour is maintained. The seasonal effects is very evident in the "Up" component.

Analysing the first 3 years (2003, 2004 and 2005) of observations for this project in which the threshold was adjusted to accept 12 hour GPS RINEX files as opposed to a threshold of 20 hours when screening RINEX files, then this period yields 2937 outliers. This equates to 42 % of the total number of outliers and 4.9 % of the total population between 2003 and 2005. This is almost double the average of 2.7 % outliers for the entire 10 year period.

This high percentage may be attributed to the 14 hour Trigtnet files (less

observations to resolve integer ambiguities), to the fewer number of available GPS stations in earlier years or to a combination of these factors.

The 12 stations that had more than 5 % of outliers were IGS stations. These 12 stations are remotely situated in terms of this project's network, hence longer baselines have to be resolved in order for their daily positions to be computed. Generally, baselines between IGS stations, and IGS and Trignet stations for this project are longer as compared to the average 200 km Trignet baselines.

Calculating the correlation between the percentage of outliers and station velocity uncertainty, which uses a white + flicker noise model, yields a value of 0.38 for stations with more than 1000 observations (and excluding stations with greater than 10 % of outliers i.e. GOUG and ANTC). Analysing the IGS and Trignet stations independently, then correlations of 0.63 and 0.37 are computed respectively.

The significant correlation computed independently for IGS suggests that an increase in the percentage of outliers is associated with an increase in the velocity uncertainty at IGS stations.

On the other hand, the independent Trignet correlation of 0.37 suggests that a decrease in percentage of outliers does not necessarily equate to a decrease in velocity uncertainty at Trignet stations.

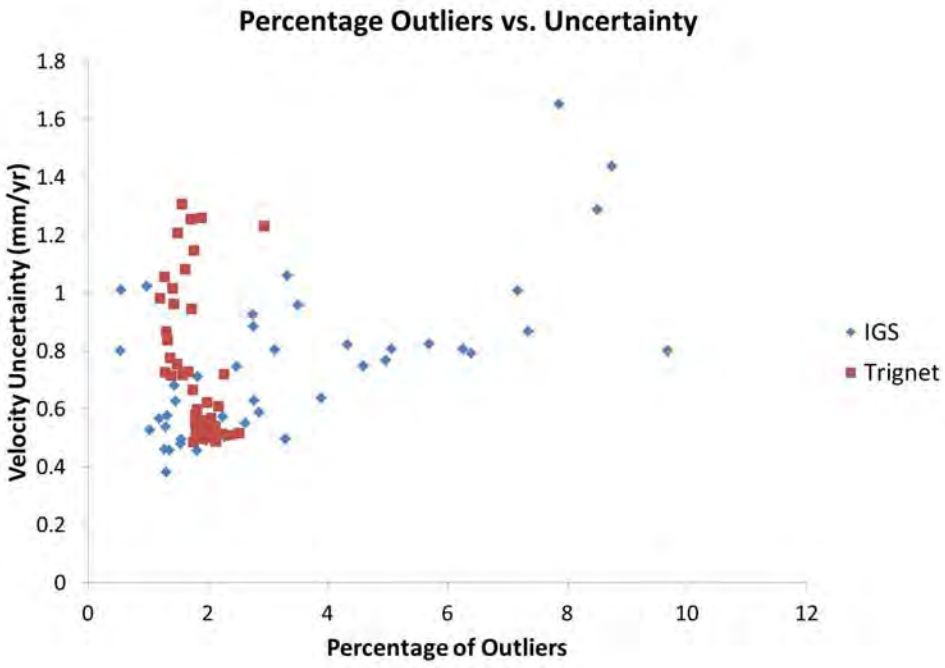

Figure 5.16: Outlier vs. velocity uncertainty graph for IGS and Trignet stations. The graph reveals the difference in uncertainty behaviour between IGS stations and Trignet stations that have more than 1000 observations.

The outlier vs. uncertainty graph in Figure 5.16 emphasises the difference in velocity uncertainty behaviour between the IGS and Trignet stations. This difference in behaviour may be due to the poor beacon construction of Trignet stations, in which the tectonic and long term station stability were not considered.

5.3 Velocity Computation

The IGS (along with the supporting organisations) is the internationally accepted organisation in determining an ITRF. In developing an ITRF, position and velocity of IGS stations are determined and published. Thus, it is interesting to verify this project's computed velocities by comparing them to the IGS published velocities. It is also understood that because this project is referenced to the ITRF, any deficiency in the ITRF is inherited by this project's results. This verification will also serve to determine whether acceptable velocities can be computed by accepting segments of the time series to represent a GPS station.

5.3.1 Velocity Estimation Precision: IGS stations

In determining station velocities with the use of 10 years of GPS data, discontinuities and outliers were considered. Time series segments with the longest observing period, that gave optimum least squares results when combining the 10 years of NEQ solutions were selected to represent the respective station velocities.

Table 5.2 summarises the comparison of the computed velocities with that of the published velocities for IGS stations. It is expected (borne from the analyses of the work by Altamimi et al. (2011)) that each velocity computation to compare better than 1 mm/yr for each of the horizontal co-ordinate components and better than 1.5 mm for the height component. Of the 48 IGS stations, only 31 stations (10 IGS stations do not have published velocities, and a further 7 were excluded) were eventually selected to align the network to the ITRF and to compute a velocity field by combining 10 years of daily NEQ files.

The 7 excluded stations are highlighted in bold print in Table 5.2.

IGS Station Exceptions

Of the chosen IGS subset of stations, a few exceptions were made. Station SYOG, MALI and SEY1 were included despite their 3.2 mm/yr Height, 1.7 mm/yr Height and 1.2 mm/yr Easting respective disagreement with the IGS.

Station SYOG was included to allow better network distribution as there are very few GPS stations between South Africa and Antarctica. Also, the properties of the SYOG time series were such that the discontinuities split the time series into three approximately equal segments (see Figure 5.7). Selecting the earliest segment gave the largest height misclosure of 4.9 mm/yr. Constraining either of the two remaining segments resulted in a similar magnitude misclosure, but opposite in orientation. Considering the two latter segments, the unconstrained SYOG segment (as opposed to the segment that is being constrained), in either scenario shows better agreement with the IGS published velocities for SYOG (within 1 mm/yr). This effect may be as result of GIA (Prawirodirdjo, 2004), which was not accounted for in this project. The final three year segment was therefore selected to represent SYOG's site velocity.

Similarly, SEY1 and MALI, which just about exceeds the threshold in Easting and Height respectively were retained to allow better GPS distribution and density on the African plate.

Excluded IGS Stations

Stations ZAMB,COCO, YIBL, PARC and IISC were all excluded because they failed the threshold test. Analysis of these stations may reveal reasons for their poor performance. Station ZAMB has very sparse data, with large data gaps which yield an unreliable velocity (data gaps should not exceed 8 weeks (Blewitt, 2002)).

Station COCO is situated close to a tectonically active plate boundary and may succumb to tectonic noise (Rebischung et al., 2011). The station beacon construction is not tied to bedrock, and has its concrete foundation settled in sand, biasing the velocity (Combrinck and Chin, 2001). Also JPL and the IGS publish different velocities for station COCO.

Despite YIBL six year data span, its data series shows a large data gap (almost a year gap between 2007 and 2009) as well as very sparse data in the year 2005, which bias the computed velocity (Blewitt, 2002). There is no continuous segment that exceeds 2.5 years.

Station PARC is constructed on a roof top of a building that is not tied to bedrock. Analysis of the time series suggest a very noisy station, which may bias the velocity solution. (e) The reason for IISC's large discrepancy is not evident.

Station RBAY and VESL were excluded despite agreeing quite well with the IGS published velocities. This exclusion was because of their sparse data time series.

Earthquake affected station: ANTC

Importantly, station ANTC was included in the network despite the 2010 earthquake that it experienced (see 5.9). For this station, only the data between 2003 and 2010 were considered to compute its velocity, to compute a network velocity, and to align the network.

Table 5.2: Difference in estimated and published IGS velocities expressed as North, East and Height components

Station Name	**NDiff (m/yr)**	**EDiff (m/yr)**	**Vdiff (m/yr)**	**Tectonic Plate**	**Segment Span (yrs)**	**Align to ITRF**
ANTC	0.0007	0.0005	0.0010	SOAM	8	Yes
BRAZ	0.0004	0.0009	-0.0004	SOAM	6	Yes
BRFT	0.0008	-0.0002	0.0012	SOAM	3.5	Yes
DAV1	0.0000	-0.0005	0.0004	ANTA	4.5	Yes
DGAR	0.0001	-0.0001	-0.0008	AUST	7.5	Yes
GRAS	0.0002	-0.0002	0.0006	EURA	8	Yes
HARB	0.0000	-0.0004	0.0004	AFRC	7	Yes
HRAO	0.0006	0.0001	-0.0010	AFRC	4	Yes
KERG	0.0003	-0.0010	0.0006	ANTA	9	Yes
MALI	0.0006	-0.0003	**0.0017**	AFRC	5.5	Yes
MAS1	0.0000	-0.0003	-0.0011	AFRC	4.5	Yes
MBAR	0.0003	-0.0003	0.0006	AFRC	6	Yes
NKLG	0.0006	-0.0005	0.0005	AFRC	7	Yes
NOT1	0.0001	-0.0002	0.0005	EURA	10	Yes
OHI2	0.0007	0.0001	-0.0008	ANTA	6	Yes
PDEL	-0.0004	-0.0005	0.0000	EURA	4.5	Yes
POL2	0.0003	-0.0003	-0.0011	EURA	7	Yes
POLV	0.0004	-0.0004	-0.0005	EURA	10	Yes
QAQ1	0.0001	-0.0002	-0.0002	NOAM	9	Yes
RABT	0.0001	-0.0002	-0.0010	AFRC	6	Yes
RAMO	0.0005	-0.0006	0.0004	ARAB	9	Yes
REUN	0.0003	-0.0005	0.0005	AFRC	3	Yes
SCH2	0.0003	0.0000	-0.0014	NOAM	5	Yes
SCUB	-0.0002	0.0006	0.0003	NOAM	9.5	Yes
SEY1	0.0004	**0.0012**	-0.0007	AFRC	6	Yes
SUTH	0.0004	-0.0003	0.0007	AFRC	5	Yes
SYOG	0.0007	-0.0005	**-0.0032**	ANTA	4	Yes
USNO	0.0003	0.0001	-0.0009	NOAM	10	Yes
WIND	0.0006	-0.0009	0.0013	AFRC	4	Yes

Tabel 5.2 continued

Station Name	NDiff (m/yr)	EDiff (m/yr)	Vdiff (m/yr)	Tectonic Plate	Segment Span (yrs)	Align to ITRF
WSRT	-0.0001	-0.0002	0.0000	EURA	10	Yes
YEBE	0.0002	-0.0001	0.0001	EURA	7	Yes
COCO	-0.0012	0.0006	0.0019	AUST	3.5	no
IISC	0.0007	-0.0011	0.0016	INDI	3	no
MAL2	0.0030	-0.0018	0.0002	AFRC	4	no
PARC	0.0013	0.0003	0.0016	SOAM	4	no
RBAY	0.0005	-0.0007	0.0003	AFRC	10	no
VESL	0.0008	-0.0007	0.0000	ANTA	10	no
YIBL	0.0008	0.0009	0.0020	AFRC	6	no
ZAMB	0.0005	-0.0005	0.0024	AFRC	10	no

Comparison between IGS computed velocities and the published velocities. Table 5.2 contains the North, East and Height difference, the tectonic plate for each station and whether the station is used in minimally constraining the network to the ITRF2008 in the combination solution. The plates are:- SOAM : S.America, AUST : Australia, NOAM : N.America, EURA : European, ARAB : Arabian, ANTA: Antarctica, AFRC : African and INDI : Indian plate.

Computing standard deviation of the agreement between this project's 31 accepted IGS computed velocities with that of the IGS08 published velocities, yields 0.0003, 0.0005, and 0.0010 m/yr for Northing, Easting and Height respectively. This agreement is indicative of the precision of the network. This high precision suggests that the alignment of the network to the ITRF is acceptable and that the computed velocities for non IGS stations within this project's network (such as Trignet stations) may have similar precision. Also, the agreement between the IGS published velocities and the computed velocities is independent of the length of the data span of the segment representative of the station velocity (that is for segments greater than 2.5 years) which is emphasised by a 0.23 computed correlation.

Excluding SYOG, MALI, and SEY1 (the IGS stations that were made exception for in aligning to the ITRF), then an RMS of the post fit velocity residuals of 0.00037, 0.00042 and 0.00072 m/yr (as listed in Table 5.3) for North, East and Height respectively is computed. This RMS of the post fit residuals is of equal magnitude to the WRMS of the post fit velocity residuals of the 14 parameter transformation between the ITRF2005 and ITRF2008 (these parameters are cited by Altamimi et al. (2011)).

Table 5.3: WRMS and RMS of the post fit velocity residuals for the 14 parameter transformation from ITRF2005 to ITRF2008 and this Projects Network to the ITRF2008 respectively, as well as average velocity uncertainty.

	North (m/yr)	**East (m/yr)**	**Height (m/yr)**
ITRF05 - ITRF08 (WRMS)	0.0004	0.0004	0.0007
Proj NetW. - ITRF08 (RMS)	0.00037	0.00042	0.00072
Velocity Uncertainty (Mean)	0.00037	0.00037	0.00076

In computing a 14 parameter transformation between the ITRF2005 and ITRF2008 using 179 common stations, the WRMS of the post fit residuals of 0.0004, 0.0004, and 0.0007 m/yr for North, East and Height components are respectively (Altamimi et al., 2011). This WRMS of the post fit residuals may be as a result of ITRF2005 deficiency, ITRF2008 deficiency, velocity precision or a combination of these factors. The GPS intrinsic precision has improved minimally overtime (Ray, 2010). This is true for GPS precision whether expressed solely in the ITRF2005 or ITRF2008 (Ray, 2010). With this in mind then the WRMS of the post fit residuals may be representative of the GPS intrinsic velocity precision, rather than being entirely dominated by ITRF system noise.

This WRMS of the post fit velocity residual between ITRF's is echoed in section 5.1.1, in which an average velocity uncertainty of 0.00037, 0.00037 and 0.00076 m/yr is computed for the North, East and Height components respectively, suggesting that the WRMS of the post fit residuals between the ITRF2005 and ITRF2008, and the RMS of the post fit residuals between this projects estimated IGS velocities and the published IGS velocities may indeed represent GPS intrinsic velocity precision.

5.3.2 Trignet velocity field

The interrogation of Trignet segment spans forms the basis of its station velocity analysis. Only segments with data spans in excess of 2.5 years were accepted to represent the relevant station's velocity. If a station has two or more segments, then the segment with the longest data span that does not have significant data gaps and has a data series that is sufficiently dense is selected to represent that station's velocity.

Table 5.4 shows the computed velocity for the North, East and Height components for the Trignet stations along with the data span of the selected stations.

Table 5.4: Computed velocities of the North, East and Height components for Trignet stations

Station Name	Northing (m/yr)	Easting (m/yr)	Height (m/yr)	Segment Span (yrs)	Type
ANTH	0.0183	0.0171	-0.0001	10	TRIGNET
BENI	0.0180	0.0167	-0.0001	3	TRIGNET
BETH	0.0178	0.0173	-0.0002	5	TRIGNET
BISO	0.0185	0.0150	0.0002	2.5	TRIGNET
BRIT	0.0182	0.0188	0.0001	4	TRIGNET
BRNK	0.0182	0.0182	-0.0001	2.5	TRIGNET
BWES	0.0187	0.0172	-0.0005	5	TRIGNET
CALV	0.0188	0.0177	-0.0005	5	TRIGNET
CTWN	0.0187	0.0171	-0.0001	4.5	TRIGNET
DEAR	0.0184	0.0175	-0.0002	10	IGS
DRBN	0.0174	0.0170	-0.0001	5	TRIGNET
ELDN	0.0180	0.0164	-0.0007	6	TRIGNET
EMLO	0.0170	0.0182	0.0010	5	TRIGNET
ERAS	0.0177	0.0188	0.0006	5	TRIGNET
GDAL	0.0181	0.0190	-0.0014	5	TRIGNET
GRHM	0.0176	0.0160	-0.0001	5	TRIGNET
GRNT	0.0186	0.0179	-0.0004	5	TRIGNET
HEID	0.0175	0.0172	0.0010	2.6	TRIGNET
HNUS	0.0188	0.0171	-0.0009	10	IGS
IXOP	0.0177	0.0169	-0.0032	2.6	TRIGNET
KLEY	0.0182	0.0180	-0.0003	10	TRIGNET
KMAN	0.0183	0.0186	-0.0002	7.5	TRIGNET
KSTD	0.0179	0.0178	0.0003	5	TRIGNET
LGBN	0.0190	0.0178	-0.0009	10	TRIGNET
LSMH	0.0177	0.0175	-0.0002	7.5	TRIGNET
MALM	0.0184	0.0176	-0.0019	3	TRIGNET
MBRG	0.0183	0.0176	-0.0012	3.5	TRIGNET
MFKG	0.0191	0.0192	-0.0008	6	IGS
MRIV	0.0174	0.0172	-0.0002	2.7	TRIGNET
NSPT	0.0174	0.0180	-0.0001	10	TRIGNET
NYLS	0.0177	0.0186	-0.0009	6	TRIGNET
PBWA	0.0173	0.0187	-0.0001	5	TRIGNET
PELB	0.0182	0.0163	-0.0004	5	TRIGNET
PMBG	0.0176	0.0167	0.0000	5	TRIGNET
PRET	0.0161	0.0186	0.0000	7	TRIGNET
PSKA	0.0185	0.0180	-0.0003	8.5	TRIGNET
PTBG	0.0180	0.0184	-0.0007	6	TRIGNET
QTWN	0.0181	0.0170	-0.0004	3.5	TRIGNET
SBOK	0.0189	0.0185	-0.0005	10	IGS
SCOT	0.0182	0.0166	-0.0007	2.7	TRIGNET
SPRT	0.0186	0.0190	-0.0014	2.8	TRIGNET

Tabel 5.4 continued

Station Name	Northing (m/yr)	Easting (m/yr)	Height (m/yr)	Segment Span (yrs)	Type
STBS	0.0189	0.0174	-0.0005	3	TRIGNET
TDOU	0.0159	0.0191	-0.0001	5	IGS
ULDI	0.0178	0.0170	-0.0024	6	IGS
UMTA	0.0176	0.0169	-0.0002	8	IGS
UPTA	0.0184	0.0185	-0.0002	5	TRIGNET
VERG	0.0179	0.0177	-0.0004	4	TRIGNET
WORC	0.0190	0.0176	-0.0023	3	TRIGNET

To improve the consistency of the combined velocity solution, eleven Trignet stations were excluded. This exclusion was based on an iterative solution, which incorporated a crude comparison with velocities generated using the NUVEL-1A velocity model, and examining the outliers. These stations are GEOR, GEOA, BFTN, KRUG, POTG, GREY, CPNT, STAN, OKNY, MBRY and DRBA.

Analysis of these stations time series reveal that: (a) stations GEOR and GEOA have multiple physical locations, and is not suitable for such study. (b) Station BFTN shows unexplainable behaviour as depicted in the time series plot in Figure 5.14. Station BFTN's unexplainable behaviour is echoed by Malservisi et al. (2013), who suggests that the station's position may succumb to hydrological effects. (c) Station KRUG has 6 unaccounted discontinuities in a 6 year period, hence no segment longer than 2.5 years. (d) Stations POTG, GREY, CPNT, STAN, OKNY, MBRY and DRBA all have less than 2.5 years of logged GPS data, or do not have resultant data segments corresponding to more than 2.5 years of logged data.

These computed velocities in Table 5.4 along with the IGS, Trignet stations HRAO, HARB and SUTH velocities as estimated for this project, will be used to solve for an Euler vector for South Africa, determine South Africa plate rigidity, and determine whether the North East Region of South Africa has a statistically different GPS velocity field to the rest of South Africa.

5.3.3 Euler Vector Estimate

This section analyses the computed Euler vector that is derived using the Trignet estimated velocities in section 5.3.2 and introducing the uncertainty value for each estimated station velocity as derived in section 5.1.1.

The consistency of the computed Euler Vector is investigated using two tests: the Altamimi et al. (2012) 3-sigma-3 test in which the residual and

its relation to the input uncertainty is considered, and the second test is a χ^2 goodness-of-fit test (GoF).

The CATS uncertainty computed for each station is used to weight the least squares Euler vector solution. Since the uncertainty is computed in a projected local system (i.e. North, East and Height), it is converted to X, Y and Z cartesian system that is compatible with the Euler vector computation. Thereafter, the weighting takes on the form $1/(uncertainty)^2$, with *uncertainty* representing the uncertainty along the respective X, Y or Z cartesian axes.

An Euler vector with an angular velocity 0.277 deg/Myr (i.e. degrees per million years) and a pole of rotation at latitude 50.768 and longitude -84.865 degrees is computed. In establishing this Euler vector an iterative method was adopted. A description of the solution is as follows. (a) Only station IXOP residual exceeded the 3 mm/yr threshold (the first part of the 3-sigma-3 test). (b) In the second part of the 3-sigma-3 test, in which the residual should not exceed three times the respective station velocity uncertainty, then PRET, TDOU and ULDI fail the test. (b) Including these stations in the solution yields a goodness-of-fit test of 2.43, suggesting very poor fit. These stations were excluded and the solution iterated. (c) Analysis after iteration: All stations passed the 3-sigma-3 test, however a poor GoF value of 1.76 was computed. (d) Eventually a GoF value of 1.07 was computed through iteration by excluding PRET, TDOU, MFKG, ULDI, MBRG, IXOP, SPRT and GDAL.

Station MFKG and IXOP fall outside of the area being investigated. However, MFKG, PRET, TDOU and GDAL have been identified in the previous study by Malservisi et al. (2013) as being problematic. PRET is stationed on top of a building, increasing its uncertainty. MFKG and TDOU are erected in gravel sand (see Table 3.1), rendering them unstable.

Station IXOP has an excessive height velocity as compared to the rest of the South African stations. The GPS height velocity is known to be poorly defined compared to the horizontal component velocities (Blewitt, 2002; Altamimi et al., 2011). For this reason an Euler vector was computed by minimising the height velocities of the input station velocities to zero. The analysis assumes the same procedure as with the height inclusive Euler vector.

Euler Vector: Minimised Height Velocity Solution

For this test, the height uncertainty is also reduced to zero before converting the uncertainty to an XYZ cartesian system.

An Euler vector with an angular velocity of 0.273 deg/Myr and a pole of rotation at latitude 50.845 and longitude -82.828 is estimated through iteration. A final 1.10 GoF is computed by excluding stations PRET, TDOU, MFKG, BENI, GRNT and EMLO. In this computation IXOP is statistically accepted as part of the solution, as well as MBRG, GDAL and SPRT.

The difference in angular velocity between the two solutions equates to 0.4 mm/yr, which is within the error bounds of GPS (error bounds as described by Altamimi et al. (2012)). That said, reducing the height velocity to zero resulted in only 6 stations being excluded as opposed to 8. Three of these stations are common. They are PRET, TDOU and MFKG.

GRNT, along with these three stations are highlighted by Malservisi et al. (2013) as misfits to the computed Euler vector in their study. GRNT may be subject to noise relating the filling of artificial lakes as suggested by Malservisi et al. (2013).

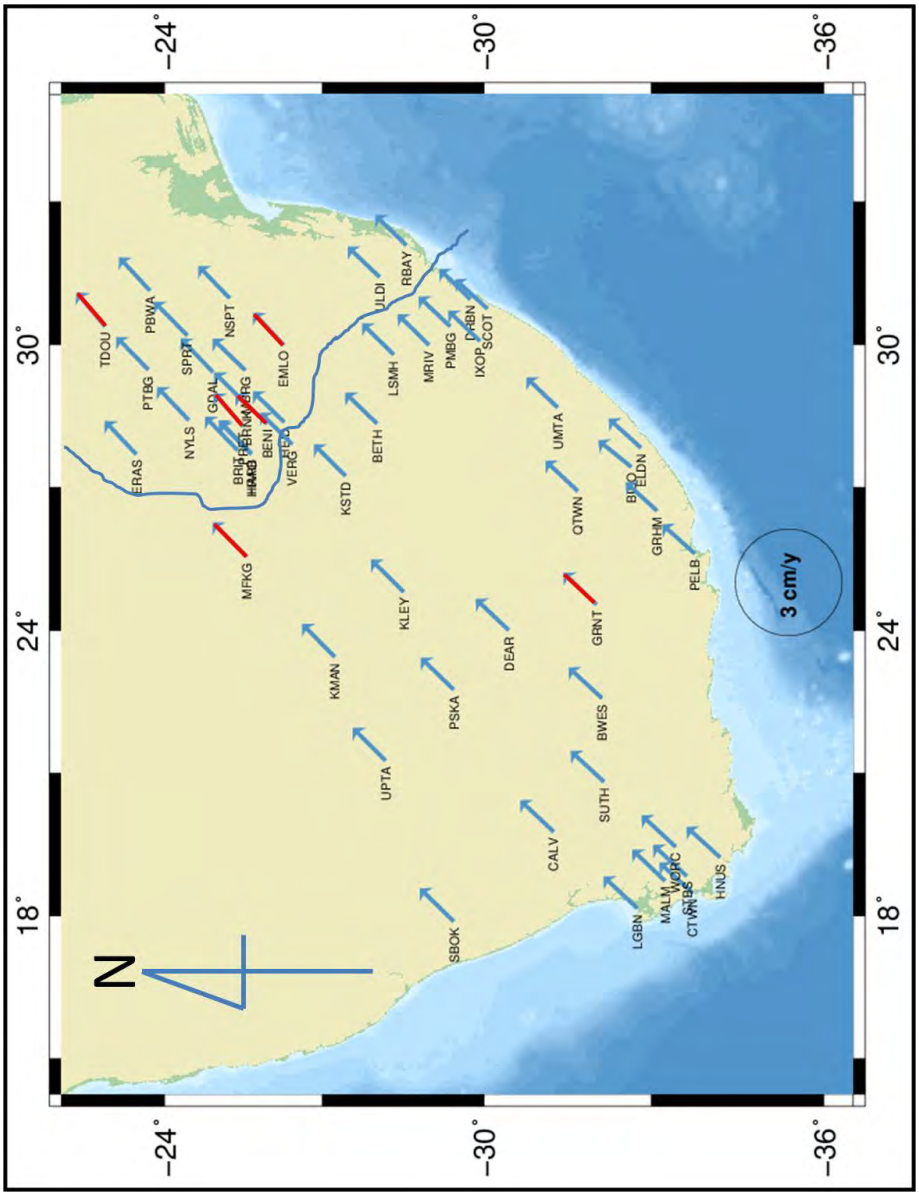

Figure 5.17: South African Velocity Field, showing the investigated North East Region divide. The Red lined arrows are misfit velocities in establishing a South African Euler Vector.

Analysing the North East Euler Vector
An Euler vector for the North East Region is computed and the consistency of the solution is analysed (following the same method of analysis as described in section 5.3.3). Here, the vertical velocity was minimised to zero. The North East boundary is estimated based on the boundary used in the Altamimi et al. (2012) global kinematic model. This boundary is depicted in Figure 5.17.

An initial χ^2 per degree of freedom value of 5.79 was computed. For this solution, stations TDOU, PRET, MBRG and BENI failed the second phase of the 3-σ-3 test. An eventual χ^2 per degree of freedom of 1.09 is computed by excluding stations TDOU, PRET, MBRG, BENI, EMLO and GDAL. The angular velocity computed for this solution is 0.269 deg/Myr, with a pole of rotation at latitude 50.936 and longitude -81.160. These results are statistically similar to the previous Euler computations as described in section 5.3.3.

Stations TDOU, PRET, BENI, GDAL and EMLO were also excluded in the previous solution in which the vertical velocity was minimised as described in section 5.3.3. Station MBRG was excluded in the previously computed solution that included vertical velocities. The fact that the same stations are excluded to attain acceptable GoF values for the computation of the kinematics of the North East Region and for the entire South African velocity network alludes to a constant GPS velocity field across South Africa. This further emphasis that these misfit stations computed velocities may not be representative of the actual site velocities.

The network of stations that surrounds these misfit stations are statistically accepted as part of the greater South Africa GPS velocity field. These misfit stations are also geographically scattered, further alluding to a uniform South African GPS velocity field. These problematic stations may not be suitable for a long term solution.

5.3.4 South African Plate Rigidity

South Africa's Euler vector consistency has been extensively investigated in this section. Within each of the 3 Euler investigations, i.e. Euler height inclusive vector, Euler height exclusive vector and North East Euler Vector, yields GoF value of approximately 1, which suggests a rigid South African plate. Stations MFKG, PRET, TDOU, GRNT, BENI and EMLO are SA velocity field misfits. These misfit station velocities may be attributed to their monumentation. This plate rigidity conclusion is confirmed by Malservisi et al. (2013) study.

5.3.5 Comparing the computed Euler Vector to Previous Work

Table 5.5 summarises the comparison of this projects computed Euler Vector to previously computed Euler vectors that may describe South Africa's velocity field.

Table 5.5: Comparison of Euler Vectors computed for South Africa and the Nubian Plate

Study	**Angular Velocity (deg/Myr)**	**Lat Deg**	**Long Deg**
Fernandes et al. (2004)	0.256	51.07	-81.11
Stamps et al. (2008)	0.244	51.24	-80.39
Altamimi et al. (2012)	0.262	50.05	-80.97
Malservisi et al. (2013)	0.275	49.71	-82.39
Computed for Project	0.273	50.85	-82.83

Fernandes et al. (2004) computes an Euler vector for the Nubian plate using 15 GPS stations. An angular velocity of 0.256 with a pole of rotation at latitude: 51.07 and longitude: -81.11 is computed in their study.

In determining a set of stations that best describes a plate, Stamps et al. (2008) chose four sensor stations that showed the best agreement in describing the Nubian Plate. Thereafter, each of the remaining GPS stations within the Nubia system were added one-by-one to the four core stations based on their statistical agreement. A subset of 14 stations best described the Nubian kinematics within the ITRF2005 reference frame. They compute

a pole of rotation at latitude: 51.2445 longitude: -80.3948 and an angular velocity of 0.2441 degrees per million years (deg/Myr).

Altamimi et al. (2012) computes the Nubian Plate kinematics using 11 GPS stations as part of a global solution within the ITRF2008 reference frame. Their solution excludes HRAO, HARB and RBAY because of these stations proximity to the proposed Nubia-Somalia plate boundary as it traverses South Africa. Their Euler vector computed for South Africa has an angular velocity of 0.262 deg/Myr with a pole of rotation at latitude: 50.0544 and longitude: -80.9733.

Malservisi et al. (2013) compute an Euler vector for South Africa of latitude: 49.71, longitude: -82.39 and 0.275 deg/Myr using 36 Trignet stations within the ITRF2005.

The difference in position is minor, however the difference in the angular velocities between certain projects are significant. Using Altamimi et al.'s (2012) study as a reference, Stamps et al. (2008) compute an angular velocity that differs by 2 mm/yr, which exceeds the current expected velocity accuracy. This may be attributed to differences in reference frame and in station selection.

The Fernandes et al.'s (2004) study agrees well with Altamimi et al.'s (2012) study (within 1 mm/yr linear velocity). However, 8 of the 15 stations had less than 2,5 years of GPS observations (see section 3.1.2) which lowers the confidence in the computation, and, hence, is not considered.

Comparing Malservisi et al.'s (2013) computed Euler vector to Altamimi et al.'s (2012) computed Euler vector, a difference of 1.4 mm/yr in the linear velocity is observed. This difference may also be attributed to differences in reference frames, as well as to the spatial distribution of the stations as Malservisi et al.'s (2013) study was centred around South Africa, rather than the entire Nubian Plate.

Similarly, this project's angular velocity agrees within 1.2 mm/yr to that computed by Altamimi et al. (2012).

This project, Malservisi et al. (2013), and Altamimi et al. (2012) Euler vectors are statistically similar. However this project shows more agreement with the Malservisi et al. (2013) study. The Altamimi et al. (2012) study made use of 11 stations across the Nubian plate, whereas this projects Euler vector is computed with South African station velocities.

The similarity between this project's solution and Malservisi et al.'s (2013)

solution may be due to (a) this study and the Malservisi et al. (2013) study being centred around South Africa; (b) both making use of Trignet data; (c) similar data spans were used in both studies; (d) both studies used the Bernese 5.0 Precise GNSS Processing software to process the data; and (e) Malservisi et al. (2013) makes use of the Alan Variance of Rate (AVR) estimator to determine GPS station velocity uncertainty which has similar performance to the CATS algorithm (Hackl et al., 2011).

The consistency of the Euler vector computations between these studies (i.e Altamimi et al. (2012), Malservisi et al. (2013) and this study) validates this project's method in determining a South African Euler Vector.

5.3.6 Synthesis of Results

In concluding this section, the optimal solution that is representative of South Africa's GPS kinematics is the minimised vertical velocity solution that incorporates all Trignet stations (with acceptable data spans) used for this project, excluding PRET, TDOU, MFKG, BENI, GRNT and EMLO. PRET is constructed on a building, MFKG and TDOU's foundation are placed in unstable ground and not tied to bedrock, GRNT may be affected by hydrological affects, and EMLO and BENI monumentation is unknown.

The Euler vector that relates to this solution has an angular velocity of 0.273 deg/Myr, with a pole of rotation at latitude 50.845 and longitude -82.828.

Analysis of an independent North East Region reveals that statistically similar Euler vectors are computed for this independent solution and for the entire Trignet network solution. Also, these solutions exclude a similar set of stations.

With respect to aligning to the ITRF2008, an RMS of the postfit velocity residuals of 0.00037, 0.00042 and 0.00072 m/yr for North, East and Height components respectively was computed. This RMS of the post fit residuals is similar to the WRMS post-fit velocity residuals of the 14 parameter transformation from ITRF2005 to ITRF2008. This suggest that this project's computed velocity may have attained the current ITRF velocity precision threshold.

This project finds that South Africa, which includes the North East Region, has a uniform velocity field. This implies that there are no intra-continental blocks and no evidence of an extension of the EAR in South Africa. The reasons for this support are: (a) a uniform GPS velocity field has been established with the use of Trignet and IGS GPS data; (b) the computed Euler vector is in agreement with previous kinematic studies (such as Altamimi

et al. (2012) and Malservisi et al. (2013)); and (c) this projects computed velocity field has similar precision to the current ITRF2008 velocity solution.

Chapter 6

Implications and Recommendations

The use of GPS in the study of tectonic plate kinematics over the years has proved very effective. For plates to be accurately modelled, the GPS data processing strategy and the management of the time series are essential. This is particularly necessary when the rifting rate between tectonic plates are small, approaching the GPS velocity precision threshold.

The EAR has one of the slowest divergent rates, with 6-7 mm/yr at the Northern end and approximately 2 mm/yr at about 25 degrees south (which coincides with the northern latitudes of South Africa). Hence, to determine the kinematics of the North East Region of South Africa, through which the Nubia-Somalian boundary may traverse, careful management of the data series is essential to avoid bias.

An extensive research method was applied to determine an accurate and precise South African GPS velocity field. The results of the research are summarised under "Synthesis of Results" in section 5.3.6. This chapter contains implications of the results and recommendations.

6.1 Implications

A high quality South African velocity field has been established for this project. Based on these Trignet velocities, an Euler vector and its consistency has been validated. The South African GPS velocity field is uniform within the scope of this project. The implications of a uniform South African velocity may be twofold:

1. If South Africa's velocity field is accepted as uniform, then the EAR is likely to extend east of South Africa, rather than through the North East

Region of South Africa.

2. Secondly, the rifting rate of the Nubian-Somalia boundary at the latitudes of South Africa is approximately 2 mm/yr. The current GPS velocity precision is 1-2 mm/yr. To be able to detect rifting velocities of this magnitude, then a system that has a velocity precision of better than 0.7 mm/yr is required. This project velocity precision exceeds this threshold.

Further implications of this study is that GPS global kinematic studies such as the ITRF2008 plate motion model, should include stations such as HRAO and HARB (rather than being excluded on the basis of tectonic boundary proximity) in its study as South Africa's GPS velocity field is uniform. This will improve the stability of the Nubian velocity computation as more stations will be available.

6.2 Recommendations

It is recommended that Trignet station beacon construction be documented and made available to users. All new Trignet stations should be tied to bedrock (if possible) to ensure a long term, stable solution.

To improve the Trignet network and to investigate poor performing stations, it is recommended that the Trignet network be computed daily. These daily computations may be combined to form various long term Trignet realizations, following the combined methodology presented in this thesis. This practice should be extended to an African Reference Frame (AFREF) in which Trignet, AFREF and the ITRF frames are aligned.

It is recommended that Trignet station events such as maintenance, antenna changes, equipment changes, etc., be documented to aid in the detection of discontinuities. The Variance Factor Discontinuity Algorithm adopted for this project should be extended to include incremental windows, so that jumps in time series that are separated by a minimal time difference can be detected.

The latest version of Bernese GNSS software (i.e. Bernese 5.2) should be used to process daily GPS solutions to determine accurate and precise station velocities. Bernese version 5.2 makes use of improved atmospheric models and processing strategies which improves the precision of the daily solution. Along with the improved processing algorithms, the ITRF2013 should be employed when available, and all daily solutions should be aligned to this latest ITRF.

With respect to station segment selection to represent site velocity, a method of tying the resultant segments before and after a time series discontinuity to compute the combined solution is an alternative approach that can be applied (rather than selecting station time series segments to represent site velocities) and should be investigated within the realms of a South African velocity field.

References

Altamimi, Z. (2003), 'Discussion on How to Express a Regional GPS Solution in the ITRF', *EUREF publication* pp. 162–167.

Altamimi, Z., Boucher, C. and Sillard, P. (2002), 'New trends for the realization of the International Terrestrial Reference System', *Advances in Space Research* **30**(2), 175–184.

Altamimi, Z. and Collilieux, X. (2008), 'IGS contribution to the ITRF', *Journal of Geodesy* **83**(3-4), 375–383.

Altamimi, Z., Collilieux, X., Legrand, J., Garayt, B. and Boucher, C. (2007), 'ITRF2005: A new release of the International Terrestrial Reference Frame based on time series of station positions and Earth Orientation Parameters', *Journal of Geophysical Research* **112**(B9), 1–19.

Altamimi, Z., Collilieux, X. and Boucher, C. (2008), 'Accuracy assessment of the ITRF datum definition', *VI Hotine-Marussi Symposium on Theoretical and Computational Geodesy* **132**, 101–110.

Altamimi, Z., Collilieux, X. and Métivier, L. (2011), 'ITRF2008: An improved solution of the International Terrestrial Reference Frame', *Journal of Geodesy* **85**(8), 457–473.

Altamimi, Z., Métivier, L. and Collilieux, X. (2012), 'ITRF2008 plate motion model', *Journal of Geophysical Research* **117**(B7), 1–14.

Bird, P. (2003), 'An updated digital model of plate boundaries', *Geochemistry, Geophysics, Geosystems* **4**(3).

Blewitt, G. (2002), 'Effect of annual signals on geodetic velocity', *Journal of Geophysical Research* **107**(B7), 2145.

Buck, W. R. (1997), 'Bending thin lithosphere causes localized 'snapping' and not distributed 'crunching': Implications for Abyssal Hill Formation', *Geophysical Research Letters* **24**(20), 2531–2534.

Calais, E., Ebinger, C., Hartnady, C., Nocquet, J. et al. (2006), 'Kinematics of the East African Rift from GPS and earthquake slip vector data', *Special Publication - Geological Society of London* pp. 1–33.

Chu, D. and Gordon, R. (1999), 'Evidence for motion between Nubia and Somalia along the Southwest Indian Ridge', *Nature* **398**(March), 64–67.

Collilieux, X., Altamimi, Z., Coulot, D., van Dam, T. and Ray, J. (2010), 'Impact of loading effects on determination of the International Terrestrial Reference Frame', *Advances in Space Research* **45**(1), 144–154.

Combrinck, W. and Chin, M. (2001), 'IGS stations: Station and regional issues', *Physics and Chemistry of the Earth, Part:A Solid Earth and Geodesy* **26**(6-8), 539 – 544. Proceedings of the First COST Action 716 Workshop Towards Operational GPS Meteorology and the Second Network Workshop of the International GPS Service (IGS).

Dach, R., Hugentobler, U., Fridez, P. and Meindl, M. (2007), 'Bernese GPS software version 5.0', *Astronomical Institute, University of Bern* .

DeMets, C., Gordon, R. G., Argus, D. F. and Stein, S. (1990), 'Current plate motions', *Geophysical Journal International* **101**(2), 425–478.

DeMets, C., Gordon, R. G. and Argus, D. F. (2010), 'Geologically current plate motions', *Geophysical Journal International* **181**(1), 1–80.

Dong, D., Fang, P., Bock, Y., Cheng, M. K. and Miyazaki, S. (2002), 'Anatomy of apparent seasonal variations from GPS-derived site position time series', *Journal of Geophysical Research: Solid Earth* **107**(B4), ETG 9–1–ETG 9–16.

Fairhead, J. and Henderson, N. (1977), 'The seismicity of southern Africa and incipient rifting', *Tectonophysics* **41**, 19–26.

Fernandes, R., Ambrosius, B., Noomen, R., Bastos, L., Combrinck, L., Miranda, J. and Spakman, W. (2004), 'Angular velocities of Nubia and Somalia from continuous GPS data: Implications on present-day relative kinematics', *Earth and Planetary Science Letters* **222**(1), 197–208.

Griffiths, J. and Ray, J. R. (2009), 'On the precision and accuracy of IGS orbits', *Journal of Geodesy* **83**(3-4), 277–287.

Hackl, M., Malservisi, R., Hugentobler, U. and Wonnacott, R. (2011), 'Estimation of velocity uncertainties from GPS time series: Examples from the analysis of the South African Trignet network', *Journal of Geophysical Research* **116**(B11), B11404.

Hales, A. and Gough, D. (1960), 'Isostatic anomalies and crustal structure in the Southern Cape', *Geophysical Journal International* **3**, 225–236.

Hartnady, C. J. H., Calais, E. and Wonnacott, R. (2007), 'ITRF2000 velocity field from the South African Trignet GPS array and the African GNSS network : Implications for Nubia- (Rovuma-Lwandle-) Somalia plate motions', *International Conference on the East African Rift System (EARS)*, July 23-25 2007, Kampala, Uganada, Extended abstract, 5pp..

Hayes, G., Jones, E., Stadler, T., Barnhart, W., McNamara, D., Benz, H. and Furlong, K. (2014), 'Seismicity of the Earth 1900-2013 East African Rift.', *U.S. Geological Survey Open-File Report 2010-1083-P* .

Hoffmann, B., Lichtenegger, H. and Collins, J. (1994), *GPS–Theory and Practice*, 3rd edn, Springer-Verlag: New York, USA.

Horner-Johnson, B. C., Gordon, R. G. and Argus, D. F. (2007), 'Plate kinematic evidence for the existence of a distinct plate between the Nubian and Somalian plates along the Southwest Indian Ridge', *Journal of Geophysical Research* **112**(B5), B05418.

Jestin, F., Huchon, P. and Gaulier, J. (1994), 'The Somalia plate and the East African Rift System: Present-day kinematics', *Geophysical Journal International* **116**(3), 637–654.

Johnson, H. O. and Agnew, D. C. (1995), 'Monument motion and measurements of crustal velocities', *Geophysical Research Letters* **22**(21), 2905–2908.

Le Gall, B., Gernigon, L., Rolet, J., Ebinger, C., Gloaguen, R., Nilsen, O., Dypvik, H., Deffontaines, B. and Mruma, A. (2004), 'Neogene-Holocene rift propagation in central Tanzania: Morphostructural and aeromagnetic evidence from the Kilombero area', *Geological Society of America Bulletin* **116**(3-4), 490–510.

Leick, A. (2004), *GPS Satellite Surveying*, 3rd edn, John Wiley & Sons,Inc.: New Jersey, USA.

Malservisi, R., Hugentobler, U., Wonnacott, R. and Chacko, R. (2010), 'How rigid is a rigid plate? Geodetic constraint from the Trignet CGPS network, South Africa .', p. 30.

Malservisi, R., Hugentobler, U., Wonnacott, R. and Hackl, M. (2013), 'How rigid is a rigid plate? Geodetic constraint from the Trignet CGPS network, South Africa', *Geophysical Journal International* **192**(3), 918–928.

Mao, A., Harrison, C. G. A. and Dixon, T. H. (1999), 'Noise in GPS coordinate time series', *Journal of Geophysical Research: Solid Earth* **104**(B2), 2797–2816.

Minster, J. B., Jordan, T. H., Molnar, P. and Haines, E. (1974), 'Numerical modelling of instantaneous plate tectonics', *Geophysical Journal International* **36**(3), 541–576.

Minster, J. B. and Jordan, T. H. (1978), 'Present-day plate motions', *Journal of Geophysical Research: Solid Earth* **83**(B11), 5331–5354.

Nikolaidis, R. (2002), 'Observation of geodetic and seismic deformation with the Global Positioning System', Dissertation (PhD), University of California, San Diego, USA.

Nocquet, J.-M. and Calais, E. (2004), 'Geodetic measurements of crustal deformation in the Western Mediterranean and Europe', *Pure and Applied Geophysics* **161**(3), 661–681.

Nocquet, J. M., Willis, P. and Garcia, S. (2006), 'Plate kinematics of Nubia-Somalia using a combined DORIS and GPS solution', *Journal of Geodesy* **80**(8-11), 591–607.

Pisani, A. R., Pietrantonio, G. and Devoti, R. (2009), 'Current geodetic deformation in the South African region'. Powerpoint Presentation: *European Geoseciences Union General Assembly 2009*, April 19-24 2009, Vienna, Austria.

Prawirodirdjo, L. (2004), 'Instantaneous global plate motion model from 12 years of continuous GPS observations', *Journal of Geophysical Research* **109**(B8), B08405.

Ray, J. (2010), 'Current positioning accuracy using Space Geodesy'. Powerpoint Presentation: *2010 American Geophysical Union Fall Meeting*, December 13-17 2010, San Francisco, California, USA.

Rebischung, P., Griffiths, J., Ray, J., Schmid, R., Collilieux, X. and Garayt, B. (2011), 'IGS08: The IGS realization of ITRF2008', *GPS Solutions* **16**(4), 483–494.

Roggero, M. (2008), Kinematic GPS batch processing, a source for large sparse problems, *in* P. Xu, J. Liu and A. Dermanis, eds, 'VI Hotine-Marussi Symposium on Theoretical and Computational Geodesy', Vol. 132 of *International Association of Geodesy Symposia*, Springer Berlin Heidelberg, pp. 160–165.

Roggero, M. (2012), Discontinuity detection and removal from data time series, *in* N. Sneeuw, P. NovÃ¡k, M. Crespi and F. Sansó, eds, 'VII Hotine-Marussi Symposium on Mathematical Geodesy', Vol. 137 of *International Association of Geodesy Symposia*, Springer Berlin Heidelberg, pp. 135–140.

Saigeetha, A. and Banyal, R. K. (2005), 'Alfred Wegener - From continental drift to plate tectonics', *Resonance* **10**(6), 43–59.

Santamaría-Gómez, A., Bouin, M.-N., Collilieux, X. and Wöppelmann, G. (2011), 'Correlated errors in GPS position time series: Implications for velocity estimates', *Journal of Geophysical Research* **116**(B1), B01405.

Sella, G. F., Dixon, T. H. and Mao, A. (2002), 'REVEL: A model for recent plate velocities from space geodesy', *Journal of Geophysical Research: Solid Earth (1978–2012)* **107**(B4), ETG–11.

Stamps, D. S., Calais, E., Saria, E., Hartnady, C., Nocquet, J.-M., Ebinger, C. J. and Fernandes, R. M. (2008), 'A kinematic model for the East African Rift', *Geophysical Research Letters* **35**(5), L05304.

Thaller, D. (2008), 'Inter-technique combination based on homogeneous normal equation systems including station coordinates, Earth orientation and troposphere parameters', Dissertation (PhD), GFZ, Helmholtz-Zentrum, Potsdam.

Williams, S. D. (2008), 'CATS: GPS coordinate time series analysis software', *GPS solutions* **12**(2), 147–153.

Williams, S. D. P. (2003*a*), 'Offsets in Global Positioning System time series', *Journal of Geophysical Research* **108**(B6), 2310.

Williams, S. D. P. (2003*b*), 'The effect of coloured noise on the uncertainties of rates estimated from geodetic time series', *Journal of Geodesy* **76**(9-10), 483–494.

Williams, S. D. P. (2004), 'Error analysis of continuous GPS position time series', *Journal of Geophysical Research* **109**(B3), B03412.

Zhang, J., Bock, Y., Johnson, H., Fang, P., Williams, S., Genrich, J., Wdowinski, S. and Behr, J. (1997), 'Southern California Permanent GPS Geodetic Array: Error analysis of daily position estimates and site velocities', *Journal of Geophysical Research: Solid Earth* **102**(B8), 18035–18055.